NASA Technical Paper 1017

Liquid Jet Impingement Normal to a Disk in Zero Gravity

Thomas L. Labus

AUGUST 1977

NASA

NASA Technical Paper 1017

Liquid Jet Impingement Normal to a Disk in Zero Gravity

Thomas L. Labus

Lewis Research Center
Cleveland, Ohio

NASA
National Aeronautics
and Space Administration

**Scientific and Technical
Information Office**

1977

LIQUID JET IMPINGEMENT NORMAL TO A DISK IN ZERO GRAVITY*

by Thomas L. Labus

Lewis Research Center

SUMMARY

An experimental and analytical investigation was conducted to determine the free-surface shapes of circular liquid jets impinging normal to sharp-edge disks under zero-gravity conditions. An order-of-magnitude analysis was conducted that indicated regions where viscous forces were not significant in the computation of free-surface shapes. The demarcation between the viscous and inviscid regions was found to depend on the flow Reynolds number and the ratio of the jet and disk radii.

Experiments conducted under zero-gravity conditions yielded three distinct flow patterns. These flow patterns were defined as surface tension flow, transition flow, and inertial flow. The flow regions were classified in terms of the relative effects of surface tension and inertial forces. The transition between regions was correlated with the system Weber number and the ratio of the jet and disk radii.

A zero-gravity inviscid analysis was performed in which the governing equations and the boundary conditions in the physical plane were transformed into an inverse plane. In the inverse plane, the stream function and the velocity potential became the coordinates. This removed the prime difficulty in free-surface problems, that of having to guess at the true position of the free surface. The governing equations were nonlinear in the inverse plane, thus requiring a numerical solution in which sets of nonlinear algebraic equations were solved simultaneously. Comparisons between experiment and numerical computations were made for the infinite- and finite-plate cases with the result that good agreement for the free-surface shapes was obtained.

INTRODUCTION

A knowledge of the dynamics of free liquid jets is required for the solution of a variety of problems associated with fluid flow within propellant tanks under low gravita-

* Submitted as a thesis in partial fulfillment of the requirements for the degree Doctor of Philosophy at the University of Toledo, Toledo, Ohio, in June 1976.

tional conditions. In particular, an understanding of the liquid-jet impact process, such as occurs when a liquid impinges upon baffles or tank walls during an inflow or reorientation maneuver, is required to predict liquid-propellant location, heat transfer rates, and pressure distributions. Liquid jet impingement also has direct applicability to spacecraft fire safety for cases in which water jets are used to extinguish fires under low-gravity conditions. To predict delivery flow rates requires the accurate prediction of flow surface coverage as a function of jet momentum flux.

There generally are three chief obstacles that have in the past prevented the solving of steady-state liquid jet - solid interaction problems. The major obstacle is the presence of the free surface. To apply numerical techniques to the solution of free-jet problems, it is necessary to define the area over which the computations are made by means of boundaries determined by the free liquid surfaces. Unfortunately, the location of the free surface is one of the solutions sought, so various complex techniques must be devised to circumvent this situation. Furthermore, analytical techniques are restricted solely to two-dimensional problems, whether a free surface exists or not. The second obstacle is gravity. Liquid jets in air (free jets), unlike liquid-into-liquid jets and gas-into-gas jets (submerged jets), are affected significantly by gravitational forces. The free-surface shape and velocity profiles depend on both the magnitude and orientation of gravity. Adding gravity necessarily complicates a model either through the governing equations or through the boundary conditions. Neglecting gravity in the model makes questionable the comparison of the theory with normal-gravity experimental data. The final obstacle is surface tension, an effect that has generally been neglected in almost all studies on free jets. Adding surface tension into a model leads to nonlinear free-surface boundary conditions.

This report presents the results of an experimental and analytical study conducted at the NASA Lewis Research Center concerning zero-gravity isothermal liquid-jet impingement. An axisymmetric liquid jet was impinged normally onto a sharp-edge disk under conditions in which both inertial and surface tension forces are of importance. The experimental free-surface shapes were correlated with known system parameters. An analytical model was formulated, and the free-surface shapes and streamlines were calculated for a number of discrete cases.

LITERATURE SURVEY

EXPERIMENTAL STUDIES

Very few experimental studies have been conducted to examine free jets impinging on solid surfaces. No work has been done where the major concern was either the shape

of the free surface or the measurement of velocity profiles within the jet. Also, only one experiment has used a two-dimensional jet. A two-dimensional jet is one in which the flow emanates from a rectangular slot so that the width of the jet is very large relative to its thickness. Schach (ref. 1) measured the pressure distributions and analytically calculated the free-surface shapes and velocity distributions for jets impinging onto flat panels at various impingement inclinations relative to the direction of flow. The jet employed had dimensions of 21 millimeters by 115 millimeters. According to Schach, the jet diverged spatially after impinging on the panel, and thus it can only be considered as truly two dimensional close to the centerline.

An excellent account of an elaborate experimental apparatus for obtaining a quiescent circular water jet in normal gravity is given by Donnelly and Glaberson (ref. 2). Their major concern was jet stability under imposed audiofrequency disturbances and, therefore, the impingement phenomenon was not directly observed. Rupe (ref. 3) and Stephens (ref. 4) experimentally measured the pressure distribution caused by circular jets striking solid surfaces in normal gravity. However, neither Rupe nor Stephens measured the free-surface shape or discussed any instabilities that occurred.

In nearly all flows where a circular liquid jet strikes a large flat surface in normal gravity, the impinging liquid jet moves radially outward from the stagnation point until a certain radial distance is reached, whereupon an instability known as a circular hydraulic jump occurs. The jump is characterized by an abrupt increase in the liquid depth and turbulent fluid motion. Koloseus and Ahmad (ref. 5) were concerned solely with predicting the behavior of the circular hydraulic jump. A water jet impinging on a flat plate of epoxy material was used in these experiments. The circular hydraulic jump was the subject of a very complete study conducted by Nirapathdongporn (ref. 6), whose report contains an excellent description of various devices for measuring jet shapes and jet diameters.

All of these studies deal with normal-gravity liquid jet - solid impingement. There have been no experimental studies on the impingement of liquid jets under zero-gravity conditions.

ANALYTICAL STUDIES

Steady Two-Dimensional Potential Flow

A number of papers and books have presented analytical studies of steady-state, two-dimensional free jets impinging on a variety of surfaces. The majority of these studies were concerned with irrotational, incompressible, inviscid flow in which the effects of gravity and surface tension were neglected. One of the major attractions of

this approach to the problem is that it can be handled by using complex potential theory and, therefore, can be treated analytically.

A two-dimensional jet striking an infinte flat surface at various angles was examined by Batchelor (ref. 7), who solved for the limiting stream thickness as a function of flow impingement angle and jet diameter. However, no attempt was made to predict free-streamline shapes. Schach (ref. 1) treated the impingement as a function of angle by using Prandtl's hodograph method and obtained the equations for free-surface shapes, flow distribution, and pressure distribution for the case of impingement on an infinitely wide plate. Kochin, et al. (ref. 8) also examined the impingement of a two-dimensional jet obliquely to an infinite flat plate and discussed the case of impingement on a plate of finite length. The equation of the free surface for the case of a two-dimensional jet striking a flat surface at right angles is presented by Milne-Thomson (ref. 9), who also solved for the velocity components within the jet. An excellent discussion of the techniques for handling two-dimensional free-jet problems is presented by Gurevich (ref. 10). Some of the two-dimensional flows examined by Gurevich include flow around a finite wedge, flow perpendicular to a finite plate, flow oblique to an infinite flat plate, and flows where a variety of solid objects are positioned adjacent to one wall or between two walls. Chang and Conly (ref. 11) analyzed the two-dimensional flow of a jet interacting with a number of flat segments at angles to one another. The results include flow turning angles but not free-surface shapes or velocity profiles. The irrotational flow pattern of a free jet discharging from a slot and flowing past a wedge was analyzed by Arbhabhirama (ref. 12).

All of these papers and books are concerned with analytical techniques for obtaining solutions. The area of steady two-dimensional potential flow represents the most complete area of research in the field of jet impingement.

Steady Axisymmetric Viscous Flow

Watson (ref. 13) has analytically investigated free-jet impingement for the case of large Reynolds numbers where the viscous forces are confined to a thin boundary layer adjacent to the plate. A similarity solution was obtained for both the two-dimensional and axisymmetric velocity profiles and free-surface shapes for the case of normal impingement. As mentioned by Watson, the similarity solution can only be expected to be valid when the radial distance is sufficiently large for the incident jet to have lost its influence. The effects of gravity and surface tension were neglected in the analysis. Watson solved for the radial position of the circular hydraulic jump.

NUMERICAL STUDIES

Steady Two-Dimensional Potential Flow

When the shape of the solid upon which the jet impinges becomes complex, numerical techniques for the solution of free-jet problems have to be applied. Jeppson (ref. 14) presents an excellent article in this regard. Jeppson used the stream function and the velocity potential as the independent variables and the coordinates as the dependent variables. A similar inversion approach has been used to solve a variety of fluid dynamics problems, as shown in references 15 to 19, and is mainly attributable to Thom and Apelt (ref. 15). Using this technique, Jeppson was able to circumvent the problem of working in the physical plane and having to guess at the true position of the free surface. The latter iterative approach was used in references 20 to 26 with limited success. Jeppson solved the problem of two-dimensional flow over a wedge and is the only one to have attempted numerical solutions of this problem. Lastly, Chan (ref. 27) applied the finite-element method to a number of free-surface flow problems, including flow from a circular orifice.

Steady Axisymmetric Potential Flow

Potential axisymmetric flow problems cannot be solved by using the powerful tool of complex analysis. Extending the mathematical treatment to axisymmetric and three-dimensional flows has so far proved intractable (ref. 9). For this reason, only numerical solutions can be attempted for problems of this nature.

LeClerc (ref. 28) studied the impingement of an axially symmetric liquid jet normal to a flat surface. The shape of the free surface was found by using an electrical analogy. This method thus fixed the position of the free surface and enabled the author to apply standard finite-differencing methods and to employ Southwell's relaxation technique in order to solve Laplace's equation. Jeppson applied his inversion technique to find the flow pattern and the free-surface shape for the case of axisymmetric flow past a variety of bodies of revolution, including cones. Jeppson applied his own technique to the solution of a jet of inviscid, incompressible fluid issuing from a nozzle into the free atmosphere. He shows how this method can be extended to a variety of other problems. Schach (ref. 29) used a semianalytical technique based on Trefftz's approximate method to find the shape of an axisymmetric free jet impinging normally on a plate. Also presented in Schach's article was the pressure distribution on the plate, which was calculated from the velocity distribution by using Bernoulli's equation. Young, et al. (ref. 30) and Brunauer (ref. 31) determined the flow pattern past two disks immersed in axisymmetric flow.

Both Young and Brunauer solved Laplace's equation in the physical plane. No analyses have been conducted for the case in which an inviscid free jet impinges on a plate of finite diameter.

References 28 to 31 encompass all the known solutions with regard to axisymmetric jet impingement. References 18, 21, 22, 25, and 27 deal specifically with numerical methods applied to free-surface problems in which no impingement occurs. Jeppson (ref. 18) used an inverse formulation; the others worked in the physical plane.

Unsteady Two-Dimensional and Axisymmetric Potential Flow

Huang, Hammit, and Yang (refs. 32 and 33) have investigated unsteady flows and considered the impact phenomena for both two-dimensional and axisymmetric jets. The major interest in these articles was in obtaining the initial pressure distribution due to liquid impact.

Steady Potential Flow Including Gravitational Effects

Adding gravity in numerical analyses for potential flows causes no serious formulation problem for either the two-dimensional or the axisymmetric case, since its effect enters only through the free-surface boundary conditions and not the governing equations. Jeppson (ref. 14) included gravity in his analysis of impingement on a two-dimensional wedge. Moayeri and Strelkoff (ref. 19), Southwell and Vaisey (ref. 22), and Chan (ref. 27) all considered the effect of gravity in dealing with steady, potential, free-surface problems in which no impingement occurs.

Steady Potential Flow Including Surface Tension

Zhukovskii (ref. 34) has indicated how to include the effects of surface tension. He examined a two-dimensional problem by using complex analysis, but his method is not extendable to either axisymmetric or three-dimensional flows.

Steady Three-Dimensional Potential Flow

Until very recently, little had been accomplished in the area of three-dimensional potential flow with a free surface, much less including impingement. Davis and Jeppson (ref. 35) developed a computer program to solve free-surface problems of this type by

the inverse method. Michelson (refs. 36 and 37) also examined jets under these conditions. He treated the case of an axisymmetric jet impinging obliquely on a flat surface and analytically showed the occurrence of wedge-shaped dry zones when the impingement angle was less than a critical value. Free-surface shapes are not obtainable by Michelson's method.

ORDER-OF-MAGNITUDE ANALYSIS

GENERAL FORMULATION

The problem under consideration is the viscous flow of a circular liquid jet as it impinges normally to a flat plate, as shown in figure 1. The objective is to determine the free-surface shape of the impinging liquid and the velocity profiles within the jet. In general, flows of this type depend on viscous, surface tension, inertial, and body forces. Physical intuition tells us that if the velocity is large and the diameter of the plate is sufficiently small, there will be regions wherein viscous forces are not of prime importance in determining the resulting flow behavior, particularly the free-surface shape. The viscous forces, in this case, will be confined to a thin boundary layer on the plate that originates from the stagnation point. The location of the stagnation point, O, is shown in figure 1. The jet or nozzle radius is R_0, and the distance between the plate and the nozzle is H. A cylindrical coordinate system (r, z) emanating from the stagnation point is chosen. An order-of-magnitude analysis will permit the governing equations to be simplified so that an analytical solution can be attempted. For axisymmetric, isothermal, incompressible steady flow under weightless conditions, the governing equations in cylindrical coordinates for a Newtonian fluid can be written as

Continuity:

$$\frac{1}{r}\frac{\partial}{\partial r}(ru) + \frac{\partial v}{\partial z} = 0 \tag{1}$$

Momentum:

r Component,

$$\rho\left(u\frac{\partial u}{\partial r} + v\frac{\partial u}{\partial z}\right) = -\frac{\partial p}{\partial r} + \mu\left\{\frac{\partial}{\partial r}\left[\frac{1}{r}\frac{\partial}{\partial r}(ru)\right] + \frac{\partial^2 u}{\partial z^2}\right\} \tag{2}$$

z Component,

$$\rho\left(u\frac{\partial v}{\partial r}+v\frac{\partial v}{\partial z}\right)=-\frac{\partial p}{\partial z}+\mu\left[\frac{1}{r}\frac{\partial}{\partial r}\left(r\frac{\partial v}{\partial r}\right)+\frac{\partial^2 v}{\partial z^2}\right] \tag{3}$$

(All symbols are defined in appendix F.)

Boundary conditions are required on the flat plate, along the axis of symmetry, at the nozzle exit, on the free surface, and at $r = L$.

On plate:

$$\left.\begin{aligned} u &= 0 \\ v &= 0 \end{aligned}\right\} \text{on } z = 0, \text{ all } r \tag{4}$$

Along axis of symmetry:

$$\left.\begin{aligned} u &= 0 \\ \frac{\partial v}{\partial r} &= 0 \end{aligned}\right\} \text{on } r = 0, \text{ all } z \tag{5}$$

At nozzle:

$$\left.\begin{aligned} v &= -\mathscr{V} \\ u &= 0 \end{aligned}\right\} \text{on } 0 \le r \le R_0, \; z = H \tag{6}$$

At $r = L$:

$$\left.\begin{aligned} u &= u(z) \\ v &= v(z) \end{aligned}\right\} \text{on } r = L, \; 0 < z \le f(L) \tag{7}$$

On the free surface, denoted by $z_s = f(r)$, two boundary conditions are required since the free-surface position is an unknown to be determined as part of the solution. The details of the calculation for the boundary conditions along the free surface are given in appendix A (see eqs. (A10) and (A14)).

On free surface:

$$\frac{1}{2}(u^2 + v^2) - \frac{\sigma}{\rho r}\frac{d}{dr}\left[\frac{r\frac{df}{dr}}{\sqrt{1 + \left(\frac{df}{dr}\right)^2}}\right] = \frac{1}{2}\mathscr{V}^2 - \frac{\sigma}{\rho R_0} \qquad \text{on } z_s = f(r) \tag{8}$$

and

$$-u\frac{df}{dr} + v = 0 \qquad \text{on } z_s = f(r) \tag{9}$$

In equation (4), the no-flow and no-slip boundary conditions are applied at the wall. Equation (5) is a statement involving the known geometrical symmetry of the problem; equation (6) imposes an initially uniform velocity profile on the incoming jet. Equation (7) simply states the velocity distribution as the liquid leaves the control volume. Equation (8) is a statement of conservation of mechanical energy along a streamline; equation (9) states that the normal velocity component on a streamline is zero. The second terms on the left and right sides of equation (8) are the contribution of surface tension to the mechanical energy balance.

The solution of the problem can be greatly facilitated by simplifying equations (1) to (8). Specifically, the method of obtaining the minimum parametric representation of a problem will be used to simplify the governing equations. This method is described in detail by Krantz (ref. 38) and is the most systematic approach for scaling the governing equations. The initial step in the minimum parametric representation method is to form dimensionless variables by introducing characteristic scale factors for all dependent and independent variables. The unknown scale factors are defined as U_0, V_0, r_0, z_0, p_0, and f_0.

Dimensionless variables are now defined as

$$u^* = \frac{u}{U_0}, \quad v^* = \frac{v}{V_0}, \quad r^* = \frac{r}{r_0}, \quad z^* = \frac{z}{z_0}, \quad p^* = \frac{p}{p_0}, \quad f^* = \frac{f}{f_0} \tag{10}$$

Introducing these dimensionless variables into the differential equations and boundary conditions and arbitrarily making the coefficient of one term in each differential equation and boundary condition equal to 1 result in

Continuity:

$$\frac{\partial v^*}{\partial z^*} + \frac{U_0 z_0}{V_0 r_0} \frac{1}{r^*} \frac{\partial}{\partial r^*} (r^* u^*) = 0 \tag{11}$$

Momentum:

r Component,

$$\frac{\rho U_0 z_0^2}{r_0 \mu} u^* \frac{\partial u^*}{\partial r^*} + \frac{\rho V_0 z_0}{\mu} v^* \frac{\partial u^*}{\partial z^*} = - \frac{p_0 z_0^2}{r_0 \mu U_0} \frac{\partial p^*}{\partial r^*} + \frac{z_0^2}{r_0^2} \frac{\partial}{\partial r^*} \left[\frac{1}{r^*} \frac{\partial}{\partial r^*} (r^* u^*) \right] + \frac{\partial^2 u^*}{\partial z^{*2}} \tag{12}$$

z Component,

$$\frac{u_0 z_0}{r_0 V_0} u^* \frac{\partial v^*}{\partial r^*} + v^* \frac{\partial v^*}{\partial z^*} = - \frac{p_0}{\rho V_0^2} \frac{\partial p^*}{\partial z^*} + \frac{\mu z_0}{r_0^2 \rho V_0} \frac{1}{r^*} \frac{\partial}{\partial r^*} \left(r^* \frac{\partial v^*}{\partial r^*} \right) + \frac{\mu}{z_0 \rho V_0} \frac{\partial^2 v^*}{\partial z^{*2}} \tag{13}$$

Boundary conditions:

On wall,

$$\left.\begin{aligned} u^* &= 0 \\ v^* &= 0 \end{aligned}\right\} \text{on } z^* = 0, \text{ all } r^* \tag{14}$$

Along axis of symmetry,

$$\left.\begin{aligned} u^* &= 0 \\ \frac{\partial v^*}{\partial r^*} &= 0 \end{aligned}\right\} \text{on } r^* = 0, \text{ all } z^* \tag{15}$$

At nozzle,

$$\left.\begin{aligned} v^* &= -\frac{\mathscr{V}}{V_0} \\ u^* &= 0 \end{aligned}\right\} 0 \le r^* \le \frac{R_0}{r_0},\ z^* = \frac{H}{z_0} \tag{16}$$

At $r^* = L/r_0$,

$$\left.\begin{aligned} u^* &= u^*(z^*) \\ v^* &= v^*(z^*) \end{aligned}\right\} \text{on } r^* = L/r_0,\ 0 < z^* \le f(L)/z_0 \tag{17}$$

On free surface,

$$\frac{1}{2}\left(u^{*2}\frac{U_0^2}{V_0^2} + v^{*2}\right) - \frac{\sigma}{\rho r^* V_0^2}\frac{f_0}{r_0^2}\frac{d}{dr^*}\left[\frac{r^*\frac{df^*}{dr^*}}{\sqrt{1+\frac{f_0^2}{r_0^2}\left(\frac{df^*}{dr^*}\right)^2}}\right] = \frac{1}{2}\frac{\mathscr{V}^2}{V_0^2} - \frac{\sigma}{\rho R_0 V_0^2} \qquad \text{on } z_s^* = \frac{f^* f_0}{z_0} \tag{18}$$

and

$$v^* - \frac{U_0 f_0}{V_0 r_0} u^* \frac{df^*}{dr^*} = 0 \qquad \text{on } z_s^* = \frac{f^* f_0}{z_0} \tag{19}$$

The scale factors must now be determined. This is done by setting some of the resulting dimensionless groups in the equations and boundary conditions equal to zero or 1. The groups chosen depend on the physical conditions for which the equations are being scaled. In what follows, the formalism of Krantz (ref. 38) is strictly followed. Characteristic lengths are usually determined from the dimensionless groups generated by the boundary conditions. Characteristic times, velocities, etc., are determined from dimensionless groups generated by the differential equations. The guidelines in determining the unknown scale factors are

(1) Do not introduce any mathematical contradictions.

(2) Do not violate physical intuition.

BOUNDARY CONDITIONS

If we examine the boundary conditions, it is apparent that the following dimensionless groups are introduced:

$$\frac{\mathscr{V}}{V_0}, \frac{R_0}{r_0}, \frac{\mu}{z_0}, \frac{L}{r_0}, \frac{f(L)}{z_0}, \frac{U_0^2}{V_0^2}, \frac{\sigma f_0}{\rho V_0^2 r_0^2}, \frac{f_0^2}{r_0^2}, \frac{\sigma}{\rho R_0 V_0^2}, \frac{f_0}{z_0}, \frac{U_0 f_0}{V_0 r_0}$$

It is known that v has the range 0 to $-\mathscr{V}$, r has the range 0 to L, z has the range 0 to H, and f(r) also has the range 0 to H. Therefore, setting

$$\left.\begin{aligned} \frac{\mathscr{V}}{V_0} &= 1 \\ \frac{L}{r_0} &= 1 \end{aligned}\right\} \tag{20}$$

implies that

$$\left.\begin{aligned} V_0 &= \mathscr{V} \\ r_0 &= L \end{aligned}\right\} \tag{21}$$

and yields two of the six unknown scale factors. Then v^* and r^* are said to be of the same or smaller order of 1. Similar statements can be applied to the remaining variables. This ordering procedure is discussed thoroughly by Lu (ref. 39).

Some of the remaining dimensionless groups cannot be set equal to 1 or zero without introducing contradictions. Setting $V_0 = \mathscr{V}$ and $r_0 = L$ into these ratios and assuming that

$$f_0 = z_0 \tag{22}$$

gives the following meaningful ratios:

$$\frac{H}{z_0}, \frac{U_0^2}{\mathscr{V}^2}, \frac{\sigma z_0}{\rho \mathscr{V}^2 L^2}, \frac{z_0^2}{L^2}, \frac{U_0 z_0}{\mathscr{V} L}$$

Setting the second or fourth ratio equal to 1 or zero would violate physical intuition. Therefore, the ratios to be considered are

$$\frac{H}{z_0}, \quad \frac{\sigma z_0}{\rho \nu^2 L^2}, \quad \frac{U_0 z_0}{\nu L}$$

At this point an attempt was made to set H/z_0 equal to 1 such that z_0 would equal H. This seemed logical because 0 to H was the range of z. However, this leads to some confusing results in terms of the physics. For a given flow condition, it is argued that for a certain (minimum) value of H up to $H = \infty$, the flow pattern in the vicinity of the plate is not expected to change. This is shown schematically in figure 2. This argument has been experimentally verified and is discussed at some length in the section EXPERIMENTATION. The major point is that H cannot be a characteristic length in the problem either with reference to z_0 or to f_0. This leaves two remaining ratios from consideration of the boundary conditions: $\sigma z_0/\rho \nu^2 L^2$ and $U_0 z_0/\nu L$. Accordingly, all possible information from the boundary conditions has been obtained. Two of the six scale factors and a relation between two others have been determined. The governing equations must now be examined.

GOVERNING EQUATIONS

Continuity Equation

From the physics of the problem, it is known that mass must be conserved. If the dimensionless derivatives $\partial v^*/\partial z^*$ and

$$\frac{1}{r^*} \frac{\partial}{\partial r^*} (r^* u^*)$$

are to be of the same order of magnitude, it is required that

$$\frac{U_0 z_0}{V_0 r_0} = 1 \tag{23}$$

With $V_0 = \nu$ and $r_0 = L$,

$$\frac{U_0 z_0}{\nu L} = 1 \tag{24}$$

Solving for U_0 gives

$$U_0 = \frac{\gamma L}{z_0} \tag{25}$$

This, of course, is an equation relating two unknowns, U_0 and z_0. The same information could have been obtained by setting the second of the two ratios remaining from the consideration of the boundary conditions equal to 1.

Momentum Equations

It is the objective of this analysis to define that portion of the flow for which an inviscid solution is valid. For this case, the pressure forces are balanced by the inertial forces. This fact allows us to determine the scale factor for the pressure p_0. If the dimensionless pressure gradient in equation (13) is to be the same order of magnitude as the dimensionless inertia term,

$$\frac{p_0}{\rho V_0^2} = 1 \tag{26}$$

it implies that

$$p_0 = \rho V_0^2 = \rho \gamma^2 \tag{27}$$

Thus, the characteristic pressure is the stagnation pressure.

Physics of z_0

The remaining unknown to be determined is z_0. At this point some physical arguments are necessary. Recall that it has been shown that H cannot be considered as a characteristic scale factor for the problem at hand for reasonably large values of H. However, the free-surface shape is expected to change as R_0 varies (fig. 3). Therefore, from physical considerations, this suggests that characteristic values of z_0 vary as R_0. By defining

$$z_0 = R_0 \tag{28}$$

U_0 can be found from equation (25):

$$U_0 = \frac{\nu L}{R_0} \tag{29}$$

In summary, the following has been determined:

$$V_0 = \nu$$

$$r_0 = L$$

$$z_0 = R_0$$

$$f_0 = R_0$$

$$U_0 = \frac{\nu L}{R_0}$$

$$p_0 = \rho \nu^2$$

These scale factors can now be substituted into the governing equations to obtain the minimum parametric representation of the problem. The results are as follows:

$$Re\ u^* \frac{\partial u^*}{\partial r^*} + Re\ v^* \frac{\partial u^*}{\partial z^*} = - Re \left(\frac{R_0}{L}\right)^2 \frac{\partial p^*}{\partial r^*} + \left(\frac{R_0}{L}\right)^2 \frac{\partial}{\partial r^*} \left[\frac{1}{r^*} \frac{\partial}{\partial r^*} (r^* u^*)\right] + \frac{\partial^2 u^*}{\partial z^{*2}} \tag{30}$$

$$Re\ u^* \frac{\partial v^*}{\partial r^*} + Re\ v^* \frac{\partial v^*}{\partial z^*} = - Re \frac{\partial p^*}{\partial z^*} + \left(\frac{R_0}{L}\right)^2 \frac{1}{r^*} \frac{\partial}{\partial r^*} \left(r^* \frac{\partial v^*}{\partial r^*}\right) + \frac{\partial^2 v^*}{\partial z^{*2}} \tag{31}$$

where Re is the Reynolds number, defined as

$$Re = \frac{\rho \nu R_0}{\mu} \tag{32}$$

The equations are now in the form from which it can be determined what the conditions must be such that viscous forces are not significant. The major parameters in this problem are R_0/L and Re. Since all the starred terms in equations (30) and (31) are of order 1 or smaller, only the coefficients of the individual terms need be considered in simplifying. Considering equation (30), it can be seen that since $(R_0/L)^2 << 1$, both the inertial and pressure forces will be an order of magnitude greater than the viscous forces, provided that

$$\left.\begin{aligned} \mathrm{Re} &>> 1 \\ \mathrm{Re}(R_0/L)^2 &>> 1 \end{aligned}\right\} \tag{33}$$

From equation (31), since $(R_0/L)^2 << 1$, no new information is obtained. The governing equations will be reduced to a simplified form of Euler's equations of motion

$$u^* \frac{\partial u^*}{\partial r^*} + v^* \frac{\partial u^*}{\partial z^*} = -\left(\frac{R_0}{L}\right)^2 \frac{\partial p^*}{\partial r^*} \tag{34}$$

$$u^* \frac{\partial v^*}{\partial r^*} + v^* \frac{\partial v^*}{\partial z^*} = -\frac{\partial p^*}{\partial z^*} \tag{35}$$

RESULTS

If the viscous forces are restricted to be at least two orders of magnitude smaller than the inertial or pressure forces, there results

$$\left.\begin{aligned} \mathrm{Re} &\geq 100 \\ \mathrm{Re}\left(\frac{R_0}{L}\right)^2 &\geq 100 \end{aligned}\right\} \tag{36}$$

Since R_0/L is less than 1 by definition, the coefficient to consider is the second one in equation (36), since this will be the limiting one. Under the restrictions $\mathrm{Re} \geq 100$ and $R_0/L < 1$, the Euler's equations of motion are obtained. The equation $\mathrm{Re}\,(R_0/L)^2 = 100$ is shown graphically in figure 4. The curve in figure 4 separates the inviscid region from the viscous region. Physical understanding of the problem is made clearer by referring to this plot. The higher the incoming jet Reynolds number becomes, the

thinner will be the boundary layer at some fixed radial position from the stagnation point. As shown in figure 4, at lower values of the ratio R_0/L (perhaps obtained by increasing the disk radius L), higher Reynolds numbers are required in order to avoid viscous influence. Finally, within the viscous region, the boundary layer will grow to a radial length that is equal to the free-surface height. The effective design of an experiment is now possible so that the flow can be considered essentially inviscid.

EXPERIMENTATION

APPARATUS AND PROCEDURE

Test Facility

The experimental investigation was conducted in the Lewis 2.2-second drop tower. The exact specifications of the facility, the mode of operation, and the release and recovery systems are described in detail in appendix B. The drop tower provides a 2.2-second weightless environment in which to conduct tests.

Experiment Package

The experiment package used to obtain the data for this study is shown in figure 5. It consists of an aluminum frame in which were mounted the jet reservoir, the disk, the 16-millimeter high-speed motion picture camera, the liquid supply tank, the backlighting scheme, and the batteries. The major functions were controlled by onboard sequence timers.

A diagram indicating the manner in which the flow system operates is shown in figure 6. This was a pressure-controlled system in which the flow was begun by opening the solenoid valve. Prior to the drop, liquid was contained in the line between the liquid supply tank and the jet reservoir. In addition, the jet reservoir was completely filled with the test liquid.

A schematic drawing of the jet reservoir, which was fabricated of acrylic plastic, is shown in figure 7. The critical feature of the jet reservoir is the 45° tapered section that leads to a circular nozzle of diameter d_0. The range of nozzle radii studied was from 0.25 to 0.75 centimeter. In addition, the transition between the circular nozzle and the tapered section was rounded smooth. This construction prevents boundary layer buildup and allows the liquid jet to exit from the reservoir with a nearly uniform velocity profile. Based on the experimental results of reference 40, this is more than sufficient

to ensure a uniform exiting velocity profile over the range of Reynolds number studied.

Sharp-edge disks, also fabricated of acrylic plastic, were mounted above the jet reservoir by means of a threaded rod such that the flat surface of the disk was at right angles to the impinging liquid jet. The radii L of the disks were 1.0 and 1.5 centimeters. A schematic drawing of the disks is shown in figure 8.

Test Liquids

Two test liquids were used, anhydrous ethanol and trichlorotrifluoroethane (Freon TF). Their properties at 20° C are listed in table I. No attempt was made to correct the fluid properties for temperature changes. Both test fluids possess a nearly 0° static contact angle on an acrylic plastic surface. However, this was not the reason why they were chosen as test fluids. They were chosen because of their relatively low viscosity and their availability.

Test Procedure

Prior to a test run, the jet reservoir, the disk, and the supply tanks were cleaned ultrasonically with a mild detergent. After these parts were rinsed with methanol, they were dried in a warm-air dryer. The supply tank was subsequently filled with the test liquid, and the jet reservoir was filled by pressurizing the supply tank. This procedure eliminated air bubbles from the lines and ensured accurate flow rates. After the jet reservoir was completely full, the supply tank was sealed and two accumulator bottles (not shown in fig. 5) were pressurized with gaseous nitrogen to a predetermined value. The accumulator bottles were designed to be of such a volume that flow rate and pressure remained essentially constant during a test. Thus, jet velocities were determined by measuring the change in liquid level in the supply tanks during a normal-gravity calibration run. It was assumed that the flow rate obtained in this fashion would remain the same in weightlessness.

Electrical timers on the experiment package were set to control the initiation and duration of all functions programmed during the drop. The experiment package was then balanced and positioned within the prebalanced drag shield. The wire support was attached to the experiment package through an access hole in the shield (fig. 29(a)). Properly sized, spiked tips were installed on the drag shield. Then the drag shield, with the experiment package inside, was hoisted to the predrop position at the top of the facility (fig. 28) and connected to an external electrical power source. The wire support was attached to the release system, and the entire assembly was suspended from the wire. After final electrical checks were made and the experiment package was

switched to internal power, the system was released. After the test was completed, the experiment package and drag shield were returned to the preparation area.

EXPERIMENTAL RESULTS

Effect of Nozzle Height

It was desired to conduct the zero-gravity tests in regions where the nondimensional distance between the nozzle and the disk H/R_0 was not of importance to the problem. Several tests were conducted that showed no effect on the free-surface shapes if the ratio of nozzle height to jet radius was greater than 6. Therefore, all zero-gravity experiments were conducted under this constraint in order to eliminate H/R_0 as a variable. This experimentally determined fact supports the argument made in the section ORDER-OF-MAGNITUDE ANALYSIS that H could not be a scale factor for the axial coordinate.

Steady-State Flow Patterns

The approximate steady-state flows in weightlessness for three different jet velocities are shown photographically in figure 9. The direction of flow of the liquid jet is vertically upward. The threaded rod and bolt shown in the figure make up the disk holder that connects the sharp-edge disk assembly to the rig frame. The jet velocity increases from left to right in the figure. Three distinct classifications of flow pattern were observed to occur and are labeled in figure 9 as surface tension flow, transition flow, and inertial flow. Surface tension flow (fig. 9(a)) is defined as that flow in which the liquid flows completely around the disk, with no separation at the disk edge. In transition flow (fig. 9(b)), surface tension and inertial forces are both important. Transition flow is defined as flow in which the liquid separates from the disk and the resulting liquid sheet either collects upon itself and forms an envelope or has the tendency to do so. Inertial flow (fig. 9(c)) is defined as that flow in which the liquid separates from the disk with no liquid returning toward the jet centerline or attempting to form an envelope.

The flow pattern shown for transition flow is not the flow pattern one would expect if steady-state conditions could have been reached. The reason for this is that some liquid always travels toward the disk from the point at which the envelope meets. This liquid flow strikes the back of the baffle and subsequently disrupts the initial configuration of the envelope. The recirculating flow is a strong function of the geometry of the disk holder. The surface tension flow is generally slow and, as a result, does not quite reach a steady-state configuration on the back of the disk. The inertial flow tests (represented by fig. 9(c)) always reached steady state.

The experimental tests were conducted for conditions that are in the inviscid region of figure 4. (Two exceptions are noted in table II.) Depending on the particular value of R_0/L, there exists a minimum Reynolds number below which the runs can no longer be considered as viscous free. The experimental results are given in table II, including all the important parameters as well as the flow classifications. One additional parameter, the Weber number, is given in table I. As will be shown in the next section, when the Reynolds number is no longer a parameter of controlling interest, the Weber number and the ratio R_0/L become important. The Weber number $\rho V^2 R_0/\sigma$, which naturally arises from consideration of the boundary conditions, is the ratio of inertial to surface tension forces. In the flow category column of table II, S indicates surface tension flow, T transition flow, and I inertial flow. Finally, note that the designated flow classification for some cases, particularly those bordering transition or inertial flow, could easily fit into either category.

Zero-Gravity Results

The data contained in table II are shown graphically in figure 10. The curves in the figure were faired by hand and separate the various flow classifications. At any particular value of the ratio R_0/L in figure 10, the flow classification depends only on the system Weber number. Two critical Weber numbers occur at a constant value of R_0/L. The lowest critical Weber number separates the surface tension flow from the transition flow; the higher critical Weber number separates the transition flow from the inertial flow. In addition, the critical Weber number between regimes decreased as R_0/L was increased over the range of parameters studied.

POTENTIAL FORMULATION

GOVERNING EQUATIONS AND BOUNDARY CONDITIONS IN PHYSICAL PLANE INCLUDING SURFACE TENSION

In the section ORDER-OF-MAGNITUDE ANALYSIS, it was shown that at any particular value of R_0/L, if the Reynolds number is sufficiently large, the flow can be considered as viscous free. It is further assumed that the jet will continue to remain viscous free after leaving the disk. There will be no shear stress between the exiting radial jet and the ambient air surrounding it.

General Formulation

Consider the flow of a circular liquid jet impinging normally on a circular disk, as shown in figure 11(a), where R_0 is the jet radius, L is the disk radius, and H is the distance between the jet reservoir and the disk. The incoming jet velocity is given as $\mathcal{V}$, and the initial velocity profile is assumed to be uniform. There will be two free surfaces involved. The upper free surface is defined as $z_s = f_1(r)$, and the lower free surface as $z_s = f_2(r)$. In addition, a third surface is required for the complete formulation of the boundary value problem. Initially, this surface was chosen as the straight line $\underline{FE}$ (fig. 11(a)). However, this proved to be inconvenient since $\underline{FE}$ is arbitrary and, thus, has no known boundary condition. Instead, $z_s = f_3(r)$ was chosen, a surface along which the velocity potential is constant. Various points in the physical plane have been designated with letters ranging from A to G for convenience. In cylindrical coordinates, the dimensional governing equations and boundary conditions in terms of the primary variables (u,v) are given as follows for a weightless environment and for inviscid, incompressible, isothermal, steady flow as

Continuity:

$$\frac{1}{r}\frac{\partial}{\partial r}(ru) + \frac{\partial v}{\partial z} = 0 \tag{38}$$

Momentum:

r Component,

$$\rho\left(u\frac{\partial u}{\partial r} + v\frac{\partial u}{\partial z}\right) = -\frac{\partial p}{\partial r} \tag{39}$$

z Component,

$$\rho\left(u\frac{\partial v}{\partial r} + v\frac{\partial v}{\partial z}\right) = -\frac{\partial p}{\partial z} \tag{40}$$

The following boundary conditions are applied:

On $\underline{DC}$:

$$v = 0 \quad \text{on } z = 0,\ 0 \le r \le L \tag{41}$$

On AB:

$$u = 0 \qquad 0 \le r \le R_0, \; z = H \tag{42}$$

On BC:

$$\frac{\partial v}{\partial r} = 0 \qquad r = 0, \; 0 < z \le H \tag{43}$$

On AG:

$$\frac{1}{2}(u^2 + v^2) - \frac{\sigma}{\rho r}\frac{d}{dr}\left(\frac{r f_1'}{\sqrt{1 + f_1'^2}}\right) = \frac{1}{2}\mathscr{V}^2 - \frac{\sigma}{\rho R_0} \qquad \text{on } z_s = f_1(r) \tag{44}$$

and

$$-u f_1' + v = 0 \qquad \text{on } z_s = f_1(r) \tag{45}$$

On DE:

$$\frac{1}{2}(u^2 + v^2) - \frac{\sigma}{\rho r}\frac{d}{dr}\left(\frac{r f_2'}{\sqrt{1 + f_2'^2}}\right) = \frac{1}{2}\mathscr{V}^2 - \frac{\sigma}{\rho R_0} \qquad \text{on } z_s = f_2(r) \tag{46}$$

and

$$-u f_2' + v = 0 \qquad \text{on } z_s = f_2(r) \tag{47}$$

On GE:

$$u + v f_3' = 0 \qquad \text{on } z_s = f_3(r) \tag{48}$$

where $f_3(r)$ for now will be assumed to be some specified surface.

The derivation for the boundary condition along GE is as follows: The velocity potential φ is constant. By definition, the velocity vector $\vec{V}$ is normal to an equipotential surface. This means that

$$\vec{V} \times \hat{n} = 0 \qquad \text{on } z_s = f_3(r) \tag{49}$$

The unit normal to $f_3(r)$ is

$$\hat{n} = - \frac{f_3' \hat{i} + \hat{j}}{\sqrt{f_3'^2 + 1}} \tag{50}$$

where $\hat{i}$ is the unit vector in the radial direction, $\hat{j}$ is the unit vector in the axial direction, and

$$\vec{V} = u\hat{i} + v\hat{j} \tag{51}$$

Applying equation (49) results in

$$\frac{u + vf_3'(r)}{\sqrt{f_3'^2 + 1}} = 0 \tag{52}$$

From which equation (48) follows.

Introduction of Stokes stream function. - The primary variables contained in the governing equations are the scalar velocity components u and v. The fact that two functions are required to describe one vector field is cumbersome. As shown in the theory of hydrodynamics, the number of functions can be reduced for several important cases, one of these being axisymmetric flow. A function ψ, defined as the Stoke's stream function, can be introduced, which automatically satisfies the continuity equation. With the additional requirement of irrotationality, the governing equation in terms of the Stokes's stream function will result.

According to Chan (ref. 27), the Stokes's stream function is a mathematical device used to describe the flow. It has the following properties: First, when the stream function is set equal to a constant, it results in different annular stream surfaces in axisymmetric flow. Second, when it is differentiated properly, it yields the velocity components. Third, the difference between the values at two adjacent stream surfaces is related to the flow rate between those surfaces.

Starting with equation (38), the continuity equation for axisymmetric flow, the following substitutions are made:

$$u = - \frac{1}{r} \frac{\partial \psi}{\partial z} \tag{53}$$

and

$$v = \frac{1}{r}\frac{\partial \psi}{\partial r} \tag{54}$$

Substituting equations (53) and (54) into equation (38) shows that continuity is identically satisfied. In addition, the assumption is made that the flow is also irrotational. As a result

$$\text{curl } \vec{V} = 0 \tag{55}$$

For axisymmetric flow, this can be written

$$\frac{\partial u}{\partial z} - \frac{\partial v}{\partial r} = 0 \tag{56}$$

Replacing u and v in equation (56) by their relations to ψ results in the governing equation for axisymmetric flow in terms of the Stokes's stream function

$$\frac{\partial^2 \psi}{\partial z^2} - \frac{1}{r}\frac{\partial \psi}{\partial r} + \frac{\partial^2 \psi}{\partial r^2} = 0 \tag{57}$$

Thus, one equation, equation (57), takes the place of the continuity equation and the two momentum equations. As mentioned, continuity is identically satisfied by substitution of equations (53) and (54). In addition, substituting equations (53) and (54) into the momentum equations and subsequently eliminating the pressure terms by cross differentiation show that it too is identically satisfied provided that $\text{curl } \vec{V} = 0$, which in essence is equation (57).

Derivation of boundary conditions in terms of ψ. - To derive the boundary conditions in terms of the Stokes stream function ψ, we need only refer to the physical-plane conditions (eqs. (41) to (48)) and the two definitions (eqs. (53) and (54)).

On DC:

$$v = 0 \qquad \text{on } z = 0,\ 0 \le r \le L \tag{58}$$

Using equation (54),

$$\frac{1}{r}\frac{\partial \psi}{\partial r} = 0 \qquad \text{on } z = 0,\ 0 \le r \le L \tag{59}$$

Therefore,

$$\frac{\partial \psi}{\partial r} = 0 \qquad \text{on } z = 0,\ 0 \le r \le L \tag{60}$$

Hence,

$$\psi \neq \psi(r) \qquad \text{on } z = 0,\ 0 \le r \le L \tag{61}$$

and at most,

$$\psi = \psi(z) \qquad \text{on } z = 0,\ 0 \le r \le L \tag{62}$$

But, $z = 0$. Therefore,

$$\psi = \text{Constant} = C$$

and DC is a streamline, as expected. Arbitrarily choosing the value of this constant equal to zero gives

On DC:

$$\psi = 0 \qquad \text{on } z = 0,\ 0 \le r \le L \tag{63}$$

Since DC, BC, and DE are all part of the same streamline, they must all have the same Stoke's stream function ($\psi = 0$). As indicated in equation (63), this value is arbitrarily chosen as zero.

Now, examine the surface AB.

On AB:

$$u = 0 \qquad 0 \le r \le R_0,\ z = H \tag{64}$$

By using equation (53), it can be seen that

$$u = -\frac{1}{r}\frac{\partial \psi}{\partial z} = 0 \qquad 0 \le r \le R_0,\ z = H \tag{65}$$

and, therefore,

$$\frac{\partial \psi}{\partial z} = 0 \qquad 0 \leq r \leq R_0, \; z = H \tag{66}$$

and generally

$$\psi = \psi(r) \qquad 0 \leq r \leq R_0, \; z = H \tag{67}$$

However, we know on AB

$$v = -\gamma \qquad 0 \leq r \leq R_0, \; z = H \tag{68}$$

so that

$$-\gamma = \frac{1}{r} \frac{\partial \psi}{\partial r} \qquad 0 \leq r \leq R_0, \; z = H \tag{69}$$

Integration yields

$$\psi = -\frac{\gamma r^2}{2} + C \qquad 0 \leq r \leq R_0, \; z = H \tag{70}$$

The value of C can now be determined by evaluating this last expression at r = 0.

$$\psi \Big|_{r=0} = C \tag{71}$$

But along BC, $\psi = 0$. Therefore C = 0 at r = 0 and

$$\psi = -\frac{\gamma r^2}{2} \qquad 0 \leq r \leq R_0, \; z = H \tag{72}$$

On AG: Since AG is a line of constant ψ, applying equation (72) yields

$$\psi = -\frac{\gamma R_0^2}{2} \tag{73}$$

In addition, equation (44) applies. Substituting equations (53) and (54) into equation (44)

yields

$$\frac{1}{2r^2}\left[\left(\frac{\partial\psi}{\partial z}\right)^2+\left(\frac{\partial\psi}{\partial r}\right)^2\right]-\frac{\sigma}{\rho r}\frac{d}{dr}\left(\frac{rf_1'}{\sqrt{1+f_1'^2}}\right)=\frac{1}{2}\gamma^2-\frac{\sigma}{\rho R_0}\qquad \text{on } z_s=f_1(r) \tag{74}$$

On DE:

$$\frac{1}{2r^2}\left[\left(\frac{\partial\psi}{\partial z}\right)^2+\left(\frac{\partial\psi}{\partial r}\right)^2\right]-\frac{\sigma}{\rho r}\frac{d}{dr}\left(\frac{rf_2'}{\sqrt{1+f_2'^2}}\right)=\frac{1}{2}\gamma^2-\frac{\sigma}{\rho R_0}\qquad \text{on } z_s=f_2(r) \tag{75}$$

On GE: Equation (48) become

$$-\frac{\partial\psi}{\partial z}+\frac{\partial\psi}{\partial r}f_3'(r)=0\qquad \text{on } z_s=f_3(r) \tag{76}$$

The second boundary conditions on the free surfaces, namely, $-uf_1'+v=0$ and $-uf_2'+v=0$, are fully equivalent to the specification of the value of the Stokes's stream function along those surfaces, $\psi=0$ on DE and $\psi=-\gamma R_0^2/2$ on AG. Since $\psi=\psi(r,z)$, it can be expanded and $d\psi$ is equal to zero along AG and ED.

Nondimensionalization of governing equations and boundary conditions in physical plane. - The governing equation in terms of the Stokes's stream function (eq. (57)) and the boundary conditions are now put into dimensionless form by introducing scale factors. Let the scale factor for the stream function be $-\gamma R_0^2$ and R_0 be the scale factor for lengths. Let dimensionless quantities be represented by stars, (i.e., ψ^* is dimensionless). The results of this manipulation are as follows: The governing equation is

$$\frac{\partial^2\psi^*}{\partial z^{*2}}+\frac{\partial^2\psi^*}{\partial r^{*2}}-\frac{1}{r^*}\frac{\partial\psi^*}{\partial r^*}=0 \tag{77}$$

The boundary conditions are

On DC:

$$\psi^*=0\qquad \text{on } z^*=0\qquad 0\le r^*\le L/R_0 \tag{78}$$

On AB:

$$\psi^* = \frac{1}{2} r^{*2} \qquad 0 \le r^* \le 1, \; z^* = H/R_0 \tag{79}$$

On BC:

$$\psi^* = 0 \qquad r^* = 0, \; 0 < z^* \le H/R_0 \tag{80}$$

On AG:

$$\psi^* = \frac{1}{2} \qquad \text{on } z_s^* = f_1^*(r^*) \tag{81}$$

and

$$\frac{1}{2r^{*2}}\left[\left(\frac{\partial\psi^*}{\partial z^*}\right)^2 + \left(\frac{\partial\psi^*}{\partial r^*}\right)^2\right] - \frac{1}{We\, r^*}\frac{d}{dr^*}\left(\frac{r^* f_1^{*\prime}}{\sqrt{1 + f_1^{*\prime 2}}}\right) = \frac{1}{2} - \frac{1}{We} \qquad \text{on } z_s^* = f_1^*(r^*) \tag{82}$$

On DE:

$$\psi^* = 0 \qquad \text{on } z_s^* = f_2^*(r^*) \tag{83}$$

and

$$\frac{1}{2r^*}\left[\left(\frac{\partial\psi^*}{\partial z^*}\right)^2 + \left(\frac{\partial\psi^*}{\partial r^*}\right)^2\right] - \frac{1}{We\, r^*}\frac{d}{dr^*}\left(\frac{r^* f_2^{*\prime}}{\sqrt{1 + f_2^{*\prime 2}}}\right) = \frac{1}{2} - \frac{1}{We} \qquad \text{on } z_s^* = f_2^*(r^*) \tag{84}$$

On GE:

$$\frac{\partial\psi^*}{\partial z^*} - \frac{\partial\psi^*}{\partial r^*} f_3^{*\prime} = 0 \qquad \text{on } z_s^* = f_3^*(r^*) \tag{85}$$

Three parameters appear in the specification of boundary conditions. They include the Weber number We and the dimensionless length ratio L/R_0. Recalling the arguments in the ORDER-OF-MAGNITUDE ANALYSIS, section H/R_0 is not really a parameter if it is larger than some minimum value. The dimensionless velocity components

can be calculated from the following expressions:

$$\frac{u}{\nu} = \frac{1}{r^*} \frac{\partial \psi^*}{\partial z^*} \tag{86}$$

$$\frac{v}{\nu} = -\frac{1}{r^*} \frac{\partial \psi^*}{\partial r^*} \tag{87}$$

The procedure for numerical solution of the boundary value problem using finite difference methods as set up in dimensionless form in the physical plane would be as follows: Initially, realistic variations for $f_1^*(r)$, $f_2^*(r)$, and $f_3^*(r)$ must be assumed. Using one of the two given boundary conditions on AG and DE (i.e., $\psi^* = 1/2$ and $\psi^* = 0$), solve for ψ^*. With the initial solution for ψ^*, check the validity of the second of the two boundary conditions on AG and GE. If the boundary conditions are not satisfied, new variations in f_1^*, f_2^*, and f_3^* must be assumed. A second iteration to ψ^* must be obtained and so on. One of the serious drawbacks of this outlined iteration scheme is the lack of knowledge concerning how to update assumed values of f_1^*, f_2^*, and f_3^* based on previous solutions. In other words, there is no logical way in which to make changes to the shape of the initially assumed control volume.

Surface-Tension-Dominated Model

For Weber numbers between 5 and 30 (depending on the ratio R_0/L), experimental data (fig. 10) show that the resulting steady-state flow pattern is surface tension dominated (fig. 9(a)). By previous definition, in surface tension flow the liquid flows completely around the disk with no separation from the edge. It is the intent to model this flow in order to solve for the theoretical free-surface shapes and velocity profiles. Assuming axisymmetry, the physical plane model is shown in figure 11(b). In the model, at some cross section far downstream, the flow is assumed to approach the initially uniform flow it possessed at AB. The exiting plane is denoted by GE in the model. Both C and C' are located at $r = 0$, $z = 0$. (The plate is assumed to be infinitely thin.) However, C is located on top of the plate, while C' is on the bottom. The free surface $f_1(r)$ is not assumed to possess mirror symmetry about the $z = 0$ position. In cylindrical coordinates, the governing equations and the boundary conditions in terms of the primary variables (u, v) are given as

Continuity:

$$\frac{1}{r}\frac{\partial}{\partial r}(ru) + \frac{\partial v}{\partial z} = 0 \tag{88}$$

Momentum:

r Component,

$$\rho\left(u\frac{\partial u}{\partial r} + v\frac{\partial u}{\partial z}\right) = -\frac{\partial p}{\partial r} \tag{89}$$

z Component,

$$\rho\left(u\frac{\partial v}{\partial r} + v\frac{\partial v}{\partial z}\right) = -\frac{\partial p}{\partial z} \tag{90}$$

The following boundary conditions are applied:

On DC:

$$v = 0 \qquad \text{on } z = 0,\ 0 \le r \le L \tag{91}$$

On DC':

$$v = 0 \qquad \text{on } z = 0,\ 0 \le r \le L \tag{92}$$

On AB:

$$u = 0 \qquad 0 \le r \le R_0,\ z = H \tag{93}$$

On BC:

$$\frac{\partial v}{\partial r} = 0 \qquad \text{on } r = 0,\ 0 < z \le H \tag{94}$$

On C'E:

$$\frac{\partial v}{\partial r} = 0 \qquad \text{on } r = 0,\ -H \le z < 0 \tag{95}$$

On GE:

$$u = 0 \qquad 0 \le r \le R_0, \; z = -H \tag{96}$$

On AG:

$$\frac{1}{2}(u^2 + v^2) - \frac{\sigma}{\rho r}\frac{d}{dr}\left(\frac{rf_1'}{\sqrt{1 + f_1'^2}}\right) = \frac{1}{2}\gamma^2 - \frac{\sigma}{\rho R_0} \qquad \text{on } z_s = f_1(r) \tag{97}$$

and

$$-uf_1' + v = 0 \qquad \text{on } z_s = f_1(r) \tag{98}$$

Equations (97) and (98) represent two distinct pieces of information concerning $z = f_1(r)$.

Direct substitution of equations (53) and (54), the relations between the velocity components and the Stoke's stream function, into the governing equations and the boundary conditions for the surface tension model results in the desired formulation after nondimensionalization. Similar to the general formulation in the last section, the various lengths in the problem are scaled with respect to R_0 and the scale factor for the Stoke's stream function is $-VR_0^2$. The equations are

$$\frac{\partial^2 \psi^*}{\partial z^{*2}} + \frac{\partial^2 \psi^*}{\partial r^{*2}} - \frac{1}{r^*}\frac{\partial \psi^*}{\partial r^*} = 0 \tag{99}$$

The boundary conditions are

On DC:

$$\psi^* = 0 \qquad \text{on } z^* = 0, \; 0 \le r^* \le L/R_0 \tag{100}$$

On DC':

$$\psi^* = 0 \qquad \text{on } z^* = 0, \; 0 \le r^* \le L/R_0 \tag{101}$$

On BC:

$$\psi^* = 0 \qquad \text{on } r^* = 0, \; 0 < z^* \le H/R_0 \tag{102}$$

On C'E:

$$\psi^* = 0 \qquad \text{on } r^* = 0,\ -H/R_0 < z^* < 0 \tag{103}$$

On AB:

$$\psi^* = \frac{1}{2} r^{*2} \qquad \text{on } 0 \le r^* \le 1,\ z^* = H/R_0 \tag{104}$$

On GE:

$$\psi^* = \frac{1}{2} r^{*2} \qquad \text{on } 0 \le r^* \le 1,\ z^* = -H/R_0 \tag{105}$$

On AG:

$$\psi^* = \frac{1}{2} \qquad \text{on } z_s^* = f^*(r^*) \tag{106}$$

and

$$\frac{1}{2r^{*2}}\left[\left(\frac{\partial\psi^*}{\partial z^*}\right)^2 + \left(\frac{\partial\psi^*}{\partial r^*}\right)^2\right] - \frac{1}{We}\frac{1}{r^*}\frac{d}{dr^*}\left[\frac{r^*}{\sqrt{\left(\frac{\partial\psi^*/\partial z^*}{\partial\psi^*/\partial r^*}\right)^2 + 1}}\right] = \frac{1}{2} - \frac{1}{We} \qquad \text{on } z_s^* = f^*(r^*) \tag{107}$$

INVERSE-PLANE FORMULATIONS

The procedure for solving for the free-surface shapes in the physical plane has already been outlined. The difficulties encountered when making adjustments to the free surfaces between iterations and the lack of a logical manner in which to make the adjustments have been cited. This would be a time-consuming task even in the absence of surface tension. A computerized scheme is sought that offers the possibility of achieving the free-surface results with a minimum of computer iteration time and user interaction.

Transformation Formulas

An alternative approach to the physical-plane solution is discussed in detail by Jeppson (ref. 14). In his article, Jeppson discusses a transformation technique into what is termed the inverse plane. The coordinate axes in the inverse plane are the velocity potential φ and the Stoke's stream function ψ. The advantage of using the $\varphi\psi$ space, or inverse plane, is that the free surface lies along a line of constant ψ and is, therefore, at a known position. The governing equation, however, is no longer linear as it was in the physical plane.

Introduction of velocity potential. - A scalar function defined as the velocity potential has been used previously in the specification of the boundary GE (the exiting plane). The continuity equation for steady incompressible axisymmetric flow is given by equation (39). The flow is also assumed to be irrotational such that the condition given by equation (56) is also valid. Equation (56) implies that there exists a scalar potential function φ such that

$$\vec{V} = \text{grad } \varphi \tag{108}$$

from which it follows that

$$u = \frac{\partial \varphi}{\partial r} \tag{109}$$

and

$$v = \frac{\partial \varphi}{\partial z} \tag{110}$$

Substituting equations (109) and (110) into equation (38) yields the governing equation for steady axisymmetric flow in terms of the velocity potential

$$\frac{\partial^2 \varphi}{\partial z^2} + \frac{1}{r}\frac{\partial \varphi}{\partial r} + \frac{\partial^2 \varphi}{\partial r^2} = 0 \tag{111}$$

Relationships between ψ and φ. - It can now be stated that the relations between the velocity potential and the Stokes's stream function are

$$u = \frac{\partial \varphi}{\partial r} = -\frac{1}{r}\frac{\partial \psi}{\partial z} \tag{112}$$

and

$$v = \frac{\partial \varphi}{\partial z} = \frac{1}{r} \frac{\partial \psi}{\partial r} \tag{113}$$

Inverse-plane formulation. - To formulate the problem in the inverse plane, r and z must be known as functions of ψ and φ. In other words, by working in the inverse plane we are attempting to reverse the roles of the dependent and independent variables. The required relations are obtained by noting that if $\psi = \psi(r, z)$ and $\varphi = \varphi(r, z)$, there then exist the inverse functions $r = r(\varphi, \psi)$ and $z = z(\varphi, \psi)$:

$$r^2 \frac{\partial^2 z}{\partial \psi^2} + \frac{\partial^2 z}{\partial \varphi^2} = -2 \frac{\partial z}{\partial \psi} \frac{\partial z}{\partial \varphi} \tag{114}$$

and

$$\frac{\partial^2 r}{\partial \psi^2} + \frac{1}{r^2} \frac{\partial^2 r}{\partial \varphi^2} - \frac{1}{r^3} \left(\frac{\partial r}{\partial \varphi} \right)^2 + \frac{1}{r} \left(\frac{\partial r}{\partial \psi} \right)^2 = 0 \tag{115}$$

Details of the derivation of these equations are contained in appendix C and were obtained from reference 14.

For further discussion, equation (114) is referred to as the z equation and equation (115) is called the r equation. Both these equations are nonlinear, with the nonlinearity in the z equation also involving r. Also, both these equations are of the elliptic type, as shown in reference 14. This means that boundary conditions are required for all boundaries in the flow region. A solution to the problem begins with a solution to the r equation (eq. (115)) since it contains only one unknown, r.

One final point involves the fact that the variables discussed in the inverse transformations are all dimensional. Nondimensionalization of these equations similar to the nondimensionalization done in the physical plane allows the same equation to be recovered. Let

$$\left.\begin{aligned} z^* &= \frac{z}{z_0} \quad \text{where } z_0 = R_0 \\ r^* &= \frac{r}{r_0} \quad \text{where } r_0 = R_0 \\ \psi^* &= \frac{\psi}{\psi_0} \quad \text{where } \psi_0 = -\gamma R_0^2 \\ \varphi^* &= \frac{\varphi}{\varphi_0} \quad \text{where } \varphi_0 = -\gamma R_0 \end{aligned}\right\} \tag{116}$$

These substitutions yield exactly the same governing equations and transformation formulas in starred notation. In other words,

$$r^{*2}\frac{\partial^2 z^*}{\partial \psi^{*2}} + \frac{\partial^2 z^*}{\partial \varphi^{*2}} = -2\frac{\partial z^*}{\partial \psi^*}\frac{\partial z^*}{\partial \varphi^*} \tag{117}$$

and

$$\frac{\partial^2 r^*}{\partial \psi^{*2}} + \frac{1}{r^{*2}}\frac{\partial^2 r^*}{\partial \varphi^{*2}} - \frac{1}{r^{*3}}\left(\frac{\partial r^*}{\partial \varphi^*}\right)^2 + \frac{1}{r^*}\left(\frac{\partial r^*}{\partial \varphi^*}\right)^2 = 0 \tag{118}$$

Infinite Flat Plate Excluding Surface Tension

The first problem to be examined in which the inverse transformation is used is the flow of a circular liquid jet normal to a flat plate (fig. 12). At this point, the starred notation to designate dimensionless quantities is dropped. It is assumed that all quantities appearing henceforth are dimensionless unless otherwise stated (i.e., r, z, ψ, φ are now dimensionless). For the case in which surface tension is excluded, some of the physical-plane boundary conditions must necessarily change. The model described in equations (77) to (85) is for the general case of a finite disk in which surface tension effects are important. The boundary conditions that remain valid for the infinite-plate case excluding surface tension are equations (79) and (80), with equation (78) modified to read "on EC." For the case of an infinite flat plate, since the free surface DE of figure 11(a) no longer exists, the designation D does not appear in

the model. Furthermore, for the case in which surface tension forces are unimportant, the boundary condition along the upper surface (referring to eq. (82)) can be written as follows:

On AG:

$$\frac{1}{r^2}\left[\left(\frac{\partial\psi}{\partial z}\right)^2 + \left(\frac{\partial\psi}{\partial r}\right)^2\right] = 1 \qquad \text{on } z_s = f(r) \tag{119}$$

This expression is obtained by allowing the Weber number (the ratio of inertial to surface tension forces) to approach infinity. The case we are examining is one in which the surface tension forces become vanishingly small or the inertial forces become large. Finally, the boundary GE will be nearly vertical, implying that the velocity there is purely radial. This is tantamount to letting $f_3^{*\prime}$ approach infinity in equation (85).

Derivation of boundary conditions in inverse plane for r formulation. - The boundary conditions in the inverse plane for r formulation are as follows:

On AB (or φ = Constant):

$$\psi = \frac{1}{2}r^2 \qquad \text{in the physical plane, eq. (79)} \tag{120}$$

$$r = \sqrt{2\psi} \qquad \text{in the inverse plane}$$

On BC (or $\psi = 0$):

$$r = 0 \qquad \text{in the inverse plane} \tag{121}$$

On EC (or $\psi = 0$):

$$v = 0$$

By equation (113), this implies that $\partial\varphi/\partial z$ and $\partial\psi/\varphi r$ equal zero. In the inverse plane (by eq. (C4)),

$$\partial r/\partial\psi = 0 \tag{122}$$

On GE (or φ = Constant): It is arbitrarily set equal to zero, $\varphi = 0$. It will be assumed that GE is nearly vertical, implying that the velocity is purely radial. From equa-

tion (85), $\partial\psi/\partial r = 0$. In the inverse plane,

$$\partial r/\partial\psi = 0 \qquad \text{since } J \neq 0 \tag{123}$$

On AG (or $\psi = 1/2$):

$$\frac{1}{r^2}\left[\left(\frac{\partial\psi}{\partial z}\right)^2 + \left(\frac{\partial\psi}{\partial r}\right)^2\right] = 1 \qquad \text{in the physical plane (from eq. (119))}$$

From equations (112) and (113),

$$\left(\frac{\partial\varphi}{\partial r}\right)^2 + \left(\frac{\partial\varphi}{\partial z}\right)^2 = 1$$

From equations (C2) and (C4),

$$J^2\left[\left(\frac{\partial z}{\partial\psi}\right)^2 + \left(\frac{\partial r}{\partial\psi}\right)^2\right] = 1$$

Substituting for J^2 from equation (C9) and then using equations (C6) and (C7) yield the final form

$$\left(\frac{\partial r}{\partial\varphi}\right)^2 + r^2\left(\frac{\partial r}{\partial\psi}\right)^2 = 1 \tag{124}$$

The results of these derivations are shown schematically in figure 13(a) in the inverse plane. The boundary conditions for the z formulation are also shown in figure 13(b).

Derivation of boundary conditions in inverse plane for z formulation. - The boundary conditions in the inverse plane for z formulation are as follows:

On AB (or φ = Constant): In the physical plane, $u = 0$, which implies that $\partial\varphi/\partial r = 0$. From equation (C2), $\partial z/\partial\psi = 0$. This implies that $z = z(\varphi)$ alone and, since AB is a line of constant φ,

$$z = \text{Constant} \qquad \text{in the inverse plane} \tag{125}$$

On BC (or $\psi = 0$): In the physical plane, $u = 0$, from which it follows, in the inverse plane, that

$$\frac{\partial z}{\partial \psi} = 0 \tag{126}$$

On EC (or $\psi = 0$):

$$z = 0 \quad \text{in the inverse plane} \tag{127}$$

On GE (or $\varphi = 0$):

$$v = 0 \quad \text{in the physical plane}$$

From equation (113), it follows that $\partial\psi/\partial r = 0$ and from equation (C3) that, in the inverse plane,

$$\frac{\partial z}{\partial \varphi} = 0 \tag{128}$$

On AG (or $\psi = 1/2$):

$$\frac{1}{r^2}\left[\left(\frac{\partial \psi}{\partial z}\right)^2 + \left(\frac{\partial \psi}{\partial r}\right)^2\right] = 1 \quad \text{in the physical plane}$$

In the inverse plane we can take over the equivalent expression given by equation (124),

$$\left(\frac{\partial r}{\partial \varphi}\right)^2 + r^2\left(\frac{\partial r}{\partial \psi}\right)^2 = 1$$

Using equations (C6) and (C7) to eliminate the derivative involving r results in

$$r^2\left(\frac{\partial z}{\partial \psi}\right)^2 + \left(\frac{\partial z}{\partial \varphi}\right)^2 = 1 \tag{129}$$

The solution technique for the infinite-plate case is as follows: The r values can be completely found once the governing equation (eq. (118)) is solved. The variable z appears nowhere in the formulation (i.e., it does not appear in either the governing

equations or the boundary conditions). Once the r values are found, the z governing equation (eq. (117)) can be solved. The z solution requires a prior knowledge of the values of r both in the interior region of flow and on the free-surface boundary.

Finite Plate Excluding Surface Tension

A second problem to be formulated is concerned with the impingement of a circular liquid jet normal to a disk of finite width. For the case in which surface tension effects are neglected, the formulation depicted in figure 13 will vary only slightly for the finite plate. In fact, all the boundary conditions are identical with the exception of the bottom free surface (ED) and the exiting plane (GE).

On ED:

$$\left(\frac{\partial r}{\partial \varphi}\right)^2 + r^2\left(\frac{\partial r}{\partial \psi}\right)^2 = 1 \tag{130}$$

There is an additional change in the boundary condition along GE (or $\varphi = 0$), the exiting plane of the jet. In the physical plane, from equation (85),

$$\frac{\partial \psi}{\partial z} - \frac{\partial \psi}{\partial r} f_3' = 0 \tag{131}$$

By using equations (C1) and (C3), this can be written

$$\frac{\partial r}{\partial \varphi} + \frac{\partial z}{\partial \varphi} f_3' = 0 \tag{132}$$

Finally, using equation (C7) to eliminate $\partial z/\partial \varphi$ yields

$$\frac{\partial r}{\partial \varphi} + r\frac{\partial r}{\partial \psi} f_3' = 0 \tag{133}$$

or

$$\frac{\partial r}{\partial \varphi} + r\left(\frac{\partial r}{\partial \psi}\right)\left(\frac{dz}{dr}\right) = 0 \tag{134}$$

The boundary conditions for the z formulation in the inverse plane can be obtained in a similar manner. Continuing with equation (134) and using equations (C6) and (C7) give

$$r\left(\frac{\partial z}{\partial \psi}\right) - \left(\frac{\partial z}{\partial \varphi}\right)\left(\frac{dz}{dr}\right) = 0 \tag{135}$$

The formulation of the problem of flow of a circular liquid jet normal to a finite disk in the inverse plane is now complete. The r solution for this case, however, can no longer be obtained independently of the z solution due to the exiting jet boundary condition. Thus, the problem will necessitate a simultaneous solution of two partial differential equations of the nonlinear elliptic type.

Surface-Tension-Dominated Model - Finite Plate

The final problem to be examined involves the surface-tension-dominated flow described in figure 11(b). The inverse-plane formulation for the r solution is indicated in figure 14(a). The boundary conditions are the same as derived previously, with the exception of the free-surface boundary and the exiting jet condition. Along AG in the physical plane,

$$\frac{1}{2r^2}\left[\left(\frac{\partial \psi}{\partial z}\right)^2 + \left(\frac{\partial \psi}{\partial r}\right)^2\right] - \frac{1}{We}\frac{1}{r}\frac{d}{dr}\left[\frac{r}{\sqrt{\left(\frac{\partial \psi / \partial z}{\partial \psi / \partial r}\right)^2 + 1}}\right] = \frac{1}{2} - \frac{1}{We} \tag{136}$$

This will now be put into inverse form. In the derivation of equation (124), it was shown that the first bracketed term on the left,

$$\frac{1}{r^2}\left[\left(\frac{\partial \psi}{\partial z}\right)^2 + \left(\frac{\partial \psi}{\partial r}\right)^2\right] = \frac{1}{\left(\frac{\partial r}{\partial \varphi}\right)^2 + r^2\left(\frac{\partial r}{\partial \psi}\right)^2} \tag{137}$$

In addition, the term within the radical becomes equation (138) by using equations (C1), (C3), and (C7).

$$\left(\frac{\frac{\partial\psi}{\partial z}}{\frac{\partial\psi}{\partial r}}\right)^2 = \frac{1}{r^2}\left(\frac{\frac{\partial r}{\partial\varphi}}{\frac{\partial r}{\partial\psi}}\right)^2 \tag{138}$$

Therefore, the inverse boundary condition along AG (or $\psi = 1/2$) becomes

$$\frac{1}{2\left[\left(\frac{\partial r}{\partial\varphi}\right)^2 + r^2\left(\frac{\partial r}{\partial\psi}\right)^2\right]} - \frac{1}{We}\frac{1}{r}\frac{d}{dr}\left[\frac{r}{\sqrt{\frac{1}{r^2}\left(\frac{\partial r/\partial\varphi}{\partial r/\partial\psi}\right)^2 + 1}}\right] = \frac{1}{2} - \frac{1}{We} \tag{139}$$

which can be written

$$\frac{1}{2\left[\left(\frac{\partial r}{\partial\varphi}\right)^2 + r^2\left(\frac{\partial r}{\partial\psi}\right)^2\right]} - \frac{1}{We}\frac{1}{r}\frac{d}{dr}\left[\frac{r^2}{\sqrt{\left(\frac{\partial r/\partial\varphi}{\partial r/\partial\psi}\right)^2 + r^2}}\right] = \frac{1}{2} - \frac{1}{We} \tag{140}$$

Multiplying through by 2 and rearranging yields

$$\left(\frac{\partial r}{\partial\varphi}\right)^2 + r^2\left(\frac{\partial r}{\partial\psi}\right)^2 = \frac{1}{1 - \frac{2}{We} + \frac{2}{We}\frac{1}{r}\frac{d}{dr}\left[\frac{r^2}{\sqrt{\left(\frac{\partial r/\partial\varphi}{\partial r/\partial\psi}\right)^2 + r^2}}\right]} \tag{141}$$

There has been no z symmetry assumed for the r formulation, only axisymmetry. The r formulation does not involve the variable z. Therefore, the r and z solutions can be obtained independently. The z formulation is shown in figure 14(b).

CENTRAL FINITE DIFFERENCE REPRESENTATION - RECTANGULAR MESH

The finite difference operators for the nonlinear r and z elliptic partial differential equations resulting from the inversion were put into difference form. It was known

from experience that considerable flexibility resulted if the difference equations were derived by using rectangular mesh. The finite difference expressions along the free surfaces (i.e., AG and ED) contain a square root, the argument of which becomes negative during iterations. The use of rectangular mesh alleviated this difficulty and also allowed us to control the size of the flow region.

GENERAL FORMULATION

General Considerations

The partial derivatives appearing in the r and z governing equations are replaced by algebraic central finite difference operators. A complete derivation of the various operators is contained in reference 41. The notation used in this report is that shown in figure 15. If the finite difference analogy of $\partial/\partial r$ is $\delta/\delta r$, the r derivatives can be written at point 0 as follows:

$$\frac{\delta r}{\delta \varphi} = \frac{r_1 - r_3}{2\,\Delta\varphi} \tag{142}$$

$$\frac{\delta r}{\delta \psi} = \frac{r_2 - r_4}{2\,\Delta\psi} \tag{143}$$

$$\frac{\delta^2 r}{\partial \varphi^2} = \frac{r_1 + r_3 - 2r_0}{\Delta\varphi^2} \tag{144}$$

$$\frac{\delta^2 r}{\partial \psi^2} = \frac{r + r_4 - 2r_0}{\Delta\psi^2} \tag{145}$$

Similarly, the central finite difference representations for the z derivatives are

$$\frac{\delta z}{\delta \varphi} = \frac{z_1 - z_3}{2\,\Delta\varphi} \tag{146}$$

$$\frac{\delta z}{\delta \psi} = \frac{z_2 - z_4}{2\,\Delta\psi} \tag{147}$$

$$\frac{\delta^2 z}{\delta \varphi^2} = \frac{z_1 + z_3 - 2z_0}{\Delta \varphi^2} \tag{148}$$

$$\frac{\delta^2 z}{\delta \psi^2} = \frac{z_2 + z_4 - 2z_0}{\Delta \psi^2} \tag{149}$$

Interior Nodal Points

If equations (142) to (145) are substituted into the r governing equation (eq. (115)) with $\alpha = \Delta\varphi/\Delta\psi$, the finite difference expression for all interior nodal points is

$$r_0^4 - \frac{r_0^3}{2}(r_2 + r_4) + r_0^2\left[\frac{1}{\alpha^2} - \frac{1}{8}(r_2 - r_4)^2\right] - \frac{r_0}{2\alpha^2}(r_1 + r_3) + \frac{1}{8\alpha^2}(r_1 - r_3)^2 = 0 \tag{150}$$

In addition, if equations (146) to (149) are substituted into the z governing equation (eq. (114)), the finite difference expression for all interior nodal points is

$$z_0 = \frac{r_0^2}{2\left(r_0^2 + \frac{1}{\alpha^2}\right)}(z_2 + z_4) + \frac{1}{2(r_0^2\alpha^2 + 1)}(z_1 + z_3) + \frac{1}{4\left(r_0^2\alpha + \frac{1}{\alpha}\right)}(z_2 - z_4)(z_1 - z_3) \tag{151}$$

where, as in the derivation of equation (150),

$$\alpha = \frac{\Delta\varphi}{\Delta\psi} \tag{152}$$

FORMULATION EXCLUDING SURFACE TENSION

The governing equations and boundary conditions were put into difference form using central finite differences. Details are contained in appendix D.

Infinite Flat Plate

The finite difference representation for the infinite flat plate is shown in figure 16. The algebraic expressions for the boundaries are derived by simultaneous application of the governing equation and the boundary conditions at a fixed point. This application involves a fictitious point, f, outside the boundary that is subsequently eliminated. Point G represents a special point in the finite difference representation for the z solution. The governing z equation (eq. (151)) was applied at point G, which resulted in two fictitious points. Then the boundary conditions along both AG and GE were applied at point G. This allowed the two fictitious points to be eliminated from the resulting finite difference expression. Detailed calculations for the boundaries are contained in appendix D for all models.

Finite Plate

The changes in inverse formulation for the finite-plate problem are now presented. For this case, the difference operator along GE is more complicated than in the infinite-plate case. The following algebraic expression is valid along GE:

$$r_0^4 - \frac{r_0^3}{2}(r_2 + r_4) + r_0^2\left[\frac{1}{\alpha^2} - \frac{1}{8}(r_2 - r_4)^2\right] - \frac{r_0}{2\alpha^2}\left[2r_1 + \alpha r_0(z_2 - z_4)\right] + \frac{r_0^2}{8}(z_2 - z_4)^2 = 0 \tag{153}$$

On DE, the following expression is valid:

$$r_0^4 - r_0^3 r_2 + r_0^2\left[\frac{1}{\alpha^2} + \frac{1}{2}\sqrt{4a^2 - \frac{1}{\alpha^2}(r_1 - r_3)^2}\right] - \frac{r_0}{2\alpha^2}(r_1 + r_3) + \frac{1}{8}\left[\frac{2}{\alpha^2}(r_1 - r_3)^2 - 4a^2\right] = 0 \tag{154}$$

In fact, both G and E represent special points in the r formulation. However, one of these, point E, is specified as a known position (r = Constant). At point G the equation to be satisfied in the r formulation is

$$r_0^4 - r_0^3 r^4 + r_0^2 \frac{1}{\alpha^2} - \left[\sqrt{a^2 - r_0^2(z_0 - z_4)^2}\right] - \frac{r_0}{\alpha^2}\left[r_1 + \alpha r_0(z_0 - z_4)\right]$$

$$+ \left[r_0^2(z_0 - z_4)^2 - \frac{a^2}{2}\right] = 0 \qquad (155)$$

For the inverse z formulation, the following changes occurred from the infinite-plate description:

On GE:

$$z_0 = \frac{r_0^2(z_2 + z_4)}{2\left(r_0^2 + \frac{1}{\alpha^2}\right)} + \frac{2z_1 - r_0\alpha(r_2 - r_4)}{2(r_0^2\alpha + 1)} + \frac{(z_2 - z_4)\left[r_0\alpha(r_2 - r_4)\right]}{4\left(r_0^2 + \frac{1}{\alpha}\right)} \qquad (156)$$

and on DE:

$$z_0 = \frac{r_0^2}{2\left(r_0^2 + \frac{1}{\alpha^2}\right)}\left[2z_2 - \frac{1}{r_0}\sqrt{4a^2 - \frac{1}{\alpha^2}(z_1 - z_3)^2}\right] + \frac{1}{2(r_0^2\alpha^2 + 1)}(z_1 + z_3)$$

$$+ \frac{z_1 - z_3}{4r_0\left(r_0^2\alpha + \frac{1}{\alpha}\right)}\sqrt{4a^2 - \frac{1}{\alpha^2}(z_1 - z_3)^2} \qquad (157)$$

Both points G and E are special points in the formulation. The following equations hold there:

At point G:

$$z_0 = \frac{r_0^2}{r_0^2 + \frac{1}{\alpha^2}} \left[\frac{1}{r_0} \sqrt{a^2 - r_0^2(r_0 - r_4)^2} + z_4 \right] + \frac{z_1 - r_0\alpha(r_0 - r_4)}{r_0^2\alpha^2 + 1}$$

$$+ \frac{r_0 - r_4}{r_0^2 + \frac{1}{\alpha^2}} \sqrt{a^2 - r_0^2(r_0 - r_4)} \qquad (158)$$

At point E:

$$z_0 = \frac{r_0^2}{r_0^2 + \frac{1}{\alpha^2}} \left[z_2 - \frac{1}{r_0} \sqrt{a^2 - r_0^2(r_2 - r_0)^2} \right] + \frac{z_1 - r_0\alpha(r_2 - r_0)}{r_0^2\alpha^2 + 1}$$

$$+ \frac{r_2 - r_0}{r_0^2 + \frac{1}{\alpha^2}} \sqrt{a^2 - r_0^2(r_2 - r_0)^2} \qquad (159)$$

Detailed calculations for all the additional boundaries encountered for the finite-plate case are contained in appendix D.

FORMULATION INCLUDING SURFACE TENSION

The finite difference formulation corresponding to the surface tension model (fig. 14) is shown in figure 17. Details of these derivations are given in appendix D. The r solution can be obtained independently of the z solution (fig. 17(a)). This implies that once the r solution has been found, there is no iteration required after the z equation has been solved.

DISCUSSION OF NUMERICAL TECHNIQUES

Since the governing equations for the r and z formulations are nonlinear in the inverse plane, in general, the finite difference operations at the interior and boundary

points will be nonlinear (eqs. (150) and (151)). For the finite-flat-plate case, as shown in figure 16(a), the solution begins with $r = r(\psi, \varphi)$. With a knowledge of the r solution, the z formulation (fig. 16(b)) is solved for $z(\psi, \varphi)$. However, in the case where the plate is finite, the r formulation also contains z along the exiting plane GE (eq. (153)). As a result, the r and z formulations must be solved simultaneously. The surface tension model described in figure 17 also allows the r equation to be solved independently of the z equation since z appears nowhere in the r formulation.

In any case, when solving the r equation, the finite difference representation of the problem results in N nonlinear algebraic equations in N unknowns. A variety of methods were applied to obtain a solution to the simultaneous nonlinear equations. These included Lieberstein's extension of Young's work on overrelaxation to nonlinear elliptic partial differential equations (ref. 42) and the familiar Newton-Raphson method. None of the methods were successful in obtaining a convergent solution.

The technique suggested by Powell (ref. 43) led to the method used in this report to obtain solutions. Basically, Powell developed a subroutine that was essentially a "compromise between the Newton-Raphson algorithm and the method of steepest descents." Powell describes a FORTRAN subroutine for solving the nonlinear set of equations

$$f_K(X_1, X_2, \ldots, X_N) = 0 \qquad K = 1, 2, \ldots, N \tag{160}$$

The objective is to minimize the function

$$F(X_1, X_2, \ldots, X_N) = \sum_{K=1}^{N} \left[f_K(X_1, X_2, \ldots, X_N)\right]^2 \tag{161}$$

As with many iteration schemes, initial guesses are required for X_K. This particular algorithm has an advantage in that the initial guessed values do not have to be close to the exact solution. The computer program for the r solution contains the main program and three subroutines. The subroutine EQUATIONS is the one supplied by Powell. The user supplies the subroutine MATINV, which inverts the matrices, and the subroutine CALFUN, which contains the nonlinear functions $F(X_K)$. A knowledge of the r solution makes the z formulation explicit in the unknown z_0 at each nodal point. As a result, a Gauss-Siedel linear iteration scheme was employed to obtain the solution. For details of the subroutines, see reference 43.

NUMERICAL RESULTS

FORMULATION EXCLUDING SURFACE TENSION

Infinite Flat Plate

Initially, the infinite-flat-plate problem (Weber number = ∞) was numerically solved by using a very coarse mesh (fig. 16(a)). The total stream function ψ was divided into five equal parts. Recall that $\psi_G = 1/2$ and $\psi_E = 0$, which meant that the parameter $a = \Delta\psi$ was set equal to 0.1. In addition, the φ-axis was divided into eight equal parts. This division was purely arbitrary. One consideration was that there would be at least two vertical lines of constant φ between points C and B. This resulted in a total of 39 unknown nodal points for the r formulation in figure 16(a) and 41 unknown nodal points for the z formulation in figure 16(b). The value of $D = 1/\alpha^2$, where $\alpha = \Delta\varphi/\Delta\psi$, was set equal to 0.0204 ($\alpha = 7$). In figure 16(a), the value of C along GE was arbitrarily chosen as 4.0; in figure 16(b) the value of $K\varphi$ for z along AB was chosen as 3.315. The major reason for the assignment of these two values for r and z was to be able to compare the results with the semianalytical work for the infinite-flat-plate case of Schach (ref. 29). Actually, the major variable choice in the entire program is $D = 1/\alpha^2$. Basically, D is a measure of how large the flow system is since rectangular mesh is being used, that is, a measure of $\Delta\varphi$ and φ_{total}. The only concern is that φ_{total} is not too small. In that event, the extent of the solution in physical space would be such that φ_{total} and the AB boundary condition would be forced too close to the plate to result in a realistic solution in the total flow domain. If $\Delta\varphi$ is chosen too large, that is, α is chosen too large or D is chosen too small, all that is lost is accuracy due to larger mesh spacings. In other words, the AB boundary is now too far from the plane. For the coarse-mesh, infinite-flat-plate problem, the results of the numerical solution are given in appendix E. For the computer listings and final output, see reference 44. The solution to the formulation (fig. 16(a)) required 1098 calls of the subroutine used to solve the simultaneous nonlinear equation. The sum of the squares of the error to the solution was reduced to 0.00357 at the last iteration.

The method applied to obtain the z solution was a simple linear iteration technique since equations explicit in z_0 can be derived both in the interior and along the boundary points. There were 249 iterations required for the z solution. Changes between the 248th and 249th iteration occurred in the fifth decimal point. In general, iterations throughout the numerical computations were continued until no significant changes in the solutions resulted.

A physical-plane description of the infinite-flat-plate solution is presented in figure 18. Only two of the four internal streamlines are shown in the figure. Curves were faired through the available calculated nodal points (r, z) by a best-fit process. There

appeared, at the onset, the question of whether the coarse mesh employed could sufficiently describe the flow. When applying boundary conditions at the free surface, a larger number of nodal points are desirable. As a result, the existing mesh was doubled. The total ψ was divided into 10 equal parts such that $a = \Delta\psi = 0.05$, and the total φ was divided into 16 equal parts. The final values for the coarse-mesh solution (r, z) were used to make initial guesses of the values for the fine-mesh solution. The r solution required the simultaneous solution of 159 nonlinear algebraic equations. The z equation, again being explicit in z_0, resulted in 164 unknown values of z. The results from the computer program (results shown in appendix E) are presented in figure 19 as computer plot. The computer connected the nodal points with straight line segments. In general, there is very little difference between the fine-mesh and coarse-mesh solutions. The fine-mesh solution required the extended-storage-space option on the 1106 Univac computer. The sum of the squares for the final r solution was reduced to 0.024 after approximately 1000 calls of the subroutine CALFUN used to solve the simultaneous nonlinear equations. For this case, 1000 passes through the flow field were required to obtain a satisfactory z solution.

Finite Plate (Inviscid, Excluding Surface Tension)

As mentioned in the section DISCUSSION OF NUMERICAL TECHNIQUES, the finite-plate formulation also contains z on the exiting jet surface (eq. (154)). Initially, values for z along GE were assumed. These values were used to compute an r solution. The computed r solution used 161 calls of the subroutine CALFUN to reduce the sum of the squares of the residuals at the nodal points to 0.00066. With this r solution, the linear iteration technique was used to calculate the complete z solution. Since the computed z solution resulted in refined approximations to the values of z along GE, changes could then be reflected in a new r computation.

For the finite-disk case in which the ratio of the radius of the liquid jet to the radius of the disk was 1/2, a second r calculation did not change when the z values were updated. A curve was faired through the calculated nodal points (fig. 20). Only two of the four available streamlines are shown in the figure. No attempt was made to refine the solution by completely doubling the number of vertical and horizontal grid lines. For this particular case, since no comparison with any existing analytical techniques existed, a more convenient value of 3.3 was chosen for $K\varphi$. The value of D employed in the solution was 0.0138. The only specification along GE was that z at point G be set equal to 0.25. The calculated r and z values at each nodal point are given in appendix E.

The same method was used to numerically compute the finite-plate case in which the ratio of the jet radius to the disk radius was 3/4. There were 38 nodal points re-

quired for the r solution and 45 for the z solution. A complete computer plot of the results is shown in figure 21. Two iterations were required for the z solution as well as for the r solution. The sum of the squares for the r solution at the final iteration was 0.001. The table is given in appendix E. Again, the value of $K\varphi$ was arbitrarily chosen as 3.3.

The z solution corresponding to the r solution was obtained and is also presented in appendix E.

SURFACE-TENSION-DOMINATED MODEL

As previously mentioned, the r formulation for the surface-tension-dominated flow can be solved independently of the z formulation (fig. 17). The initial case examined had a Weber number of 4, and the ratio of the radius of the jet to the radius of the disk was 1/2. Also, the first solution to this problem assumed only axisymmetry. The results of the numerical solution, when a coarse mesh was used, resulted in a symmetrical r solution - symmetrical about the equipotential line emanating from point D. This simplified the problem in that, not only can axisymmetry be assumed, but also mirror-image symmetry (i.e., symmetry about the $z = 0$ plane). This is significant for problems in which the surface tension effects are to be taken into account since the surface tension forces are highly dependent on the curvature of the free surface. By taking advantage of the symmetry involved, additional nodal points can be placed on the free surface without using extended computer storage.

Referring to figure 17(a), if a vertical line were to be drawn (equipotential line) from point D, where $r = RD$, the intersection of this equipotential line with the free surface AG would be defined as point M. Along DM, it is known that $z = 0$. The variation of r with ψ can be computed along this line. The equipotential line DM is depicted in figure 22. Since DM is an equipotential line, the velocity along this line must be equal to V, the incoming jet velocity, with the exception of the point $r = L$ in the physical plane. At point D, a velocity discontinuity will exist.

In the physical plane, on DM,

$$\left.\begin{aligned} u &= 0 \\ v &= -V \end{aligned}\right\} \quad \text{on } z = 0,\ L \le r \le R_{max} \tag{162}$$

where R_{max} is the maximum radius of the liquid flow pattern.

An expression for the stream function along DM can now be derived, since the radial velocity component along DM is 0:

$$-\frac{1}{r}\frac{\partial\psi}{\partial z} = 0 \tag{163}$$

This implies that $\psi = \psi(r)$ alone. To find what the function is, the definition of the axial velocity is used, namely,

$$v = \frac{1}{r}\frac{\partial\psi}{\partial r}$$

On DM,

$$-\gamma = \frac{1}{r}\frac{\partial\psi}{\partial r} \tag{164}$$

Integrating this gives

$$\psi = -\frac{\gamma r^2}{2} + \text{Constant} \tag{165}$$

By applying the boundary condition that $\psi = 0$ at $r = L$, we can calculate the constant in equation (165). The following expression results:

$$\psi = -\frac{\gamma r^2}{2} + \frac{\gamma L^2}{2} \tag{166}$$

If this equation is nondimensionalized,

$$\psi^* = \frac{r^{*2}}{2} - \frac{1}{2}\left(\frac{L}{R_0}\right)^2 \tag{167}$$

Dropping the starred notation, as was done in the past derivations, gives

$$\psi = \frac{r^2}{2} - \frac{1}{2}\left(\frac{L}{R_0}\right)^2 \tag{168}$$

Solving for r yields

$$r = + \sqrt{2\psi + (RD)^2} \tag{169}$$

where

$$\frac{L}{R_0} = RD \tag{170}$$

Equation (169) represents the boundary condition used along DM in the inverse plane for the r formulation. The condition z = 0 was used for the z formulation.

In the course of finding the solution to the z formulation (fig. 17(b)), it was necessary to solve a cubic equation for the parameter T along the free surface. Physical as well as mathematical interpretation was required when choosing the proper root of the cubic since a possibility of three real roots existed. In equation (D78), appendix D, the only mathematically meaningful roots were those in which the absolute value of the parameter T was greater than or equal to 1. However, the possibility still existed that all three roots would be real and in addition, satisfy the requirement that their absolute values be greater than 1. As a result, some physical insight was required when deciding which roots to use in the equation relating T to the fictitious point f (eq. (D84)). For example, it is known that, as the nozzle exit is approached along the free surface, z = f(r) becomes steeper (i.e., f'(r) approaches infinity). This would coincide with the curvature terms dropping out of the boundary condition in the physical-plane formulation. An alternative approach to viewing this is that the fictitious point f approaches the image point z_4. As a result, the value of the parameter T approaches 1. The algorithm selected for choosing the proper root of the cubic was to select the value of T closest to 1 but to ensure that its absolute value was greater than or equal to 1. During the course of finding the solution, problems in implementing this algorithm occurred, particularly close to the nozzle, since the T values closest to 1 were slightly less than 1 and were automatically discarded by the algorithm. The resulting potential lines and streamlines appeared to be inaccurate when plotted. The only way found to circumvent this problem was to set up an additional algorithm that set T identically equal to 1 for several free-surface nodal points in the vicinity of the nozzle (i.e., those nodal points in which the computed r value was ≤ 1.009). Physically, this reasoning is justified since it is known that f'(r) must approach infinity there.

The results of the numerical solution are shown in figure 23. The Weber number for this solution was 4, and the ratio of the radius of the liquid jet to the radius of the disk was 1/2. A value of 3.5 was chosen for $K\varphi$, and D was set equal to 0.0204. In appendix E, the computed r and z values for the nodal points are given.

The sum of the squares for the r solution was 0.77×10^{-6}, and since the r solution was independent of the z solution, a second iteration was unnecessary.

DISCUSSION OF RESULTS

The numerical solutions were compared with the available semianalytical results of Schach (ref. 29) for the case of an infinite flat plate. The method employed by Schach is attributed to Trefftz. Schach's method did not appear to be readily extendable to more-complicated geometrical flows and could not account for the effects of surface tension. In making the comparison between reference 29 and the numerical results, the fine-mesh solution presented in figure 19 was used. The results of the comparison for an infinite flat plate are shown in figure 24. The data points in the figure were obtained from figure 11 of Schach's paper by using an expandable scale. As a result, there is some unknown error associated with the process of taking the results from the reference. In any case, the agreement looks particularly good, with the sole exception of the first r coordinate greater than 1.

One final point with respect to the infinite-flat-plate solution concerns the extreme left coordinate in figure 24, namely, $r = 4$, $z = 0.125$. These two values are fixed by continuity, both in this numerical program and in the semianalytical results of Schach. This result was obtained as follows: assuming constant density, the volumetric flow rate into the control volume at AB must balance the flow out of the control volume at GE. In physical coordinates, the flow in is given by $\pi R_0^2 V$ and the flow out by $2\pi R_{jet} z_g V$. Equating these and canceling lead to the fact that z_g must equal $R_0^2/2R_{jet}$. Nondimensionalizing with respect to R_0 yields

$$z_g^* = \frac{1}{2R_{jet}^*} \tag{171}$$

Dropping the starred notation and observing that $R_{jet} = 4$ at the left boundary of the control volume show that z_0 must equal 1/8.

As far as the finite plate is concerned, there were no available comparisons with past experimental or analytical work. As a result, comparisons were made with respect to the zero-gravity experimental data obtained in this work. The results are shown in dimensionless coordinates in figures 25 and 26. Figure 25 is for the case where the ratio of the jet radius to the disk radius is 1/2, and figure 26 for a ratio of 3/4. The comparisons were made with respect to the outer (or top) free surface since it was impossible to view the lower free surface because of the way in which the flow occurred. The results were generally good for both ratios compared. Experimental data points were obtained from both sides of the axisymmetric sheet as it flowed around the disk. The average values to the left and right of the jet centerline were used to plot the solid lines in figures 25 and 26. The analysis corroborated the experiments in the sense that,

as the ratio R_0/L becomes smaller, the jet appears to leave the disk in a more nearly tangent manner (fig. 27).

SUMMARY OF RESULTS

An experimental and analytical investigation was conducted to determine the free-surface shapes of circular liquid jets impinging normal to sharp-edge disks in zero gravity. The test liquids were anhydrous ethanol and trichlorotrifluoroethane (Freon TF). Nozzle radii were varied from 0.25 to 0.75 centimeter, and disk radii of 1.0 and 1.5 centimeters were used. The jet velocity was varied between 12 and 365 centimeters per second. Under the stipulation that the nozzle be located at least 5 centimeters from the disk, the investigation yielded the following results:

1. It was analytically determined that flow regions exist where viscous forces are not significant in the computation of free-surface shapes. It was shown that the Reynolds number $\rho V R_0/\mu$ and the ratio of jet to disk radii R_0/L uniquely define the flow regions. It was further shown that the Reynolds number specifying the transition between viscous and nonviscous flow decreased with an increasing ratio of jet radius to disk radius.

2. Within the inviscid region, three distinct flow regimes were experimentally found that depend uniquely on the Weber number $\rho V^2 R_0/\sigma$ and the ratio of jet to disk radii R_0/L. These flows were defined as surface tension flow, transition flow, and inertial flow. The critical Weber number between regimes also decreased with an increasing ratio of jet to disk radii.

3. A numerical solution yielding free-surface shapes and streamlines was obtained for the case of impingement normal to an infinite flat plate and compared favorably with semianalytical techniques in the literature.

4. A numerical solution yielding free-surface shapes and streamlines was obtained for inertially dominated flows at ratios of jet to disk radii of 1/2 and 3/4. The comparison with experiments showed good agreement for the upper free surface.

5. A surface-tension-dominated flow was formulated and solved numerically. The system Weber number was 4, and the ratio of jet to disk radii was 1/2.

Lewis Research Center,
National Aeronautics and Space Administration,
Cleveland, Ohio, May 6, 1977,
506-21.

APPENDIX A

DETAILED CALCULATIONS OF FREE-SURFACE BOUNDARY CONDITIONS

Two boundary conditions are required to solve for a free surface in a fluid dynamics problem. In comparison, for known boundaries, only one boundary condition is required. The two conditions to be satisfied are

(1) Conservation of energy along a streamline

(2) Zero velocity normal to the streamline

Consider the following geometry:

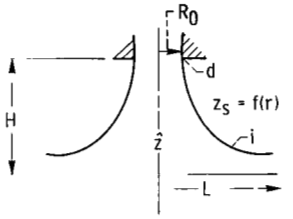

where i represents any point on the free surface $z_s = f(r)$ and d designates the reference point, which is chosen as the point where the liquid jet exits from the nozzle.

CONSERVATION OF ENERGY ALONG A STREAMLINE

Bernoulli's equation written between points i and d becomes for inviscid incompressible, steady flow.

$$\frac{1}{2}(u^2 + v^2) + \frac{p_i}{\rho} = \frac{1}{2}\mathcal{V}^2 + \frac{p_d}{\rho} \qquad \text{on } z_s = f(r) \tag{A1}$$

The pressure at point i, p_i, is not the same as the pressure at point d, p_d, because of the effects of surface tension. In general,

$$p_g - p = \sigma J \tag{A2}$$

where p_g is the known gas pressure and

$$J = \frac{1}{R_1} + \frac{1}{R_2} \tag{A3}$$

where R_1 and R_2 are radii of curvature and

$$\frac{1}{R_1} = \frac{f''}{\left(1 + f'^2\right)^{3/2}} \tag{A4}$$

$$\frac{1}{R_2} = \frac{f'}{r\left(1 + f'^2\right)^{1/2}} \tag{A5}$$

Combining equations (A4) and (A5) with (A2) gives

$$p_g - p = \sigma \left[\frac{f''}{\left(1 + f'^2\right)^{3/2}} + \frac{f'}{r\left(1 + f'^2\right)^{1/2}} \right] \tag{A6}$$

which can be combined to yield

$$p_g - p = \frac{\sigma}{r} \frac{d}{dr} \left(\frac{rf'}{\sqrt{1 + f'^2}} \right) \tag{A7}$$

If at point d we apply $z = H$, $r = R_0$, and $df/dr = f' = \infty$, then for large f', $\sqrt{1 + f'^2} \doteq \sqrt{f'^2} = f'$. Therefore, substitution into equation (A7) yields

$$p_g - p_d = \frac{\sigma}{R_0} \tag{A8}$$

Similarly, at point i,

$$p_g - p_i = \frac{\sigma}{r} \frac{d}{dr} \left(\frac{rf'}{\sqrt{1 + f'^2}} \right) \tag{A9}$$

Now equations (A8) and (A9) can be substituted into equation (A1) to obtain

$$\frac{1}{2}(u^2 + v^2) - \frac{\sigma}{\rho r}\frac{d}{dr}\left(\frac{rf'}{\sqrt{1 + f'^2}}\right) = \frac{1}{2}\gamma^2 - \frac{\sigma}{\rho R_0} \qquad \text{on } z_s = f(r) \tag{A10}$$

ZERO VELOCITY NORMAL TO FREE SURFACE

A portion of the free surface $z_s = f(r)$ is shown in sketch (b)

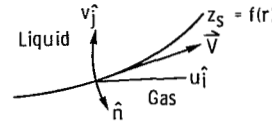

(b)

where $\hat{n}$ is the unit outward normal to the surface at some point and u and v are the velocity components such that $\vec{V} = u\hat{i} + v\hat{j}$. Since the velocity normal to the surface is zero,

$$\vec{V} \cdot \hat{n} = 0 \tag{A11}$$

With the surface given by $z_s = f(r)$, the unit normal is given as

$$\hat{n} = -\frac{f'\hat{i} - \hat{j}}{\sqrt{1 + f'^2}} \tag{A12}$$

Taking the gradient at the surface and dividing that result by the absolute value of the gradient (i.e., $\hat{n} = \nabla\varphi / |\nabla\varphi|$, where $\hat{i}$ is a unit vector in the radial direction and $\hat{j}$ is a unit vector in the axial direction, yield

$$\vec{V} \cdot \hat{n} = -\frac{uf'}{\sqrt{1 + f'^2}} + \frac{v}{\sqrt{1 + f'^2}} = 0 \tag{A13}$$

which simplifies to

$$-uf' + v = 0 \qquad \text{on } z_s = f(r) \tag{A14}$$

APPENDIX B

ZERO-GRAVITY DROP TOWER TEST FACILITY

The experimental data for this study were obtained in the Lewis Research Center's 2.2-second zero-gravity facility. A schematic diagram of this facility is shown in figure 28. The facility consists of a building 6.4 meters square by 30.5 meters tall. Contained within the building is a drop area 27 meters high with a cross section 1.5 meters by 2.75 meters.

The service building has a shop and service area, a calibration room, and a controlled-environment room. Those components of the experiment that required special handling were prepared in the controlled-environment room. This air-conditioned and filtered room contains an ultrasonic cleaning system and the laboratory equipment necessary for handling test liquids.

MODE OF OPERATION

A 2.2-second period of weightlessness is obtained by allowing the experiment package to free fall from the top of the drop area. To minimize drag on the experiment package, it is enclosed in a drag shield designed with a high ratio of weight to frontal area and a low drag coefficient. The relative motion of the experiment package with respect to the drag shield during a test is shown in figure 29. Throughout the test, the experiment package and drag shield fall freely and independently of each other; that is, no guide wires or electrical lines, etc., are connected to either. Therefore, the only force acting on the freely falling experiment package is the air drag associated with the relative motion of the package within the enclosure of the drag shield. This air drag results in an equivalent gravitational acceleration acting on the experiment, which is estimated to be below 10^{-5} g's.

RELEASE SYSTEM

The experiment package, installed within the drag shield, is suspended at the top of the drop area by means of a highly stressed music wire attached to the release system. This release system consists of a double-acting air cylinder with a hard-steel knife edge attached to the piston. Pressurization of the air cylinder drives the knife edge against the wire, which is backed by an anvil. The resulting notch causes the wire to fail, smoothly releasing the experiment. No measurable disturbances are imparted to the package by this release procedure.

RECOVERY SYSTEM

After the experiment package and drag shield have traversed the total length of the drop area, they are recovered by a deceleration in a 2.2-meter-deep container filled with sand. The deceleration rate (averaging 15 g's) is controlled by selectively varying the tips of the deceleration spikes mounted on the bottom of the drag shield (fig. 28). At the time of impact of the drag shield in the deceleration container, the experiment package has traversed the vertical distance within the drag shield (compare figs. 29(a) and (c)).

APPENDIX C

DERIVATION OF INVERSE-PLANE EQUATIONS

FORMULATION

Assume that there exist functions $\psi = \psi(r, z)$ and $\varphi = \varphi(r, z)$. Then, there are inverse functions $r = r(\psi, \varphi)$ and $z = z(\varphi, \psi)$ such that

$$\frac{\partial r}{\partial \varphi} = -\frac{1}{J}\frac{\partial \psi}{\partial z} \tag{C1}$$

$$\frac{\partial z}{\partial \psi} = -\frac{1}{J}\frac{\partial \varphi}{\partial r} \tag{C2}$$

$$\frac{\partial z}{\partial \varphi} = \frac{1}{J}\frac{\partial \psi}{\partial r} \tag{C3}$$

$$\frac{\partial r}{\partial \psi} = \frac{1}{J}\frac{\partial \varphi}{\partial z} \tag{C4}$$

and where the Jacobian J is defined as

$$J = \begin{vmatrix} \frac{\partial \varphi}{\partial r} & \frac{\partial \varphi}{\partial z} \\ \frac{\partial \psi}{\partial r} & \frac{\partial \psi}{\partial z} \end{vmatrix} = \left(\frac{\partial \varphi}{\partial r}\right)\left(\frac{\partial \psi}{\partial z}\right) - \left(\frac{\partial \varphi}{\partial z}\right)\left(\frac{\partial \psi}{\partial r}\right) \tag{C5}$$

From these equations follow two important relations. Substituting the values of $\partial\varphi/\partial r$ and $\partial\psi/\partial z$ from equations (C1) and (C2) into equation (112) yields

$$\frac{\partial z}{\partial \psi} = -\frac{1}{r}\frac{\partial r}{\partial \varphi} \tag{C6}$$

Similarly, substituting the values for $\partial\varphi/\partial z$ and $\partial\psi/\partial r$ from equations (C3) and (C4) into equation (113) yields

$$\frac{\partial r}{\partial \psi} = \frac{1}{r}\frac{\partial z}{\partial \varphi} \tag{C7}$$

For subsequent relations, it is necessary to express the Jacobian in terms of the inverse functions $r(\psi, \varphi)$ and $z(\psi, \varphi)$. Substituting equations (C1) to (C4) into equation (C5) results in

$$J = J^2 \left[\left(\frac{\partial z}{\partial \psi} \right) \left(\frac{\partial r}{\partial \varphi} \right) - \left(\frac{\partial r}{\partial \psi} \right) \left(\frac{\partial z}{\partial \varphi} \right) \right] \tag{C8}$$

Now, using equations (C6) and (C7) in equation (C8) yields

$$J = - \frac{1}{r \left[\left(\frac{\partial z}{\partial \psi} \right)^2 + \left(\frac{\partial r}{\partial \psi} \right)^2 \right]} = - \frac{r}{\left(\frac{\partial r}{\partial \varphi} \right)^2 + \left(\frac{\partial z}{\partial \varphi} \right)^2} \tag{C9}$$

GOVERNING EQUATIONS FOR INVERSE FUNCTIONS

Differentiating equation (C6) with respect to ψ yields

$$\frac{\partial^2 z}{\partial \psi^2} = - \frac{1}{r} \frac{\partial^2 r}{\partial \psi \, \partial \varphi} + \frac{1}{r^2} \frac{\partial r}{\partial \psi} \frac{\partial r}{\partial \varphi} \tag{C10}$$

and combining this with the derivative of equation (C7) with respect to φ, which is

$$\frac{\partial^2 r}{\partial \varphi \, \partial \psi} = - \frac{1}{r^2} \left(\frac{\partial r}{\partial \varphi} \right) \left(\frac{\partial z}{\partial \varphi} \right) + \frac{1}{r} \frac{\partial^2 z}{\partial \varphi^2} \tag{C11}$$

gives

$$\frac{\partial^2 z}{\partial \psi^2} = \frac{1}{r^3} \frac{\partial r}{\partial \varphi} \frac{\partial z}{\partial \varphi} - \frac{1}{r^2} \frac{\partial^2 z}{\partial \varphi^2} + \frac{1}{r^2} \frac{\partial r}{\partial \varphi} \frac{\partial r}{\partial \psi} \tag{C12}$$

By using equations (C6) and (C7), the following important equation is obtained:

$$r^2 \frac{\partial^2 z}{\partial \psi^2} + \frac{\partial^2 z}{\partial \varphi^2} = -2 \frac{\partial z}{\partial \psi} \frac{\partial z}{\partial \varphi} \tag{C13}$$

On the other hand, differentiating equation (C6) with respect to φ and equation (C7) with respect to ψ and combining the result lead to the equation

$$\frac{\partial^2 r}{\partial \psi^2} = -\frac{1}{r^2}\frac{\partial^2 r}{\partial \varphi^2} + \frac{1}{r^3}\left(\frac{\partial r}{\partial \varphi}\right)^2 - \frac{1}{r^2}\frac{\partial r}{\partial \psi}\frac{\partial z}{\partial \varphi} \tag{C14}$$

By substituting for $\partial z/\partial \varphi$ from equation (C7), the following equation for $r(\varphi, \psi)$ is obtained:

$$\frac{\partial^2 r}{\partial \psi^2} + \frac{1}{r^2}\frac{\partial^2 r}{\partial \varphi^2} - \frac{1}{r^3}\left(\frac{\partial r}{\partial \varphi}\right)^2 + \frac{1}{r}\left(\frac{\partial r}{\partial \psi}\right)^2 = 0 \tag{C15}$$

APPENDIX D

DETAILED DERIVATIONS OF FINITE DIFFERENCE OPERATORS ALONG BOUNDARIES

INFINITE FLAT PLATE

The finite difference representations for the derivatives are those shown in the text (eqs. (142) to (149)). Refer to figure 13.

$$\frac{\partial r}{\partial \psi} = 0 \quad \text{on Line } \underline{EC}$$

The line $\underline{EC}$ is shown in sketch c. Applying the r difference equation (eq. (150))

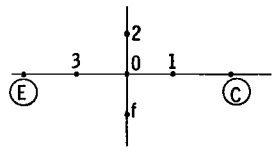

(c)

at point 0, where f is a fictitious point outside the boundary, gives

$$r_0^4 - \frac{r_0^3}{2}(r_2 + r_f) + r_0^2\left[\frac{1}{\alpha^2} - \frac{1}{8}(r_2 - r_f)^2\right] - \frac{r_0}{2\alpha^2}(r_1 + r_3) + \frac{1}{8\alpha^2}(r_1 - r_3)^2 = 0 \qquad \text{(D1)}$$

Along $\underline{EC}$, $\partial r/\partial \psi = 0$. This implies that

$$\frac{r_2 - r_f}{2\,\Delta\psi} = 0 \qquad \text{(D2)}$$

Therefore,

$$r_2 \equiv r_f \qquad \text{(D3)}$$

Equation (D1) then becomes

$$r_0^4 - r_0^3 r_2 + r_0^2\left(\frac{1}{\alpha^2}\right) - \frac{r_0}{2\alpha^2}(r_1 + r_3) + \frac{1}{8\alpha^2}(r_1 - r_3)^2 = 0 \qquad \text{(D4)}$$

$$\frac{\partial r}{\partial \psi} = 0 \quad \text{on Line } \underline{GE}$$

Applying $\partial r/\partial \psi$ on $\underline{GE}$ (sketch d) yields $r_2 = r_4$ and does not involve the unknown

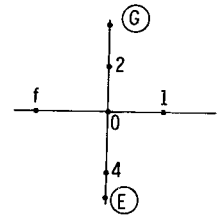

(d)

fictitious point f. However, $\partial r/\partial \psi = 0$ implies that $r \neq r(\psi)$. Therefore, r must only be a function of φ, $r = r(\varphi)$. But, along $\underline{GE}$, φ is constant ($\varphi = 0$). Hence, r is constant along $\underline{GE}$.

$$\left(\frac{\partial r}{\partial \varphi}\right)^2 + r^2\left(\frac{\partial r}{\partial \psi}\right)^2 = 1 \quad \text{on Line } \underline{AG}$$

For line $\underline{AG}$ (sketch e), the r difference equation can be written

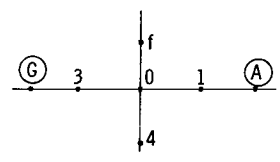

(e)

$$r_0^4 - \frac{r_0^3}{2}(r_f + r_4) + r_0^2\left[\frac{1}{\alpha^2} - \frac{1}{8}(r_f - r_4)^2\right] - \frac{r_0}{2\alpha^2}(r_1 + r_3) + \frac{1}{8\alpha^2}(r_1 - r_3)^2 = 0 \qquad \text{(D5)}$$

Along AG,

$$\left(\frac{\partial r}{\partial \varphi}\right)^2 + r^2\left(\frac{\partial r}{\partial \psi}\right)^2 = 1$$

This implies that

$$\left(\frac{r_1 - r_3}{2\,\Delta\varphi}\right)^2 + r_0^2\left(\frac{r_f - r_4}{2\,\Delta\psi}\right)^2 = 1 \qquad \text{(D6)}$$

Rearranging and letting $\Delta\psi = a$ (recalling that $\alpha = \Delta\varphi/\Delta\psi$) gives

$$(r_f - r_4)^2 = \frac{1}{r_0^2}\left[4a^2 - \frac{1}{\alpha^2}(r_1 - r_3)^2\right] \qquad \text{(D7)}$$

Upon which we can obtain

$$r_f - r_4 = \frac{1}{r_0}\sqrt{4a^2 - \frac{1}{\alpha^2}(r_1 - r_3)^2} \qquad \text{(D8)}$$

or, rewriting,

$$r_f + r_4 = \frac{1}{r_0}\sqrt{4a^2 - \frac{1}{\alpha^2}(r_1 - r_3)^2} + 2r_4 \qquad \text{(D9)}$$

Inserting equations (D8) and (D9) into (D5) yields the desired relation

$$r_0^4 - r_0^3 r_4 + r_0^2\left[\frac{1}{\alpha^2} - \frac{1}{2}\sqrt{4a^2 - \frac{1}{\alpha^2}(r_1 - r_3)^2}\right] - \frac{r_0}{2\alpha^2}(r_1 + r_3)$$

$$+ \frac{1}{8}\left[\frac{2}{\alpha^2}(r_1 - r_3)^2 - 4a^2\right] = 0 \qquad \text{(D10)}$$

Constant z on Line AB

For z to be constant on AB, let $z = K\varphi$ and $\partial z/\partial \varphi = 0$ on BC (sketch f). Apply-

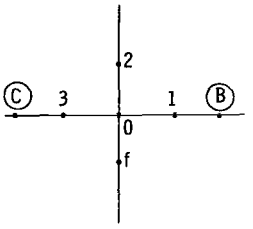

(f)

ing the z difference equation (eq. (151)) at point 0, where f is a fictitious point outside the boundary, gives

$$z_0 = \frac{r_0^2}{2\left(r_0^2 + \frac{1}{\alpha^2}\right)}(z_2 + z_f) + \frac{1}{2(r_0^2\alpha^2 + 1)}(z_1 + z_3) + \frac{1}{4\left(r_0^2\alpha + \frac{1}{\alpha}\right)}(z_2 - z_f)(z_1 - z_3) \tag{D11}$$

Along BC, $\partial z/\partial \psi = 0$. This implies that $z_2 - z_f = 0$ or

$$z_f = z_2 \tag{D12}$$

Therefore, equation (D11) becomes

$$z_0 = \frac{r_0^2 z_2}{r_0^2 + \frac{1}{\alpha^2}} + \frac{1}{2(r_0^2\alpha^2 + 1)}(z_1 + z_3) \tag{D13}$$

$$\frac{\partial z}{\partial \varphi} = 0 \text{ on Line GE}$$

For the line GE (sketch g), the z difference equation can be written

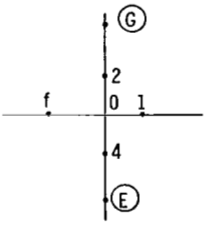

(g)

$$z_0 = \frac{r_0^2}{2\left(r_0^2 + \frac{1}{\alpha^2}\right)}(z_2 + z_4) + \frac{1}{2(r_0^2\alpha^2 + 1)}(z_1 + z_f) + \frac{1}{4\left(r_0^2\alpha + \frac{1}{\alpha}\right)}(z_2 - z_4)(z_1 - z_f) \tag{D14}$$

Along GE, $\partial z/\partial \varphi = 0$. This implies that $z_1 - z_f = 0$ or

$$z_f \equiv z_1 \tag{D15}$$

Therefore, equation (D14) becomes

$$z_0 = \frac{r_0^2}{2\left(r_0^2 + \frac{1}{\alpha^2}\right)}(z_2 + z_4) + \frac{z_1}{r_0^2\alpha^2 + 1} \tag{D16}$$

$$r^2\left(\frac{\partial z}{\partial \psi}\right)^2 + \left(\frac{\partial z}{\partial \varphi}\right)^2 = 1 \quad \text{on Line AG}$$

For the line AG (sketch h), the z difference equation can be written

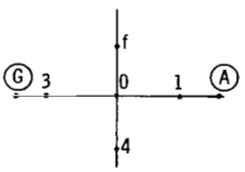

(h)

$$z_0 = \frac{r_0^2}{2\left(r_0^2 + \frac{1}{\alpha^2}\right)}(z_f + z_4) + \frac{1}{2(r_0^2\alpha^2 + 1)}(z_1 + z_3) + \frac{1}{4\left(r_0^2\alpha + \frac{1}{\alpha}\right)}(z_f - z_4)(z_1 - z_3) \tag{D17}$$

Along AG,

$$r^2\left(\frac{\partial z}{\partial \psi}\right)^2 + \left(\frac{\partial z}{\partial \varphi}\right)^2 = 1$$

Hence,

$$r_0^2\left(\frac{z_f - z_4}{2\,\Delta\psi}\right)^2 + \left(\frac{z_1 - z_3}{2\,\Delta\varphi}\right)^2 = 1 \tag{D18}$$

which can be expressed as

$$(z_f - z_4)^2 = \frac{1}{r_0^2}\left[4a^2 - \frac{1}{\alpha^2}(z_1 - z_3)^2\right] \tag{D19}$$

This yields

$$z_f - z_4 = \frac{1}{r_0}\sqrt{\left[4a^2 - \frac{1}{\alpha^2}(z_1 - z_3)^2\right]} \tag{D20}$$

$$z_f + z_4 = \frac{1}{r_0}\sqrt{\left[4a^2 - \frac{1}{\alpha^2}(z_1 - z_3)^2\right]} + z_4 \tag{D21}$$

Inserting these last two equations in (D17) eliminates the fictitious point z_f and yields

$$z_0 = \frac{r_0^2}{2\left(r_0^2 + \frac{1}{\alpha^2}\right)}\left[\frac{1}{r_0}\sqrt{4a^2 - \frac{1}{\alpha^2}(z_1 - z_3)^2} + 2z_4\right] + \frac{1}{2(r_0^2\alpha^2 + 1)}(z_1 + z_3)$$

$$+ \frac{z_1 - z_3}{4r_0\left(r_0^2\alpha + \frac{1}{\alpha}\right)}\sqrt{4a^2 - \frac{1}{\alpha^2}(z_1 - z_3)^2} \tag{D22}$$

A special boundary condition is required for point G since it is a part of two separate boundaries (sketch i). Applying the z difference equation yields

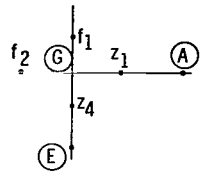

(i)

$$z_0 = \frac{r_0^2}{2\left(r_0^2 + \frac{1}{\alpha^2}\right)}(f_1 + z_4) + \frac{1}{2(r_0^2\alpha^2 + 1)}(z_1 + f_2) + \frac{1}{4\left(r_0^2\alpha + \frac{1}{\alpha}\right)}(f_1 - z_4)(z_1 - f_2) \tag{D23}$$

Applying the boundary condition along GE, namely, $\partial z/\partial \varphi = 0$, gives $f_2 = z_1$. Therefore,

$$z_0 = \frac{r_0^2}{2\left(r_0^2 + \frac{1}{\alpha^2}\right)}(f_1 + z_4) + \frac{z_1}{r_0^2\alpha^2 + 1} \tag{D24}$$

The boundary condition along AG (eq. (D20)) gives

$$f_1 = z_4 + \frac{1}{r_0}\sqrt{\left[4a^2 - \frac{1}{\alpha^2}(z_1 - f_2)^2\right]} \tag{D25}$$

but $f_z = z_1$. Hence,

$$f_1 = z_4 + \frac{2a}{r_0} \tag{D26}$$

Equation (D23) becomes

$$z_0 = \frac{r_0^2\left(z_4 + \frac{a}{r_0}\right)}{r_0^2 + \frac{1}{\alpha^2}} + \frac{z_1}{r_0^2\alpha^2 + 1} \tag{D27}$$

such that $z_0 = z_0(z_1, z_4)$ at point G.

FINITE PLATE (EXCLUDING SURFACE TENSION)

The differences in the boundary conditions between the infinite and finite plates involve GE and the addition of the free surface ED. In addition, G becomes a special point in the r formulation, and both G and E become special points in the z formulation.

$$\left(\frac{\partial r}{\partial \varphi}\right) + r\left(\frac{\partial r}{\partial \psi}\right)\left(\frac{dz}{dr}\right) = 0 \quad \text{on Line GE}$$

Along the line GE (sketch j), the r difference equation is

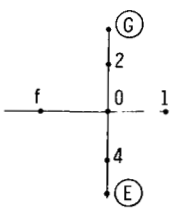

(j)

$$r_0^4 - \frac{r_0^3}{2}(r_2 + r_4) + r_0^2\left[\frac{1}{\alpha^2} - \frac{1}{8}(r_2 - r_4)^2\right] - \frac{r_0}{2\alpha^2}(r_1 + f) + \frac{1}{8\alpha^2}(r_1 - f)^2 = 0 \tag{D28}$$

In finite difference form, the boundary condition, with

$$\frac{dz}{dr} = \frac{z_2 - z_4}{r_2 - r_4}$$

is

$$\frac{r_1 - f}{\Delta\varphi} + \frac{r_0}{\Delta\psi}(z_2 - z_4) = 0 \tag{D29}$$

In equation (D29), central finite difference was not used. Solving for f gives

$$f = r_1 + \alpha r_0(z_2 - z_4)$$

and inserting this into the r difference equation yields the desired result:

$$r_0^4 - \frac{r_0^3}{2}(r_2 + r_4) + r_0^2\left[\frac{1}{\alpha^2} - \frac{1}{8}(r_2 - r_4)^2\right] - \frac{r_0}{2\alpha^2}\left[2r_1 + \alpha r_0(z_2 - z_4)\right] + \frac{r_0^2}{8}(z_2 - z_4)^2 = 0 \tag{D31}$$

$$\left(\frac{\partial r}{\partial\varphi}\right)^2 + r^2\left(\frac{\partial r}{\partial\psi}\right)^2 = 1 \quad \text{on the Free Surface } \underline{ED}$$

On the free surface ED (sketch k), the r difference equation can be written

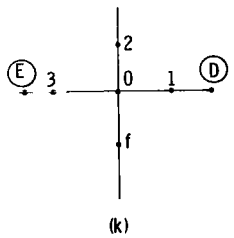

(k)

$$r_0^4 - \frac{r_0^3}{2}(r_2 + r_f) + r_0^2\left[\frac{1}{\alpha^2} - \frac{1}{8}(r_2 - r_f)^2\right] - \frac{r_0}{2\alpha^2}(r_1 + r_3) + \frac{1}{8\alpha^2}(r_1 - r_3)^2 = 0 \tag{D32}$$

Using

$$\left(\frac{\partial r}{\partial \varphi}\right)^2 + r^2\left(\frac{\partial r}{\partial \psi}\right)^2 = 1$$

on ED gives

$$\left(\frac{r_1 - r_3}{2\,\Delta\varphi}\right)^2 + r_0^2\left(\frac{r_2 - r_f}{2\,\Delta\psi}\right)^2 = 1 \qquad \text{(D33)}$$

which yields (with $a = \Delta\psi$)

$$(r_2 - r_f)^2 = \frac{1}{r_0^2}\left[4a^2 - \frac{1}{\alpha^2}(r_1 - r_3)^2\right] \qquad \text{(D34)}$$

and

$$r_2 + r_f = 2r_2 - \frac{1}{r_0}\sqrt{4a^2 - \frac{1}{\alpha^2}(r_1 - r_3)^2} \qquad \text{(D35)}$$

Substituting equations (C34) and (C35) into (C32) gives

$$r_0^4 - r_0^3 r_2 + r_0^2\left[\frac{1}{\alpha^2} + \frac{1}{2}\sqrt{4a^2 - \frac{1}{\alpha^2}(r_1 - r_3)^2}\right] - \frac{r_0}{2\alpha^2}(r_1 + r_3) + \frac{1}{8}\left[-4a^2 + \frac{2}{\alpha^2}(r_1 - r_3)^2\right] = 0 \qquad \text{(D36)}$$

Now, points E and G will be special points since equation (D31) cannot be directly applied there. One of these positions can be specified as known, r_E = Constant. Let us examine the special point G (sketch l). Applying equation (D10) at point G yields

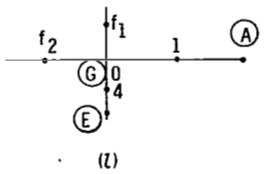

(l)

$$r_0^4 - r_0^3 r_4 + r_0^2\left[\frac{1}{\alpha^2} - \frac{1}{2}\sqrt{4a^2 - \frac{1}{\alpha^2}(r_1 - f_2)^2}\right] - \frac{r_0}{2\alpha^2}(r_1 + f_2)$$

$$+ \frac{1}{8}\left[\frac{2}{\alpha^2}(r_1 - f_2)^2 - 4a^2\right] = 0 \qquad \text{(D37)}$$

Now, applying

$$\left(\frac{\partial r}{\partial \varphi}\right) + r\left(\frac{\partial r}{\partial \psi}\right)\left(\frac{dz}{dr}\right) = 0$$

along $\underline{GE}$ without involving f_1 gives

$$\left(\frac{r_1 - f_2}{2\,\Delta\varphi}\right) + r_0\left(\frac{r_0 - r_4}{\Delta\psi}\right)\left(\frac{z_0 - z_4}{r_0 - r_4}\right) = 0 \qquad \text{(D38)}$$

Note again that central finite difference was not used to derive this expression. Solving for f_2 gives

$$f_2 = r_1 + 2\alpha r_0(z_0 - z_4) \qquad \text{(D39)}$$

Therefore, equation (D37) becomes

$$r_0^4 - r_0^3 r_4 + r_0^2\left[\frac{1}{\alpha^2} - \sqrt{a^2 - r_0^2(z_0 - z_4)^2}\right] - \frac{r_0}{\alpha^2}\left[r_1 + \alpha r_0(z_0 - z_4)\right]$$

$$+ \left[r_0^2(z_0 - z_4)^2 - \frac{a^2}{2}\right] = 0 \qquad \text{(D40)}$$

$$r\left(\frac{\partial z}{\partial \psi}\right) - \left(\frac{\partial z}{\partial \varphi}\right)\left(\frac{dz}{dr}\right) = 0 \quad \text{on Line } \underline{GE}$$

Along the line $\underline{GE}$ (sketch m), applying the z difference equation yields

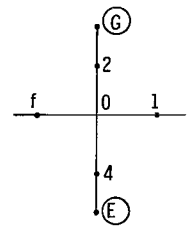

(m)

$$z_0 = \frac{r_0^2}{2\left(r_0^2 + \frac{1}{\alpha^2}\right)}(z_2 + z_4) + \frac{z_1 + f}{2(r_0^2\alpha^2 + 1)} + \frac{(z_2 - z_4)(z_1 - f)}{4\left(r_0^2\alpha + \frac{1}{\alpha}\right)} \tag{D41}$$

Now, along $\underline{GE}$,

$$r\left(\frac{\partial z}{\partial \psi}\right) - \left(\frac{\partial z}{\partial \varphi}\right)\left(\frac{dz}{dr}\right) = 0$$

which in difference form can be written

$$r_0\left(\frac{z_2 - z_4}{2\,\Delta\psi}\right) - \left(\frac{z_1 - f}{2\,\Delta\varphi}\right)\left(\frac{z_2 - z_4}{r_2 - r_4}\right) = 0 \tag{D42}$$

Solving for f gives

$$f = z_1 - r_0\alpha(r_2 - r_4) \tag{D43}$$

Hence, equation (D41) becomes

$$z_0 = \frac{r_0^2}{2\left(r_0^2 + \frac{1}{\alpha^2}\right)}(z_2 + z_4) + \frac{2z_1 - r_0\alpha(r_2 - r_4)}{2(r_0^2\alpha^2 + 1)} + \frac{(z_2 - z_4)\, r_0\alpha(r_2 - r_4)}{4\left(r_0^2\alpha + \frac{1}{\alpha}\right)} \qquad \text{(D44)}$$

$$r^2\left(\frac{\partial z}{\partial \psi}\right)^2 + \left(\frac{\partial z}{\partial \varphi}\right)^2 = 1 \quad \text{on Free Surface } \underline{\text{ED}}$$

On the free surface ED (sketch n), the z difference equation can be written

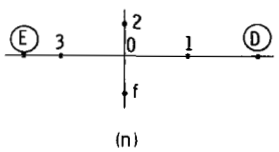

(n)

$$z_0 = \frac{r_0^2}{2\left(r_0^2 + \frac{1}{\alpha^2}\right)}(z_2 + z_f) + \frac{1}{2(r_0^2\alpha^2 + 1)}(z_1 + z_3) + \frac{1}{4\left(r_0^2\alpha + \frac{1}{\alpha}\right)}(z_2 - z_f)(z_1 - z_3) \qquad \text{(D45)}$$

Applying

$$r^2\left(\frac{\partial z}{\partial \psi}\right)^2 + \left(\frac{\partial z}{\partial \varphi}\right)^2 = 1$$

on ED gives

$$r_0^2\left(\frac{z_2 - z_f}{2\,\Delta\psi}\right)^2 + \left(\frac{z_1 - z_3}{2\,\Delta\varphi}\right)^2 = 1 \qquad \text{(D46)}$$

Solving for $z_2 - z_f$ yields

$$z_2 - z_f = \frac{1}{r_0}\sqrt{4a^2 - \frac{1}{\alpha^2}(z_1 - z_3)^2} \tag{D47}$$

Also,

$$z_f + z_2 = 2z_2 - \frac{1}{r_0}\sqrt{4a^2 - \frac{1}{\alpha^2}(z_1 - z_3)^2} \tag{D48}$$

Substituting equations (D47) and (D48) into (D45) yields the desired expression

$$z_0 = \frac{r_0^2}{2\left(r_0^2 + \frac{1}{\alpha^2}\right)}\left[2z_2 - \frac{1}{r_0}\sqrt{4a^2 - \frac{1}{\alpha^2}(z_1 - z_3)^2}\right] + \frac{z_1 + z_3}{2(r_0^2\alpha^2 + 1)}$$

$$+ \frac{z_1 - z_3}{4\left(r_0^2\alpha + \frac{1}{\alpha}\right)}\frac{1}{r_0}\sqrt{4a^2 - \frac{1}{\alpha^2}(z_1 - z_3)^2} \tag{D49}$$

Applying equation (D22) at point G (sketch o) yields

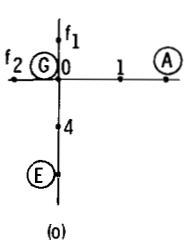

(o)

$$z_0 = \frac{r_0^2}{2\left(r_0^2 + \frac{1}{\alpha^2}\right)}\left[\frac{1}{r_0}\sqrt{4a^2 - \frac{1}{\alpha^2}(z_1 - f_2)^2} + 2z_4\right] + \frac{z_1 + f_2}{2(r_0^2\alpha^2 + 1)}$$

$$+ \frac{z_1 - f_2}{4r_0\left(r_0^2\alpha + \frac{1}{\alpha}\right)}\sqrt{4a^2 - \frac{1}{\alpha^2}(z_1 - f_2)^2} \qquad \text{(D50)}$$

To find f_2, we apply

$$r\left(\frac{\partial z}{\partial \psi}\right) - \left(\frac{\partial z}{\partial \varphi}\right)\left(\frac{dz}{dr}\right) = 0$$

Without involving f_1,

$$r_0\left(\frac{z_0 - z_4}{\Delta\psi}\right) - \left(\frac{z_1 - f_2}{2\,\Delta\varphi}\right)\left(\frac{z_0 - z_4}{r_0 - r_4}\right) = 0 \qquad \text{(D51)}$$

Solving for f_2,

$$f_2 = z_1 - 2r_0\alpha(r_0 - r_4) \qquad \text{(D52)}$$

Substitution into equation (D50) yields

$$z_0 = \frac{r_0^2}{r_0^2 + \frac{1}{\alpha^2}}\left[\frac{1}{r_0}\sqrt{a^2 - r_0^2(r_0 - r_4)^2} + z_4\right] + \frac{z_1 - r_0\alpha(r_0 - r_4)}{r_0^2\alpha^2 + 1}$$

$$+ \frac{r_0 - r_4}{r_0^2 + \frac{1}{\alpha^2}}\sqrt{a^2 - r_0^2(r_0 - r_4)^2} \qquad \text{(D53)}$$

Let us examine the special point at E (sketch p). Applying equation (D49) at point E

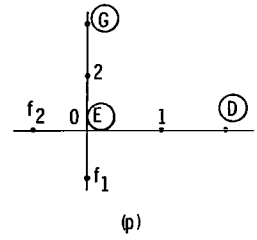

results in

$$z_0 = \frac{r_0^2}{2\left(r_0^2 + \frac{1}{\alpha^2}\right)} 2z_2 - \frac{1}{r_0}\sqrt{4a^2 - \frac{1}{\alpha^2}(z_1 - f_2)^2} + \frac{1}{2(r_0^2\alpha^2 + 1)}(z_1 + f_2)$$

$$+ \frac{z_1 - f_2}{4r_0\left(r_0^2\alpha + \frac{1}{\alpha}\right)}\sqrt{4a^2 - \frac{1}{\alpha^2}(z_1 - f_2)^2} \qquad \text{(D54)}$$

In order to find the fictitious point f_2, we apply

$$r\left(\frac{\partial z}{\partial \psi}\right) - \left(\frac{\partial z}{\partial \varphi}\right)\left(\frac{dz}{dr}\right) = 0$$

on $\underline{GE}$, without involving f_1:

$$\frac{r_0(z_2 - z_0)}{\Delta\psi} - \left(\frac{z_1 - f_2}{2\,\Delta\varphi}\right)\left(\frac{z_2 - z_0}{r_2 - r_0}\right) = 0 \qquad \text{(D55)}$$

Solving for f_2,

$$f_2 = z_1 - 2r_0\alpha(r_2 - r_0) \qquad \text{(D56)}$$

$$z_0 = \frac{r_0^2}{r_0^2 + \frac{1}{\alpha^2}} \left[z_2 - \frac{1}{r_0} \sqrt{a^2 - r_0^2 (r_2 - r_0)^2} \right] + \frac{z_1 - r_0 \alpha (r_2 - r_0)}{r_0^2 \alpha^2 + 1}$$

$$+ \frac{r_2 - r_0}{r_0^2 + \frac{1}{\alpha^2}} \sqrt{a^2 - r_0^2 (r_2 - r_0)^2} \qquad \text{(D57)}$$

FINITE PLATE (INCLUDING SURFACE TENSION)

$$\left(\frac{\partial r}{\partial \varphi}\right)^2 + r^2 \left(\frac{\partial r}{\partial \psi}\right)^2 = \frac{1}{1 - \frac{2}{We} + \frac{2}{We} \frac{1}{r} \frac{d}{dr} \frac{r^2}{\sqrt{\left(\frac{\partial r / \partial \varphi}{\partial r / \partial \psi}\right)^2 + r^2}}} \quad \text{on Line } \underline{AG}$$

Applying the r difference equation (eq. (115)) at point o on the line AG (sketch q),

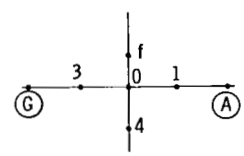

(q)

where f is a fictitious point outside the boundary, gives

$$r_0^4 - \frac{r_0^3}{2}(r_f + r_4) + r_0^2 \left[\frac{1}{\alpha^2} - \frac{1}{8}(r_f - r_4)^2 \right] - \frac{r_0}{2\alpha^2}(r_1 + r_3) + \frac{1}{8\alpha^2}(r_1 - r_3)^2 = 0 \qquad \text{(D58)}$$

In difference form, the free-surface boundary condition becomes

$$\left(\frac{r_1 - r_3}{2\,\Delta\varphi}\right)^2 + r_0^2\left(\frac{r_f - r_4}{2\,\Delta\psi}\right)^2 = \frac{1}{1 - \frac{2}{We} + \frac{2}{We}\frac{1}{r_0}\frac{d}{dr_0}\left[\frac{r_0^2}{\sqrt{\left(\frac{(r_1 - r_3)/2\,\Delta\varphi}{(r_f - r_4)/2\,\Delta\psi}\right)^2 + r_0^2}}\right]} \tag{D59}$$

Simplifying by using $\alpha = \Delta\varphi/\Delta\psi$ and defining

$$Q = \left[\frac{\frac{(r_1 - r_3)}{\Delta\varphi}}{\frac{(r_f - r_4)}{\Delta\psi}}\right]^2$$

yields

$$\frac{1}{\alpha^2}(r_1 - r_3)^2 + r_0^2(r_f - r_4)^2 = \frac{4a^2}{1 - \frac{2}{We} + \frac{2}{We}\frac{1}{r_0}\frac{d}{dr_0}\left(\frac{r_0^2}{\sqrt{Q + r_0^2}}\right)} \tag{D60}$$

Now, examine

$$\frac{1}{r_0}\frac{d}{dr_0}\left(\frac{r_0^2}{\sqrt{Q + r_0^2}}\right)$$

As an approximation to this derivative Q is assumed as a constant. In actuality, $Q = f(r_f)$ and $r_f = f(r_0)$. Expanding

$$\frac{1}{r_0}\frac{d}{dr_0}\left(\frac{r_0^2}{\sqrt{Q + r_0^2}}\right)$$

yields

$$\frac{1}{r_0}\frac{d}{dr_0}\left(\frac{r_0^2}{\sqrt{Q + r_0^2}}\right) = \frac{2Q + r_0^2}{\sqrt{Q + r_0^2}\,(Q + r_0^2)} \tag{D61}$$

Therefore, the finite difference representation for the free surface becomes

$$\frac{1}{\alpha^2}(r_1 - r_3)^2 + r_0^2(r_f - r_4)^2 = \frac{4a^2}{1 - \frac{2}{We} + \frac{2}{We}\left[\frac{2Q + r_0^2}{\sqrt{Q + r_0^2\,(Q + r_0^2)}}\right]} \tag{D62}$$

The term r_f must be eliminated between equations (D58) and (D62). If we define x as

$$x = r_f - r_4 \tag{D63}$$

equation (D62) can be written

$$\frac{1}{\alpha^2}(r_1 - r_3)^2 + r_0^2 x^2 = \frac{4a^2}{1 - \frac{2}{We} + \frac{2}{We}\left[\frac{4a^2}{\sqrt{Q + r_0^2\,(Q + r_0^2)}}\right]} \tag{D64}$$

where

$$Q = \frac{(r_1 - r_3)^2}{x^2}\left(\frac{1}{\alpha^2}\right) \tag{D65}$$

Inserting (D63) into (D58) yields

$$\frac{r_0^2 x^2}{8} + \frac{r_0^3}{2}x - r_0^4 + r_0^3 r_4 - \frac{r_0^2}{\alpha^2} + \frac{r_0}{2\alpha^2}(r_1 + r_3) - \frac{1}{8\alpha^2}(r_1 - r_3)^2 = 0 \tag{D66}$$

This is of the form

$$A'\chi^2 + B'\chi + C' = 0$$

Hence,

$$\chi = -\frac{B' + \sqrt{B'^2 - 4A'C'}}{2A'} \tag{D67}$$

where

$$A' = \frac{r_0^2}{8} \tag{D68}$$

$$B' = \frac{r_0^3}{2} \tag{D69}$$

$$C' = -r_0^4 + r_0^3 r_4 - \frac{r_0^2}{\alpha^2} + \frac{r_0}{2\alpha^2}(r_1 + r_3) - \frac{1}{8\alpha^2}(r_1 - r_3)^2 \tag{D70}$$

The sign in front of the square root in equation (D67) was chosen as positive since x must be greater than or equal to zero. In addition, employing equation (141) and the results of appendix C yield

$$r^2\left(\frac{\partial z}{\partial \psi}\right)^2 + \left(\frac{\partial z}{\partial \varphi}\right)^2 = \frac{1}{1 - \frac{2}{We} + \frac{2}{We}\frac{1}{r}\frac{d}{dr}\left[\frac{r}{\sqrt{r^2\left(\frac{\partial z/\partial \psi}{\partial z/\partial \varphi}\right)^2 + 1}}\right]}$$

on AG.

Applying the z difference equation (eq. (114)) at point 0 (sketch q), where f is a fictitious point outside the boundary, yields

$$z_0 = \frac{r_0^2}{2\left(r_0^2 + \frac{1}{\alpha^2}\right)}(f + z_4) + \frac{1}{2(r_0^2\alpha^2 + 1)}(z_1 + z_3) + \frac{(f - z_4)(z_1 - z_3)}{4\left(r_0^2\alpha + \frac{1}{\alpha}\right)} \tag{D71}$$

In finite difference form, the free-surface boundary condition can be written

$$r_0^2(f - z_4)^2 + \frac{1}{\alpha^2}(z_1 - z_3)^2 = \frac{4a^2}{1 - \frac{2}{We} + \frac{2}{We}\frac{1}{r_0}\frac{d}{dr_0}\left(\frac{r_0}{\sqrt{r_0^2Q^* + 1}}\right)} \tag{D72}$$

where

$$Q^* = \alpha^2 \frac{(f - z_4)^2}{(z_1 - z_3)^2} \tag{D73}$$

As an approximation Q^* is assumed to be a constant. Expanding

$$\frac{1}{r_0}\frac{d}{dr_0}\left(\frac{r_0}{\sqrt{r_0^2Q^* + 1}}\right)$$

gives

$$\frac{1}{r_0}\frac{d}{dr_0}\left(\frac{r_0}{\sqrt{r_0^2Q^* + 1}}\right) = \frac{1}{r_0(r_0^2Q^* + 1)\sqrt{r_0^2Q^* + 1}} \tag{D74}$$

Therefore, the finite difference representation along the free surface becomes

$$r_0^2(f - z_4)^2 + \frac{1}{\alpha^2}(z_1 - z_3)^2 = \frac{4a^2}{1 - \frac{2}{We} + \frac{2}{We}\frac{1}{r_0}\frac{1}{(r_0^2Q^* + 1)\sqrt{r_0^2Q^* + 1}}} \tag{D75}$$

The point f must now be eliminated between equations (D76) and (D75). This is done as follows: Equation (D75) is solved for $f = fct(z_1, z_3, z_4)$. The results are then inserted into equation (D71). In this way, equation (D71) remains explicit in z_0. Actually, it will be more convenient to solve for the variable $(f - z_4)$ instead of f since equation (D71) can be expressed as

$$z_0 = \frac{r_0^2 z_4}{r_0^2 + \frac{1}{\alpha^2}} + \frac{z_1 + z_3}{2(r_0^2\alpha^2 + 1)}(f - z_4)\left[\frac{2\alpha r_0^2 + (z_1 - z_3)}{4\alpha\left(r_0^2 + \frac{1}{\alpha^2}\right)}\right] \tag{D76}$$

Equation (D75) is solved for $(f - z_4)$

$$\frac{\alpha^2 r_0^2 (f - z_4)^2}{(z_1 - z_3)^2} + 1 = \frac{\frac{4a^2\alpha^2}{(z_1 - z_3)^2}}{1 - \frac{2}{We} + \frac{2}{We}\frac{1}{r_0}\frac{1}{\left[\frac{r_0^2\alpha^2(f - z_4)^2}{(z_1 - z_3)^2} + 1\right]\sqrt{\frac{r_0^2\alpha^2(f - z_4)^2}{(z_1 - z_3)^2} + 1}}} \tag{D77}$$

A new variable, T^2, is introduced:

$$T^2 = \frac{\alpha^2 r_0^2 (f - z_4)^2}{(z_1 - z_3)^2} + 1 \tag{D78}$$

Also, let

$$C_0 = \frac{4a^2\alpha^2}{(z_1 - z_3)^2} \tag{D79}$$

$$C_1 = 1 - \frac{2}{We} \tag{D80}$$

$$C_2 = \left(\frac{2}{We}\right)\left(\frac{1}{r_0}\right) \tag{D81}$$

Making these substitutions into equation (D77) results in a cubic equation for T:

$$T^3 - \frac{C_0}{C_1} T + \frac{C_2}{C_1} = 0 \tag{D82}$$

Rewriting this gives

$$T^3 + aT + b = 0 \tag{D83}$$

Once T is found from equation (D83), $(f - z_4)$ is calculated from equation (D78) as follows:

$$f - z_4 = \pm \frac{(z_1 - z_3)}{\alpha r_0} \sqrt{T^2 - 1} \tag{D84}$$

The choice of sign in equation (D84) depends on whether z is less than, equal to, or greater than zero, since the fictitious point f by definition must lie outside the boundary.

APPENDIX E

COMPUTER SOLUTIONS

INFINITE FLAT PLATE

Coarse-Mesh Solution for r and z

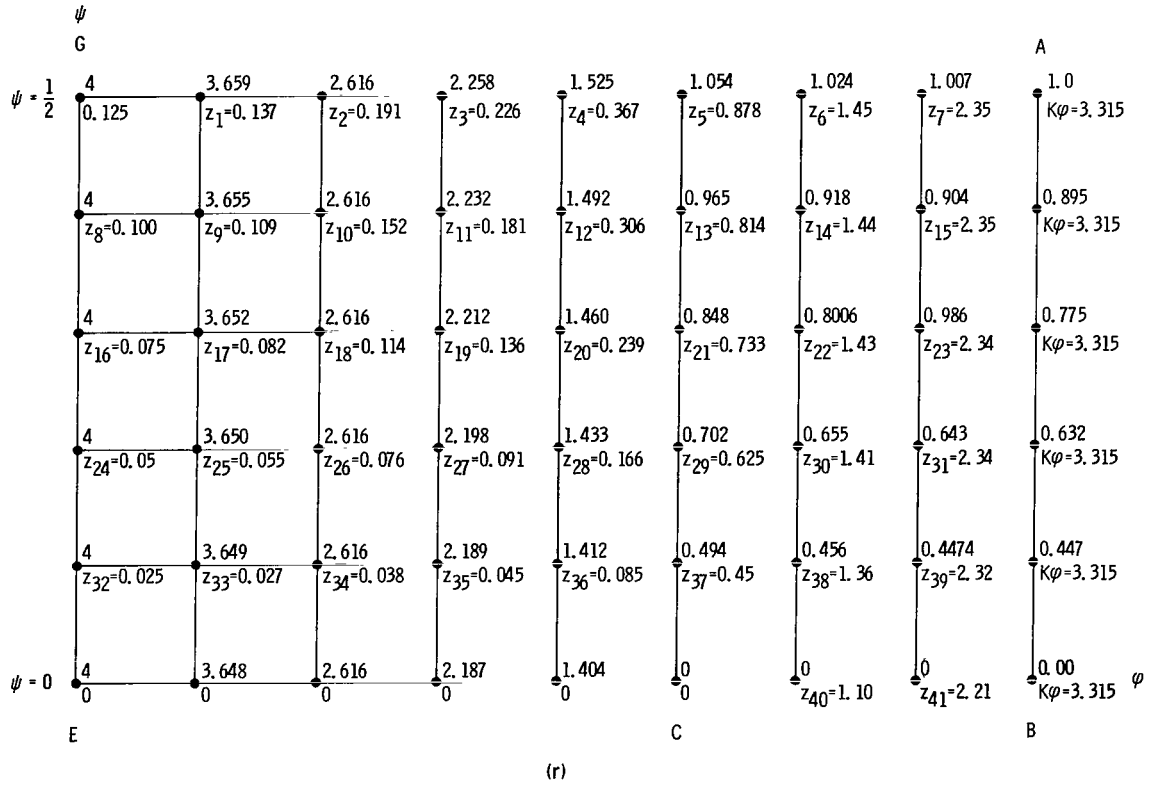

Fine-Mesh Solution for r and z

FINITE PLATE

Coarse-Mesh Solution ($R_0/L = 1/2$)

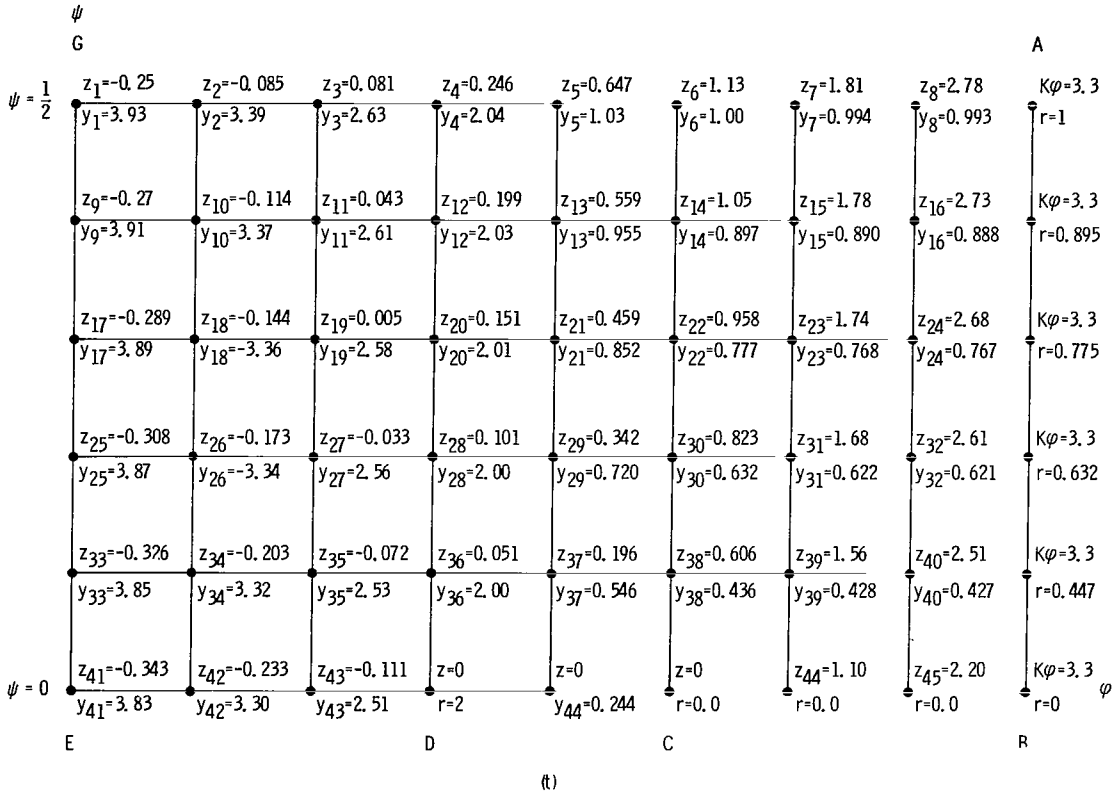

(t)

Coarse-Mesh Solution ($R_0/L = 3/4$)

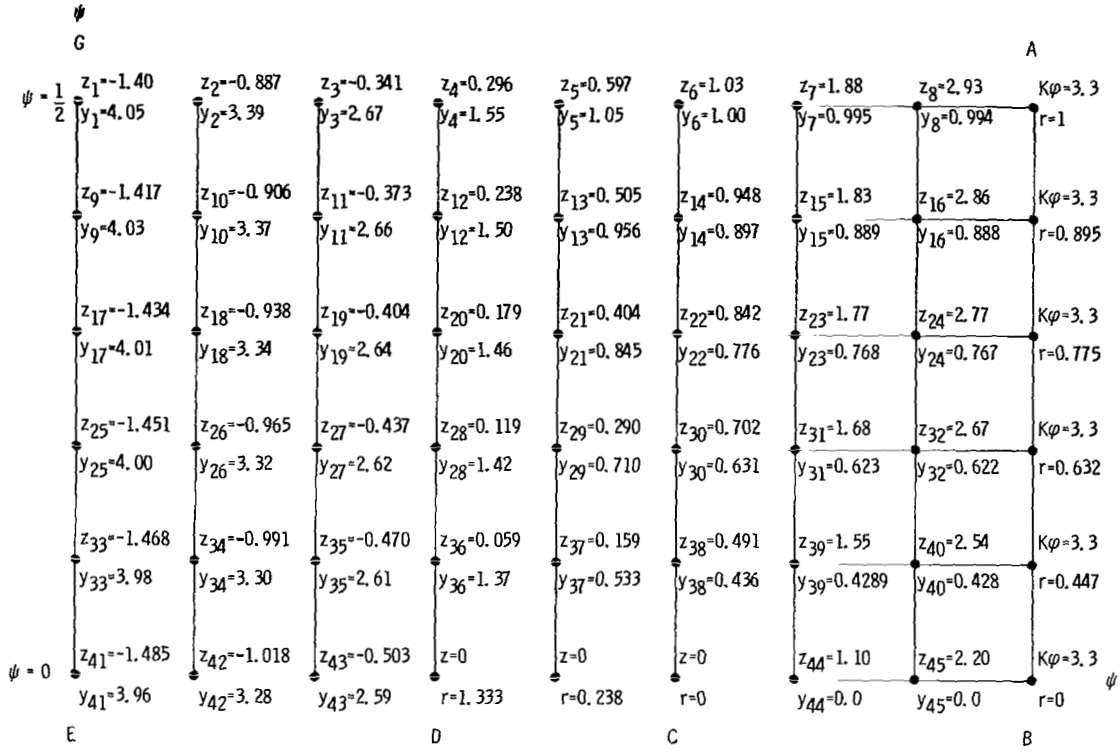

(u)

r Solution

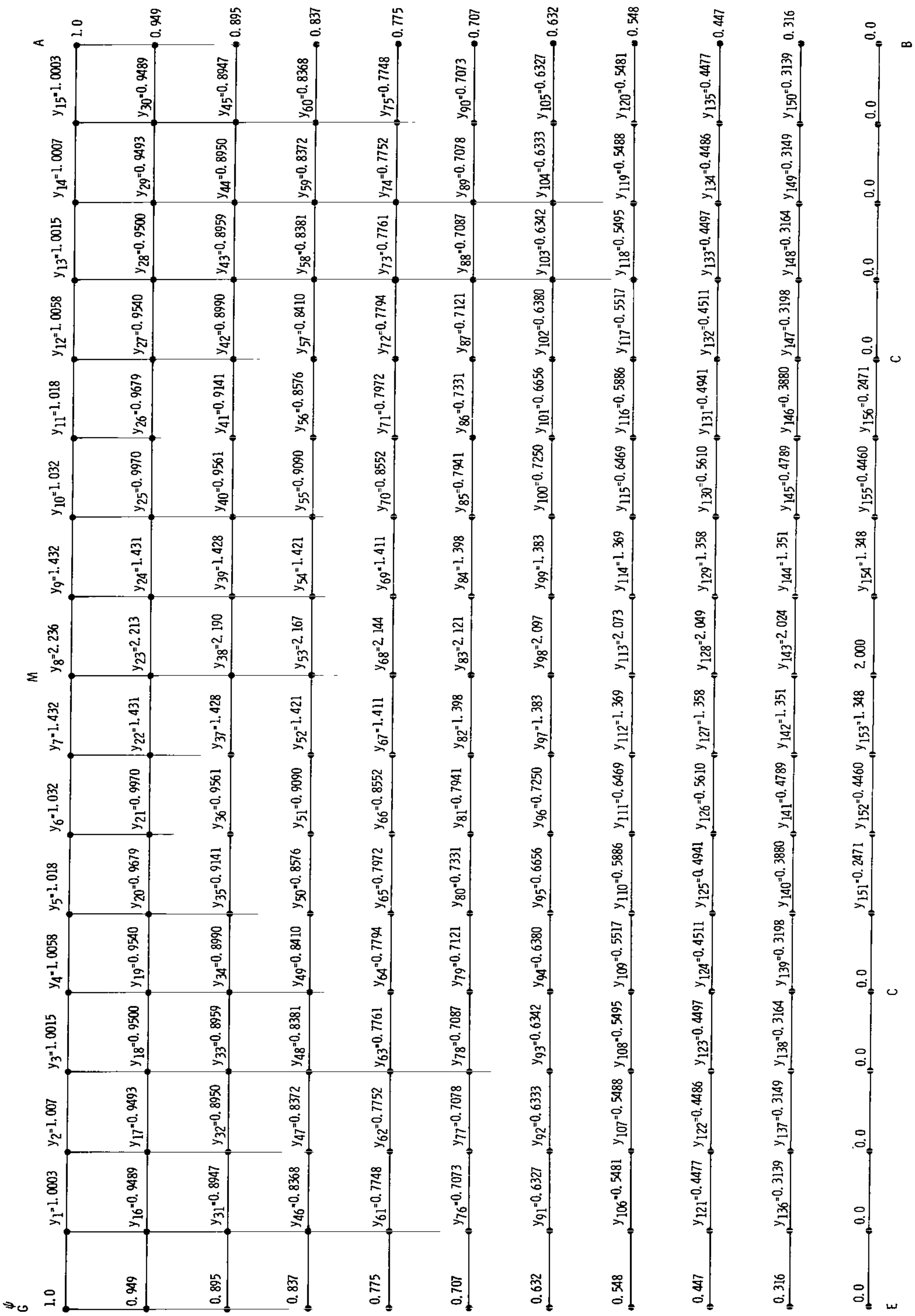
ψ
G
A
M
E
C
(v)
C
B
1.0
0.949
0.895
0.837
0.775
0.707
0.632
0.548
0.447
0.316
0.0
y1=1.0003 y2=1.007 y3=1.0015 y4=1.0058 y5=1.018 y6=1.032 y7=1.432 y8=2.236 y9=1.432 y10=1.032 y11=1.018 y12=1.0058 y13=1.0015 y14=1.0007 y15=1.0003
y16=0.9489 y17=0.9493 y18=0.9500 y19=0.9540 y20=0.9679 y21=0.9970 y22=1.431 y23=2.213 y24=1.431 y25=0.9970 y26=0.9679 y27=0.9540 y28=0.9500 y29=0.9493 y30=0.9489
y31=0.8947 y32=0.8950 y33=0.8959 y34=0.8990 y35=0.9141 y36=0.9561 y37=1.428 y38=2.190 y39=1.428 y40=0.9561 y41=0.9141 y42=0.8990 y43=0.8959 y44=0.8950 y45=0.8947
y46=0.8368 y47=0.8372 y48=0.8381 y49=0.8410 y50=0.8576 y51=0.9090 y52=1.421 y53=2.167 y54=1.421 y55=0.9090 y56=0.8576 y57=0.8410 y58=0.8381 y59=0.8372 y60=0.8368
y61=0.7748 y62=0.7752 y63=0.7761 y64=0.7794 y65=0.7972 y66=0.8552 y67=1.411 y68=2.144 y69=1.411 y70=0.8552 y71=0.7972 y72=0.7794 y73=0.7761 y74=0.7752 y75=0.7748
y76=0.7073 y77=0.7078 y78=0.7087 y79=0.7121 y80=0.7331 y81=0.7941 y82=1.398 y83=2.121 y84=1.398 y85=0.7941 y86=0.7331 y87=0.7121 y88=0.7087 y89=0.7078 y90=0.7073
y91=0.6327 y92=0.6333 y93=0.6342 y94=0.6380 y95=0.6656 y96=0.7250 y97=1.383 y98=2.097 y99=1.383 y100=0.7250 y101=0.6656 y102=0.6380 y103=0.6342 y104=0.6333 y105=0.6327
y106=0.5481 y107=0.5488 y108=0.5495 y109=0.5517 y110=0.5886 y111=0.6469 y112=1.369 y113=2.073 y114=1.369 y115=0.6469 y116=0.5886 y117=0.5517 y118=0.5495 y119=0.5488 y120=0.5481
y121=0.4477 y122=0.4486 y123=0.4497 y124=0.4511 y125=0.4941 y126=0.5610 y127=1.358 y128=2.049 y129=1.358 y130=0.5610 y131=0.4941 y132=0.4511 y133=0.4497 y134=0.4486 y135=0.4477
y136=0.3139 y137=0.3149 y138=0.3164 y139=0.3198 y140=0.3880 y141=0.4789 y142=1.351 y143=2.024 y144=1.351 y145=0.4789 y146=0.3880 y147=0.3198 y148=0.3164 y149=0.3149 y150=0.3139
0.0 0.0 0.0 0.0 0.0 y151=0.2471 y152=0.4460 y153=1.348 2.000 y154=1.348 y155=0.4460 y156=0.2471 0.0 0.0 0.0 0.0 0.0

z Solution

APPENDIX F

SYMBOLS

A	numerical constant
a	stream function increment, numerical constant
B	numerical constant
b	numerical constant
C	numerical constant; integration constant
C_0, C_1, C_2	numerical constants
c	numerical constant
D	$1/\alpha^2$
d	designated reference point
d_0	nozzle diameter, cm
E	special point
F	function
f_0	unknown scale factor, m
f_K	functions
f, f_1, f_2, f_3	fictitious points; functions
G	special point
g	gas
H	distance between plate and nozzle, m
i	any point on free surface
$\hat{i}, \hat{j}$	unit vectors in radial and axial directions, respectively
J	Jacobian; local curvature
$K\varphi$	numerical constant
L	disk radius, m
N	index
$\hat{n}$	unit normal on free surface
O	stagnation point

p	pressure, N/m^2
p_0	unknown scale factor, N/m^2
Q	$\frac{(r_1 - r_3)^2}{(r_f - r_4)^2}\left(\frac{1}{\alpha^2}\right)$
Q^*	$\frac{\alpha^2(f - z_4)^2}{(z_1 - z_3)^2}$
R_{max}	maximum radius for surface tension model, m
R_0	radius of nozzle, m
R_1, R_2	radii of curvature, m
RD	L/R_0
Re	Reynolds number, $\rho V R_0/\mu$
r	radial coordinate, m
r_E	radial dimension, m
r_0	unknown scale factor, m
r_0^*, r_0^{**}	nozzle radii, m
T^2	$\alpha^2 r_0^2(f - z_4)^2/(z_1 - z_3)^2 + 1$
U_0	unknown scale factor, m/sec
u	radial velocity component, m/sec
$\mathscr{V}$	jet velocity, m/sec
$\vec{V}$	vector velocity, m/sec
V_0	unknown scale factor, m/sec
v	axial velocity component, m/sec
We	Weber number, $\rho V^2 R_0/\sigma$
z	axial coordinate, m
z_0	unknown scale factor, m
α	$\Delta\varphi/\Delta\psi$
β	specific surface tension, σ/ρ, m^3/sec^2
$\delta/\delta r$	finite difference analogy of $\partial/\partial r$

μ	liquid viscosity, g/m^2-sec
ρ	liquid density, kg/m^3
σ	liquid surface tension, N/m
φ	velocity potential, m^2/sec
χ	$r_f - r_4$, m
ψ	Stoke's stream function, m^3/sec

Subscripts:

cr	critical
d	datum
E, G	special points
g	gas
i, k, n	free indices
jet	jet
max	maximum
s	surface
0	stagnation point, subscript for z
0, 1, 2, 3, 4	nodal point locations

Superscripts:

'	differentiation with respect to r
*	dimensionless quantity
**	dimensionless quantity

REFERENCES

1. Schach, Von W.: Umlenkunk eines freien Flussigkeitsstrahles an einer ebenen Platte. (Deflection of a Free Fluid Jet at a Flat Panel.) Ingenidur-Archiv, vol. 5, 1934, pp. 245-265.

2. Donnelly, R. J.; and Glaberson, W.: Experiments on the Capillary Instability of a Liquid Jet. Proc. Roy. Soc. (London), vol. A290, 1966, pp. 547-556.

3. Rupe, Jack H.: On the Dynamic Characteristics of Free-Liquid Jets and a Partial Correlation with Orifice Geometry. JPL-TR-32-207, Jet Propulsion Lab., 1962.

4. Stephens, David G.: Experimental Investigation of Liquid Impact in Model Propellant Tank. NASA TN D-2913, 1965.

5. Koloseus, H. J.; and Ahmad, D.: Circular Hydraulic Jump. Am. Soc. Civil Eng. Proc. (J. Hydraulics Div.), vol. 95, no. HY1, Jan. 1969, pp. 409-422.

6. Nirapathdongporn, S.: Circular Hydraulic Jump. M.S. Thesis, Asian Inst. of Tech., Bangkok (Thailand), 1968.

7. Batchelor, George K.: An Introduction to Fluid Mechanics. Cambridge Univ. Press, 1967.

8. Kochin, N. E.; Kibel, I. A.; and Roze, N. V.: Theoretical Hydromechanics. Interscience Publ., 1964.

9. Milne-Thomson, Louis M.: Theoretical Hydrodynamics. Macmillan Book Co., Inc., 1968.

10. Gurevich, Maksim J.: Theory of Jets in Ideal Fluids. Academic Press, 1965.

11. Chang, H. Y.; and Conly, J. F.: Potential Flow of Segmental Jet Deflectors. J. Fluid Mech., vol. 46, pt. 3, Apr. 1971, pp. 465-475.

12. Arbhabhirama, A.: Free Streamline Analysis of Two-Dimensional Jet. Am. Soc. Civil Eng. Proc. (J. Hydraulic Div.), vol. 95, no. HY4, July 1969, pp. 1139-1148.

13. Watson, E. J.: The Radial Spread of a Liquid Jet Over a Horizontal Plane. J. Fluid Mech., vol. 20, pt. 3, Nov. 1964, pp. 481-499.

14. Jeppson, Roland W.: Techniques for Solving Free-Streamline, Cavity, Jet, and Seepage Problems by Finite Differences. TR-68, Stanford Univ., (AD-654922), 1966.

15. Thom, Alexander; and Apelt, C. J.: Field Computations in Engineering and Physics. D. Van Nostrand Co., 1961.

16. Yih, Chio-Shun: Dynamics of Nonhomogeneous Fluids. MacMillan Book Co., Inc., 1965.

17. Brennan, Christopher: A Numerical Solution of Axisymmetric Cavity Flows. J. Fluid Mech., vol. 37, pt. 4, July 1969, pp. 671-688.

18. Jeppson, Roland W.: Inverse Formulation and Finite Difference Solution for Flow from a Circular Orifice. J. Fluid Mech., vol. 40, pt. 1, Jan. 1970, pp. 215-223.

19. Moayeri, Mohmmad S.; and Strelkoff, Theodor S.: Potential Flow at a Two-Dimensional Conduit Outlet. Am. Soc. Civil Eng. Proc. (J. Hydraulics Div.), vol. 99, no. HY4, Apr. 1973, pp. 653-671.

20. Fox, L.: A Short Account of Relaxation Methods. Q. J. Mech. Appl. Mathematics, vol. 1, pt. 3, Sept. 1948, pp. 253-280.

21. McNown, J. S.; Hsu, E.; and Yih, C. S.: Applications of the Relaxation Techniques in Fluid Mechanics. Amer. Soc. Civil Engs. Proc., vol. 79, no. 223, July 1953.

22. Southwell, R. V.; and Vaisey, Gillian: Relaxation Methods Applied to Engineering Problems. XII. Fluid Motions Characteristics by "Free" Stream-Lines. Phil. Trans. Roy. Soc. (London), vol. 240, 1948, pp. 117-161.

23. Allen, Deryck N. G.: Relaxation Methods. McGraw-Hill Book Co., Inc., 1954.

24. Moss, W. D.: Flow Separation at the Upstream Edge of a Square-Edged Broad-Crested Weir. J. Fluid Mech., vol. 52, pt. 2, Mar. 1972, pp. 307-320.

25. Chan, Stevens T. K.; and Larock, Brock E.: Fluid Flows from Axisymmetric Orifices and Valves. Am. Soc. Civil Eng. Proc. (J. Hydraulics Div.), vol. 99, no. HY1, Jan. 1973, pp. 81-97.

26. Rouse, Hunter; and Abul-Fetouh, Abdel-Hode: Characteristics of Irrotational Flow through Axially Symmetric Orifices. J. Appl. Mech., vol. 17, no. 12, Dec. 1950, pp. 421-426.

27. Chan, S. T. K.: Finite Element Analysis of Irrotational Flows of an Ideal Fluid. Ph. D. Thesis, Univ. California, 1971.

28. LeClerc, A.: Deflection of a Liquid Jet by a Perpendicular Boundary. M.S. Thesis, Univ. Iowa, 1948.

29. Schach, Von W.: Umlenkung eines Kreisformigen Flussigkeitsstrahles an einer ebenen Platte Senkrecht zur Stromungs Trichtung. (Deflection of a Circular Liquid Jet on a Plane Plate Normal to the Stream.) Ingenieur Archiv, vol. 6, 1935, pp. 51-59.

30. Young, D. M.; et al.: The Computation of an Axially Symmetric Free Boundary Problem on NORC. Rept. 1413, Naval Proving Ground, 1955.

31. Brunauer, E. A.: Axially Symmetric Free Streamline Flow about Tandem Discs. M.S. Thesis, Illinois Inst. Tech., 1951.

32. Huang, Yen C.; Hammit, F. C.; and Yang, W.-J.: Hydrodynamic Phenomena during High-Speed Collision between Liquid Droplet and Rigid Plane. J. Fluids Eng., vol. 95, no. 2, June 1973, pp. 276-294.

33. Huang, Y. C.; Hammit, F. G.; and Yang, W.-J.: Normal Impact of a Finite Cylindrical Liquid Jet on a Flat Rigid Plane. Rept. 03371-91T, Univ. Michigan, 1971.

34. Zhukovskii, N. Ye.: Opred' Leniye Dvisheniya Zhidkosti Pri Kakom'-Nibud' Uslovii, Dannom' Na Linii Toka. (Determining the Movement of a Liquid for a Condition Specified on a Streamline.) Zh. Obshch. Khim., vol. 23, no. 2, 1891, pp. 89-100.

35. Davis, A. L.; and Jeppson, R. W.: Solving Three-Dimensional Potential Flow Problems by Means of an Inverse Formulation and Finite Differences. Utah State Univ., 1973.

36. Michelson, I.: Fluid Jet Impingement - Analytical Solution and Novel Physical Characteristic. Nature, vol. 223, Aug. 9, 1969, pp. 610-611.

37. Michelson, I.: A Solution of the Three-Dimensional Oblique-Incidence Liquid Jet Problem. Rev. Roum. Math. Pures Et Appl., vol. 15, no. 2, 1970, pp. 279-284.

38. Krantz, W. B.: Scaling Initial and Boundary Value Problems. Chem. Eng. Educ., vol. 4, no. 3, Summer 1970, pp. 145-151.

39. Lu, Pau-Chang: Introduction to the Mechanics of Viscous Fluids. Holt, Rinehart and Winston, Inc., 1973, pp. 87-89.

40. Labus, Thomas L.; and Symons, Eugene P.: Experimental Investigation of an Axisymmetric Free Jet with an Initially Uniform Velocity Profile. NASA TN D-6783, 1972.

41. Roache, Patrick J.: Computational Fluid Dynamics. Hermosa Publ., 1972, pp. 18-23.

42. Lieberstein, H. M.: Overrelaxation for Non-linear Elliptic Partial Differential Problems. Tech. Summary Rept. 80, Mathematics Research Center, Univ. Wisconsin, 1959.

43. Powell, M. J. D.: A FORTRAN Subroutine For Solving Systems of Non-linear Algebraic Equations. AERE-R-5947, Atomic Energy Research Establishment (England), 1968.

44. Labus, Thomas L.: Liquid Jet Impingement Normal to a Disk in Zero Gravity. NASA TM X-73405, 1976.

TABLE I. - LIQUID PROPERTIES AT 20° C

Liquid	Surface tension, N/cm	Density, g/cm^3	Absolute viscosity, g/cm-sec
Anhydrous ethanol	22.3×10^{-5}	0.789	1.200×10^{-2}
Trichlorotrifluoroethane	18.6	1.579	.700

TABLE II. - SUMMARY OF PARAMETERS

Test liquid	Nozzle radius, R_0, cm	Disk radius, L, cm	Ratio, R_0/L	Velocity of jet, cm/sec	Reynolds number, $\rho V R_0/\mu$	Weber number, $\rho V^2 R_0/\sigma$	Flow category
Freon TF	0.25	1.0	0.25	34.3	1934	24.8	S
Freon TF				38.0	2133	30.5	S
Freon TF				43.7	2464	40.4	T
Ethanol[a]				77.0	1278	52.2	
Freon TF				50.5	2848	54.0	
Freon TF				58.8	3316	73.4	
Ethanol				101.0	1662	90.1	
Freon TF				79.6	4460	113.2	
Ethanol				131.3	2160	151.9	I
Freon TF				88.6	5000	161.5	
Ethanol				149.8	2465	197.8	
				237.7	3911	498	
				282.2	4642	703	
				365.6	6014	1180	
Ethanol[a]	.50	1.5	.33	26.4	868	12.2	S
Freon TF				19.5	1815	16.1	S
Ethanol				37.7	1240	25.1	S
Freon TF				27.4	3090	31.8	T
Ethanol				46.0	1513	37.2	
Ethanol				53.9	1773	51.2	
Freon TF				37.6	4240	60.0	
Ethanol				59.6	1900	62.0	
Freon TF				42.75	4830	77.6	I
Ethanol	.75		.50	15.4	760	6.2	S
	.75			19.1	942	9.6	
	.75			19.9	986	10.5	
	.50	1.0		26.4	868	12.2	
Freon TF	.50	1.0		17.7	1996	13.2	
Ethanol	.75	1.5		28.2	1891	21.0	
Ethanol	.50	1.0		34.9	1148	21.3	T
Freon TF	.50	1.0		23.3	2628	23.0	
Ethanol	.75	1.5		34.4	1697	31.2	
Ethanol	.50	1.0		46.1	1516	37.4	
Freon TF	.50	1.0		31.9	3490	43.2	
Ethanol	.75	1.5		41.2	2036	44.7	I
Ethanol	.50	1.0		52.3	1720	48.2	T
Freon TF	.50	1.0		37.5	4230	59.5	I
Ethanol	.75	1.5		47.5	2347	59.6	I
	.50	1.0		85.7	2820	129.0	I
	.75		.75	12.7	630	4.2	S
				22.5	1110	13.3	S
				24.8	1227	16.2	S
				27.3	1350	19.7	T
				29.4	1454	22.9	
				32.0	1580	27.0	
				35.0	1730	32.3	
				39.1	1930	40.2	I

[a]Do not satisfy minimum-Reynolds-number criterion, but included as data and in data points.

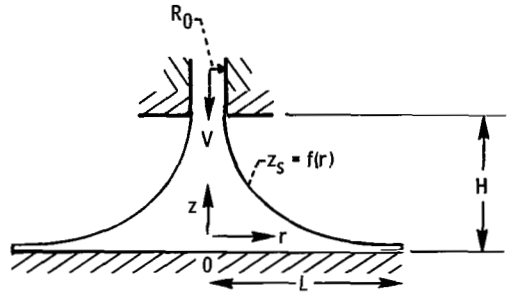

Figure 1. - Schematic of liquid jet impinging on a flat plate.

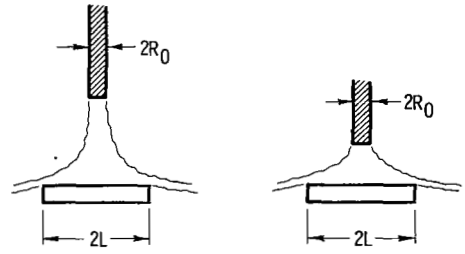

Figure 2. - Flow pattern as a function of nozzle height.

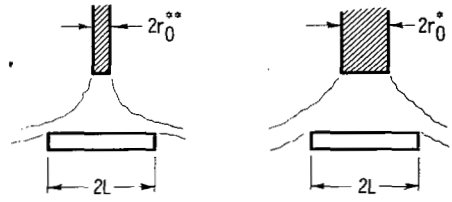

Figure 3. - Flow pattern as a function of jet radius.

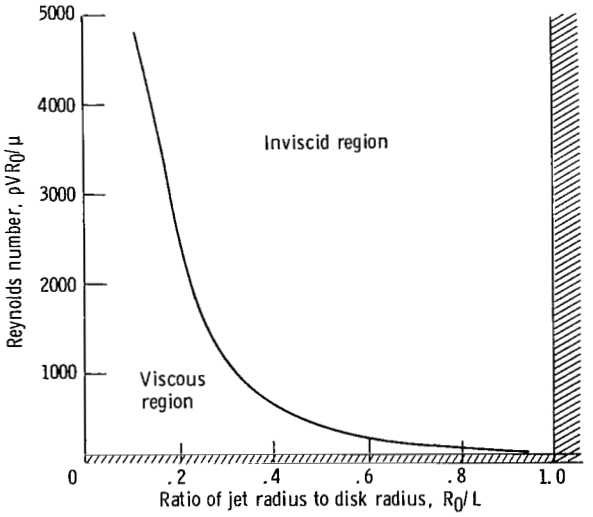

Figure 4. - Results of order-of-magnitude analysis.

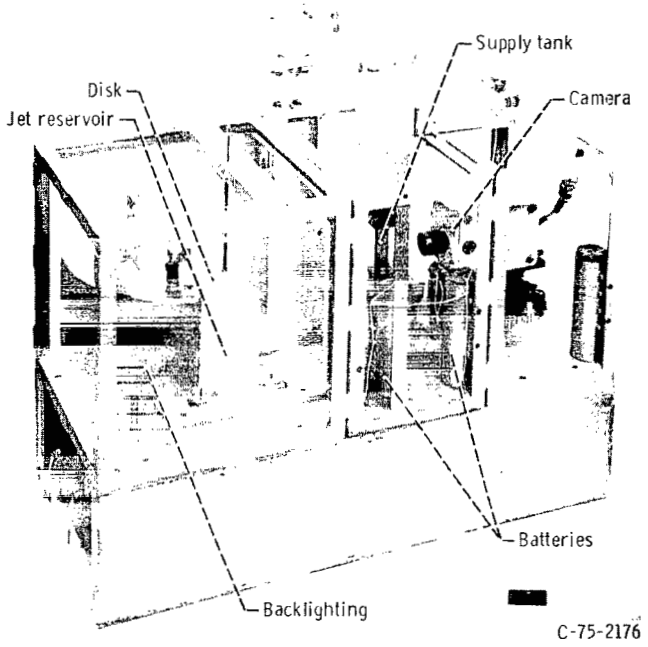

Figure 5. - Experiment package.

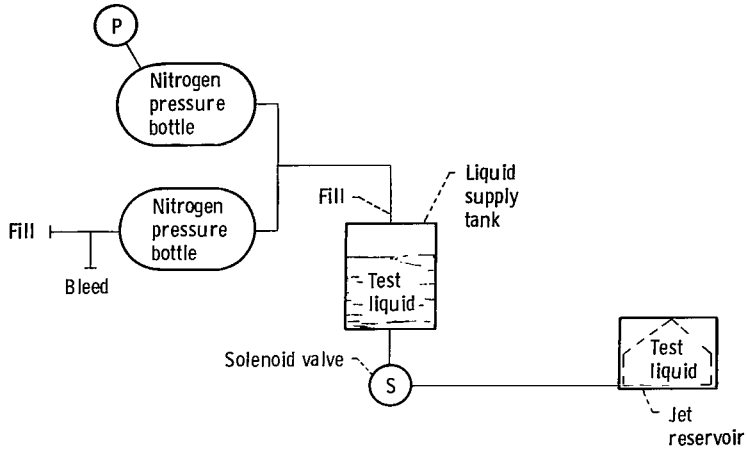

Figure 6. - Schematic of flow system.

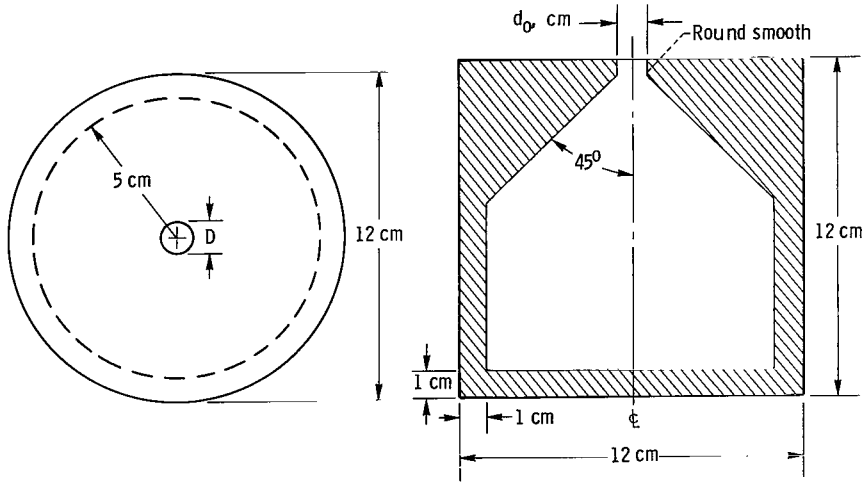

(a) Top view. (b) Side view.

Figure 7. - Jet reservoir.

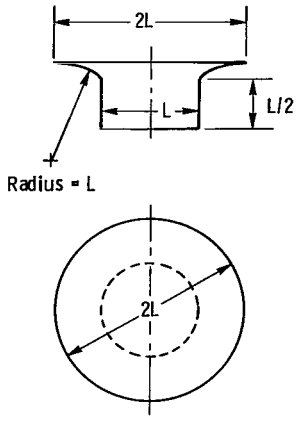

Figure 8. - Schematic diagram of sharp-edge disk.

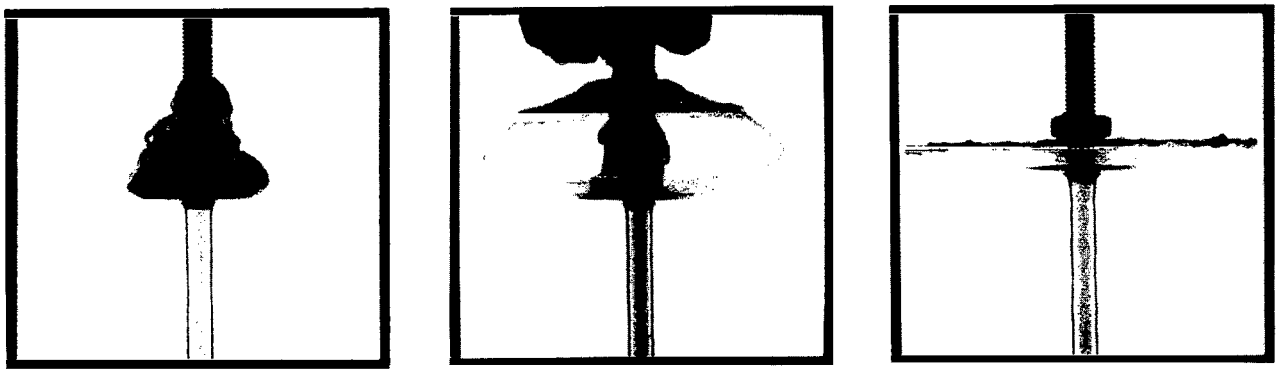

(a) Surface tension flow.

(b) Transition flow.

(c) Inertial flow.

Figure 9. - Liquid jet impinging on flat solid disk.

C-75-128

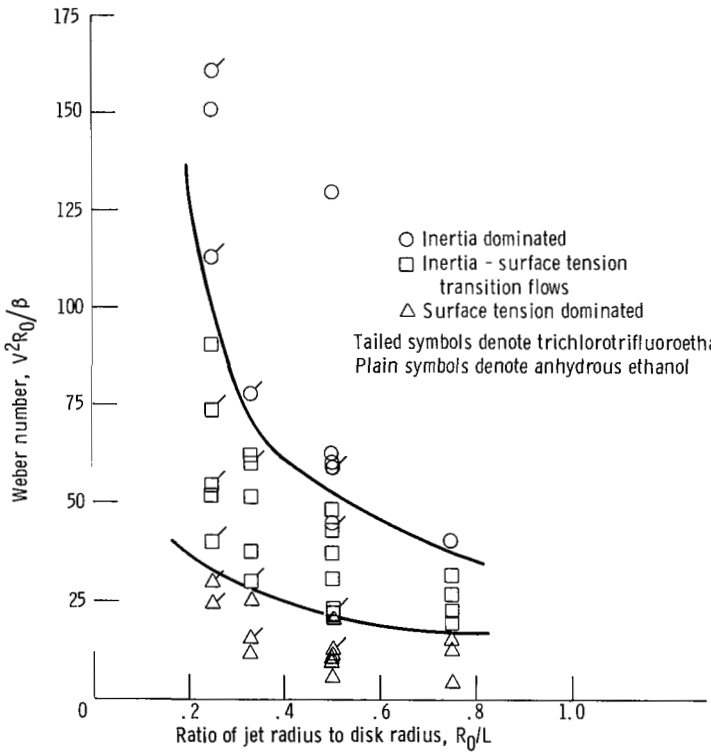

Figure 10. - Zero-gravity experimental results.

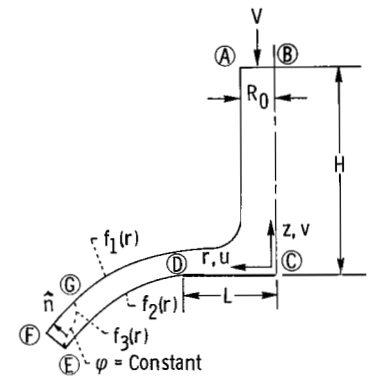

(a) Liquid jet impingement.

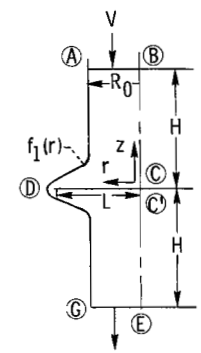

(b) Surface tension.

Figure 11. - Models in physical plane.

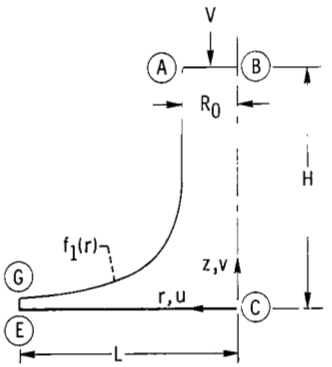

Figure 12. - Circular liquid jet impinging on infinite plate.

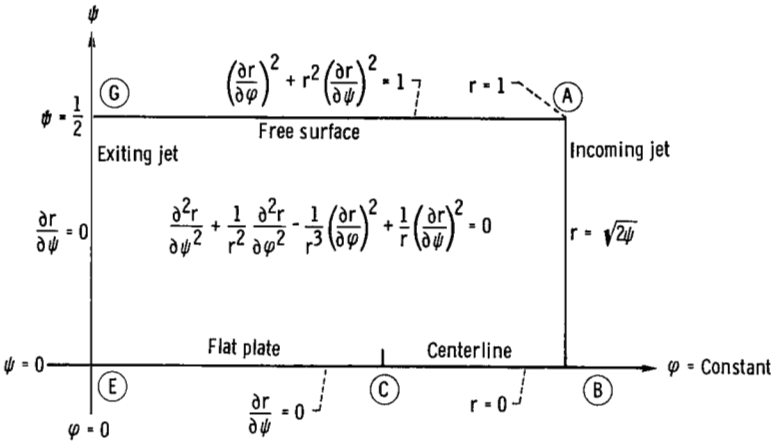

(a) r Solution.

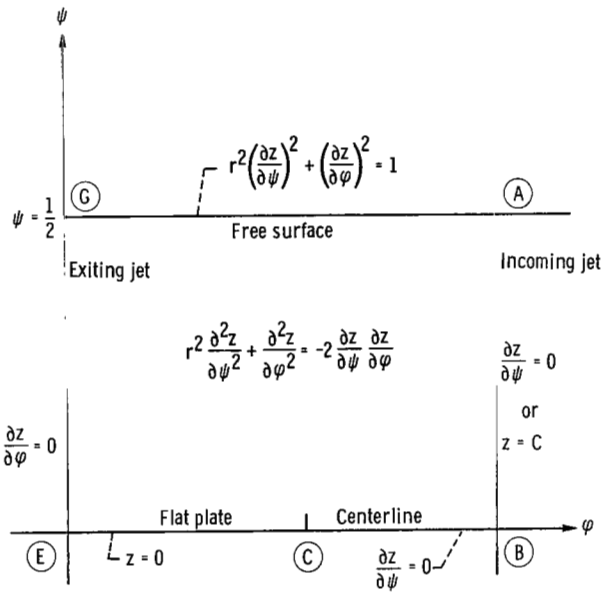

(b) z Solution.

Figure 13. - Inverse formulation excluding surface tension for finite plate.

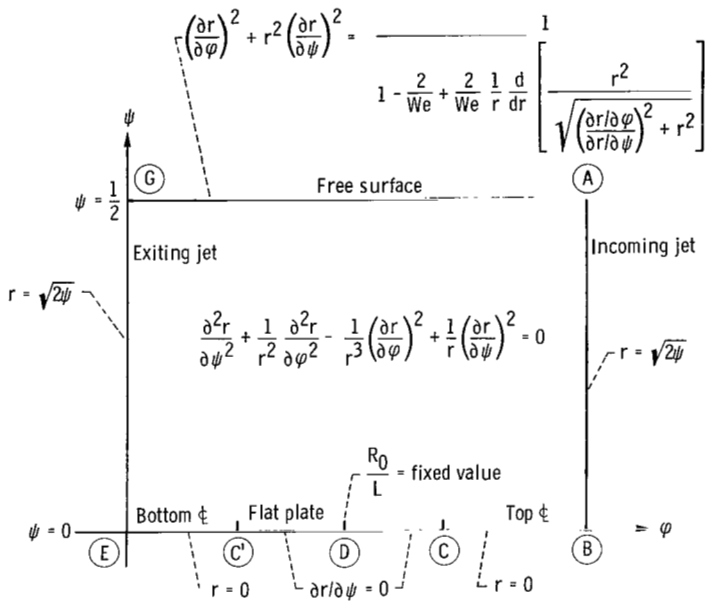

(a) r Solution.

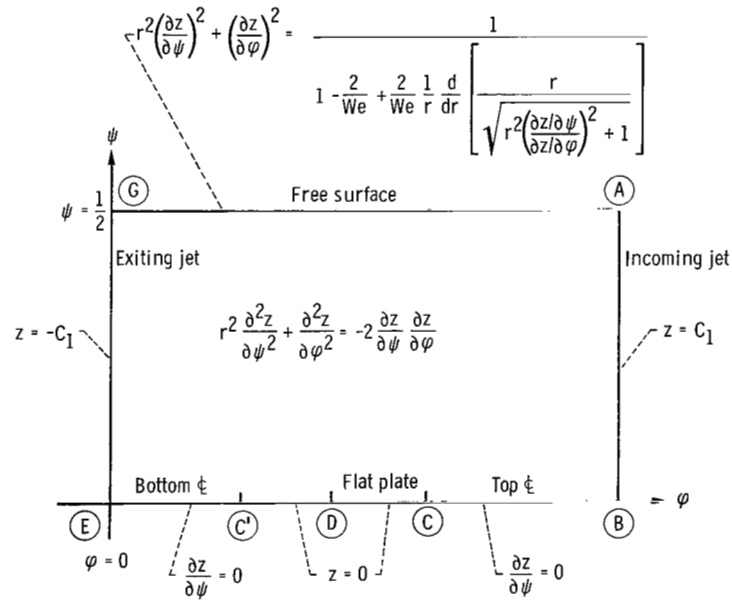

(b) z Solution.

Figure 14. - Surface tension model - inverse formulation for finite plate.

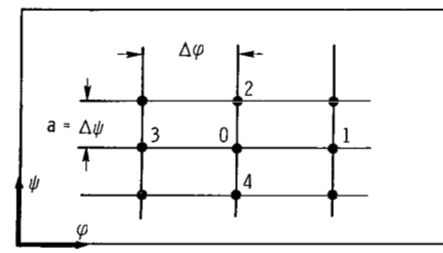

Figure 15. - Nodal point representation for rectangular mesh.

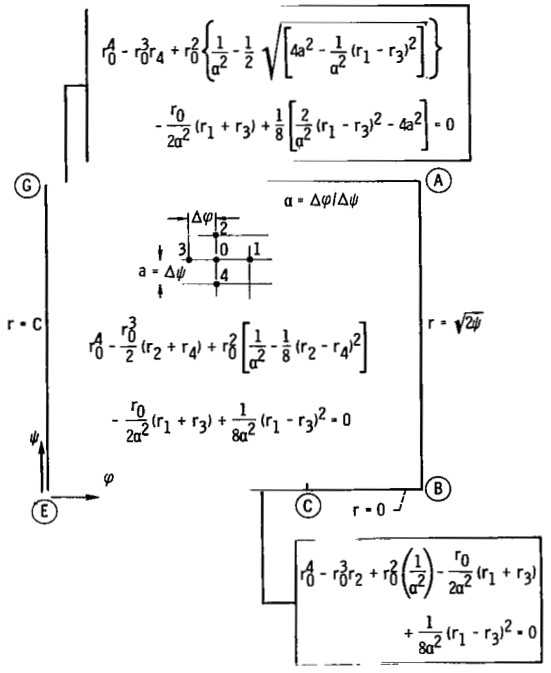

(a) r Solution.

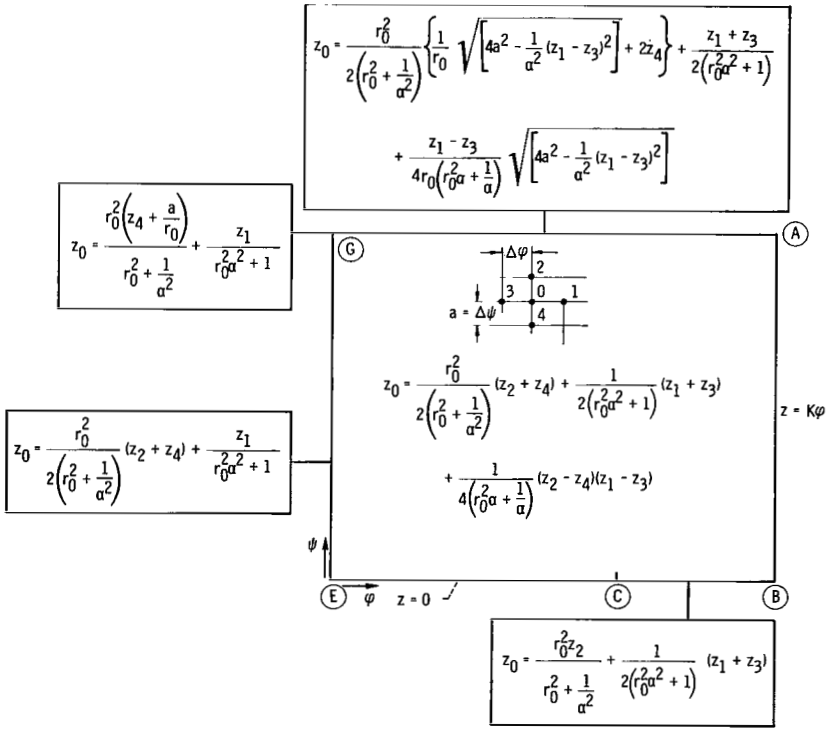

(b) z Solution.

Figure 16. - Finite difference representation for infinite plate.

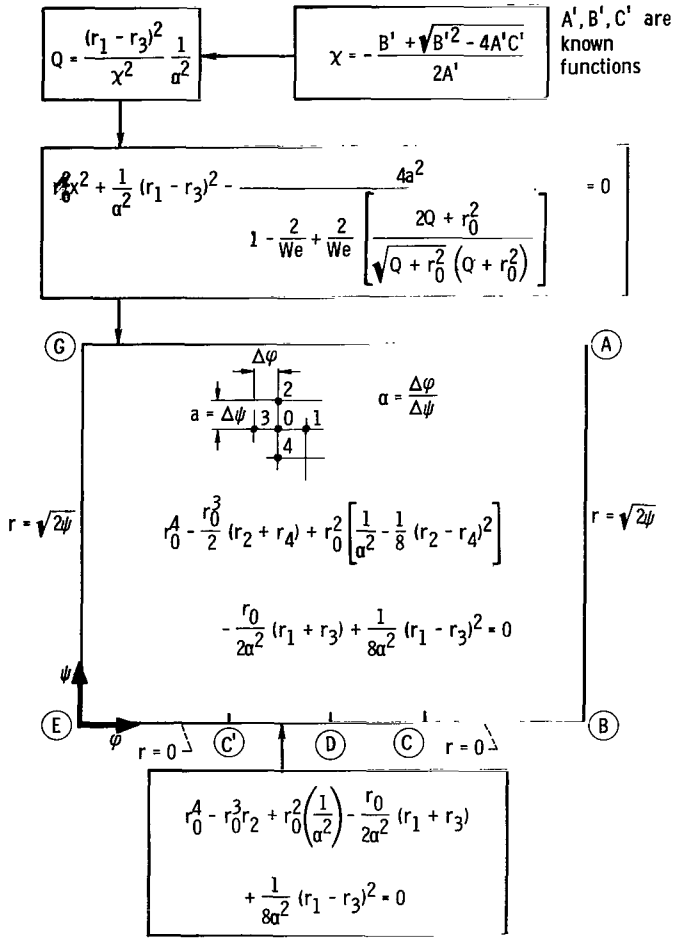

(a) r Solution.

Figure 17. - Finite difference representation for surface-tension-dominated model.

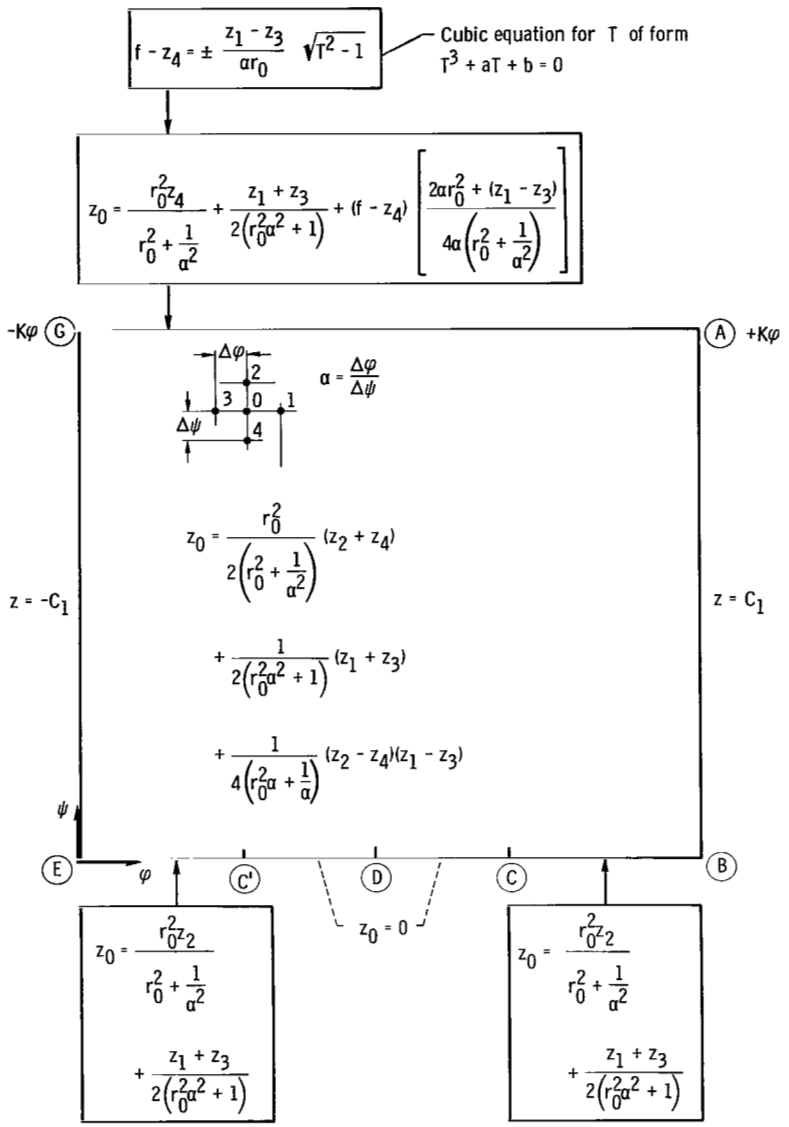

(b) z Solution.

Figure 17. - Concluded.

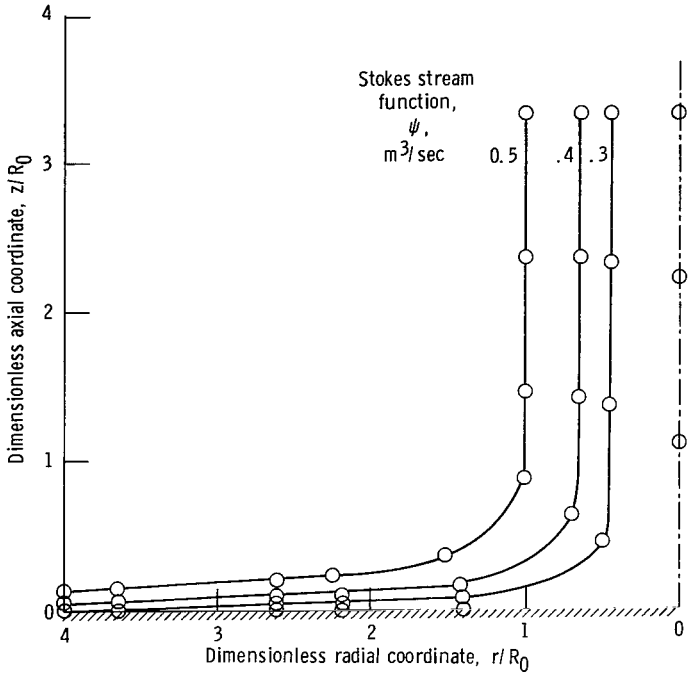

Figure 18. - Numerical solution of liquid jet impinging on infinite flat plate (coarse mesh) for inviscid flow, excluding surface tension.

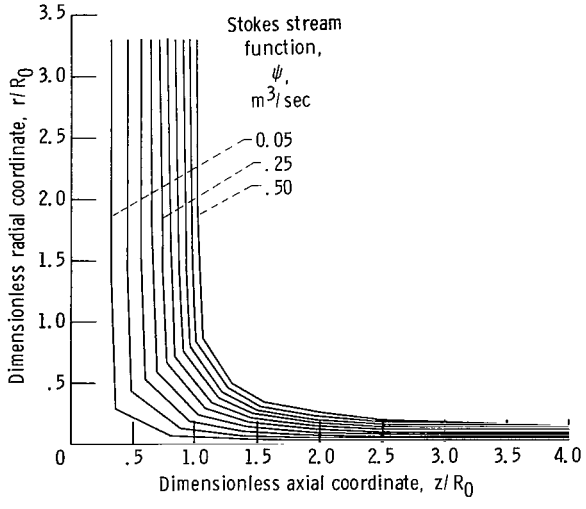

Figure 19. - Computer plot of liquid jet impinging on infinite flat plate (fine mesh) for inviscid flow, excluding surface tension.

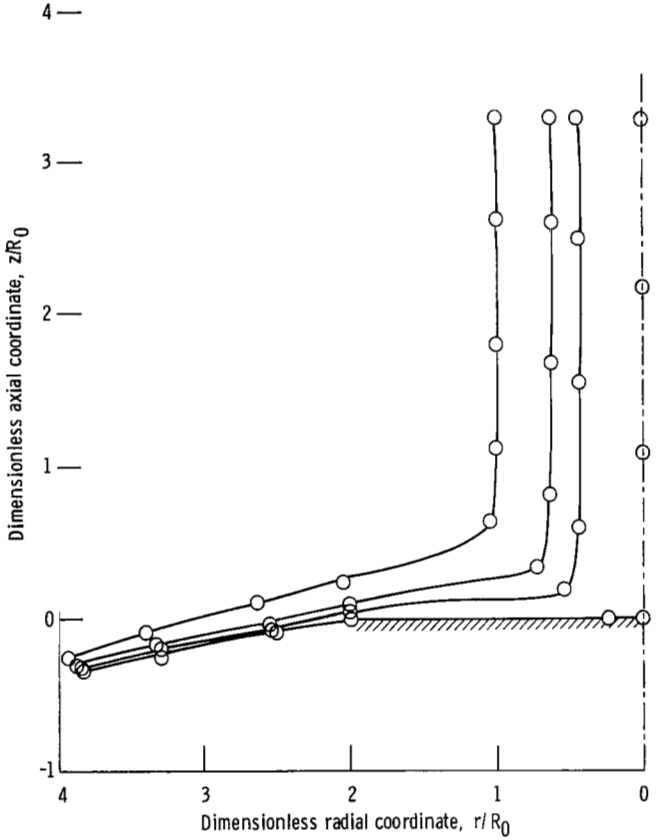

Figure 20. - Numerical solution of liquid jet impinging on finite plate, excluding surface tension, for ratio of jet radius to disk radius R_0/L of 1/2.

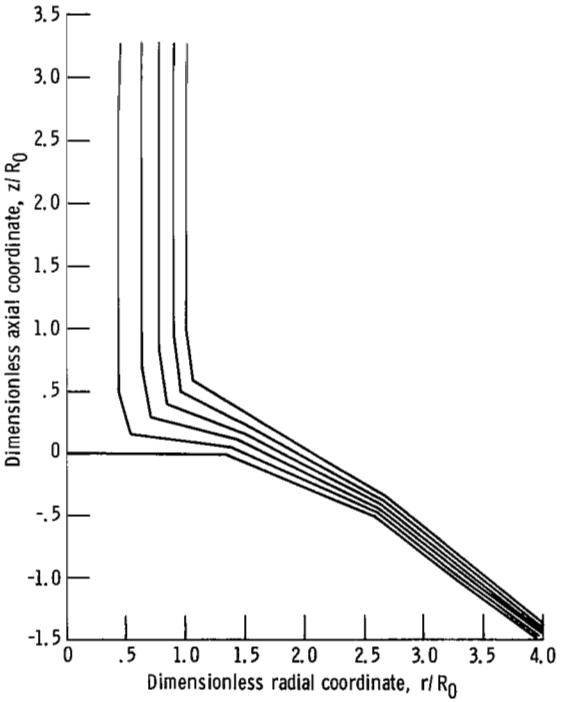

Figure 21. - Computer plot of numerical solution for impingement on finite plate, excluding surface tension, for ratio of jet radius to disk radius R_0/L of 1/2.

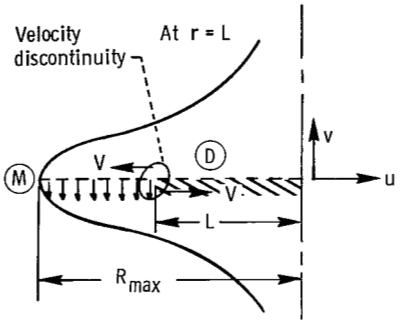

Figure 22. - Schematic of velocity discontinuity occurring in surface tension model.

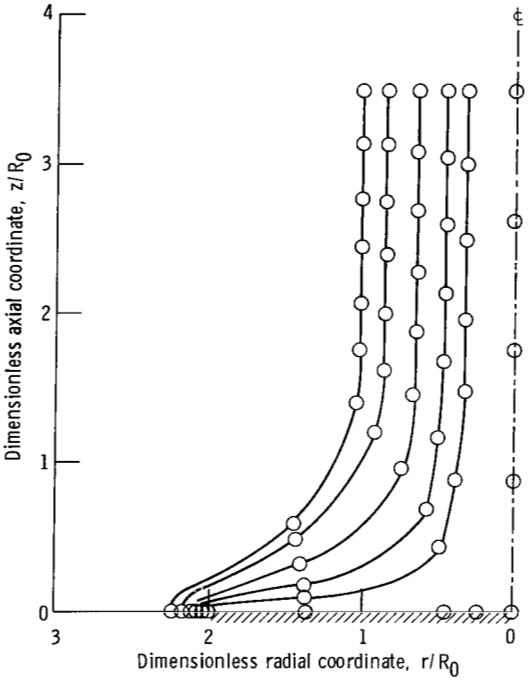

Figure 23. - Numerical solution of surface-tension-dominated model. Weber number, We, 4; ratio of jet radius to disk radius, R_0/L, 1/2.

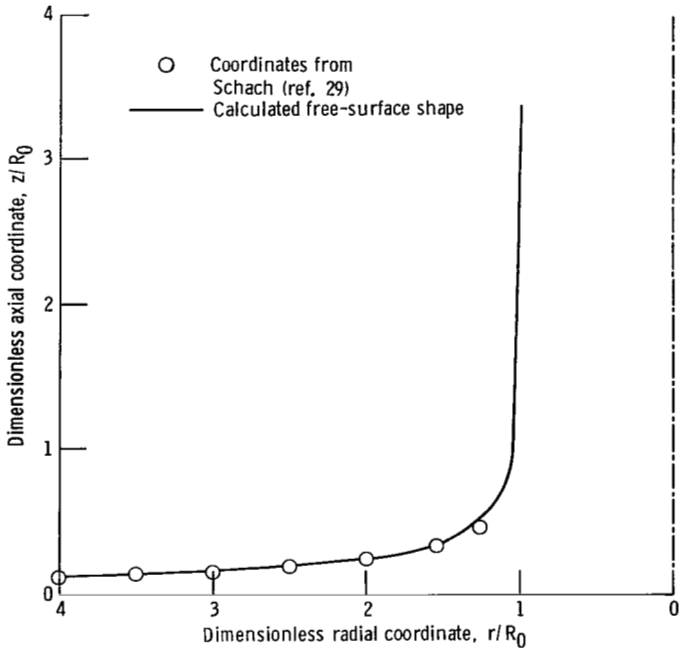

Figure 24. - Comparison of numerical results for infinite plate with reference 29.

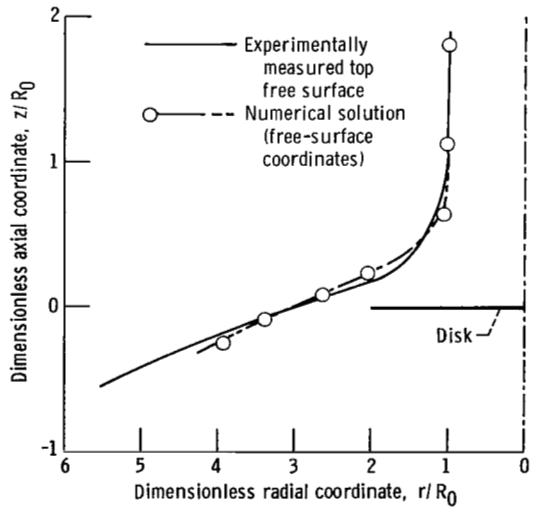

Figure 25. - Comparison of numerical results for finite-plate inertial flow with experiments for ratio of jet radius to disk radius R_0/L of 1/2.

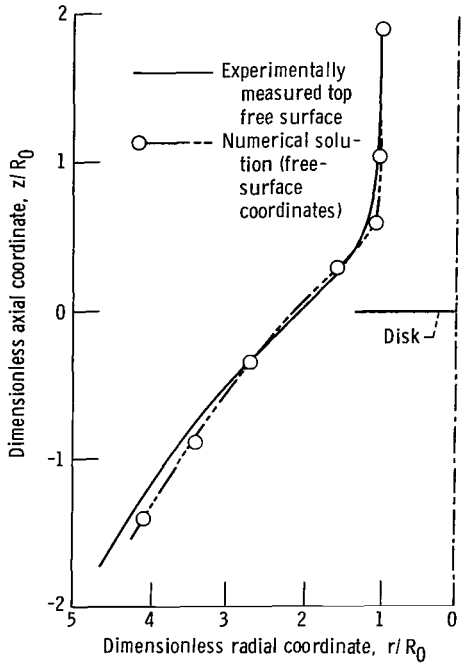

Figure 26. - Comparison of numerical results for finite-plate inertial flow with experiments for ratio of jet radius to disk radius R_0/L of 3/4.

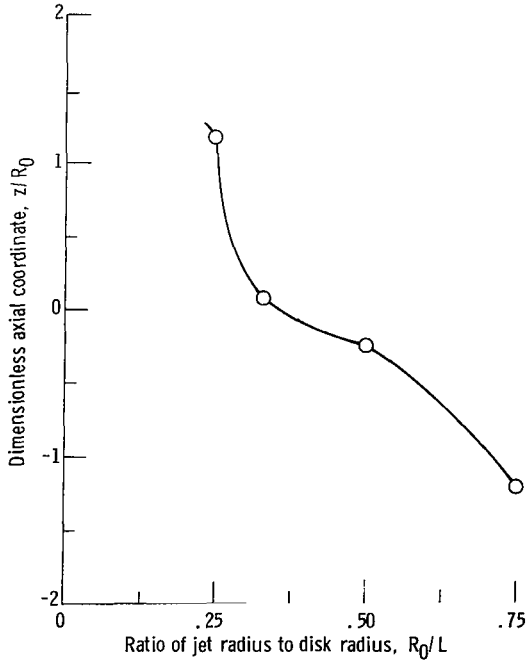

Figure 27. - Experimentally obtained free-surface data showing downward trend of jet at higher ratios of jet radius to disk radius. Dimensionless radial coordinate, r/R_0, 4.

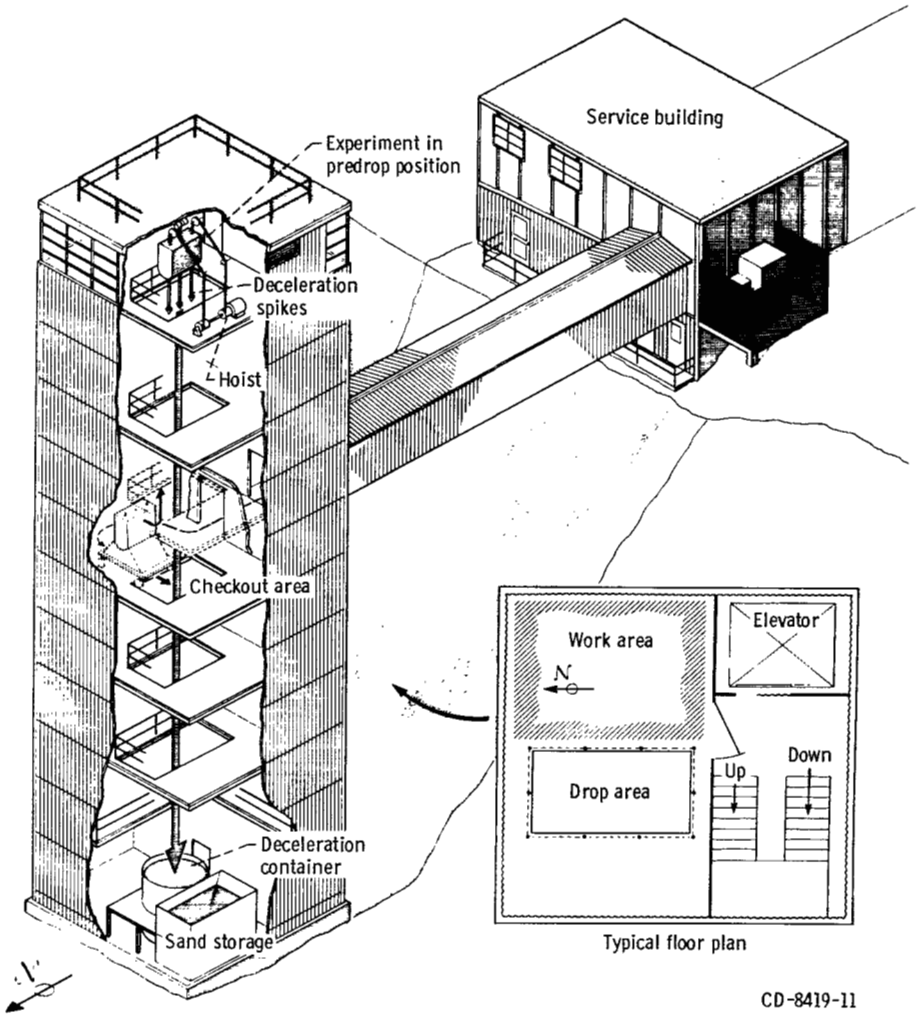

Figure 28. - 2.2-Second zero-gravity facility.

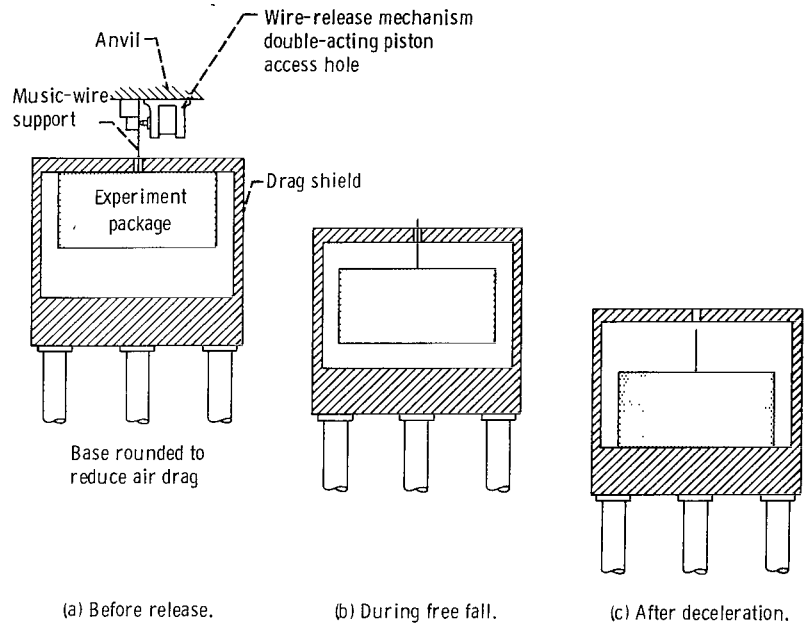

Figure 29. - Position of experiment package and drag shield before, during, and after test drop.

1. Report No.	2. Government Accession No.	3. Recipient's Catalog No.
NASA TP-1017		

4. Title and Subtitle	5. Report Date
LIQUID JET IMPINGEMENT NORMAL TO A DISK IN ZERO GRAVITY	August 1977
	6. Performing Organization Code
7. Author(s)	8. Performing Organization Report No.
Thomas L. Labus	E-8668
	10. Work Unit No.
9. Performing Organization Name and Address	506-21
National Aeronautics and Space Administration Lewis Research Center Cleveland, Ohio 44135	11. Contract or Grant No.
	13. Type of Report and Period Covered
12. Sponsoring Agency Name and Address	Technical Paper
National Aeronautics and Space Administration Washington, D.C. 20546	14. Sponsoring Agency Code

15. Supplementary Notes

16. Abstract

An experimental and analytical investigation was conducted to determine the free-surface shapes of circular liquid jets impinging normal to sharp-edge disks in zero gravity. Experiments conducted in a zero-gravity drop tower yielded three distinct flow patterns that were classified in terms of the relative effects of surface tension and inertial forces. An order-of-magnitude analysis was conducted that indicated regions where viscous forces were not significant in the computation of free-surface shapes. The free-surface analysis was simplified by transforming the governing potential flow equations and boundary conditions into the inverse plane, where the stream function and velocity potential became the coordinates. The resulting nonlinear equations were solved by standard finite difference methods, and comparisons were made with the experimental data for the inertia-dominated regime.

17. Key Words (Suggested by Author(s))	18. Distribution Statement
Axisymmetric flow; Free jets; Weightless fluids; Laminar flow; Isothermal flow; Steady flow	Unclassified - unlimited STAR Category 34

19. Security Classif. (of this report)	20. Security Classif. (of this page)	21. No. of Pages	22. Price*
Unclassified	Unclassified	117	A06

* For sale by the National Technical Information Service, Springfield, Virginia 22161

NASA-Langley, 1977 E-8668

9 1 1U,D, 080577 S00903DS
DEPT OF THE AIR FORCE
AF WEAPONS LABORATORY
ATTN: TECHNICAL LIBRARY (SUL)
KIRTLAND AFB NM 87117

Mixed
States